Stochastic Model Predictive Control and its Application for Small Satellite Attitude Control

Roni Yadlin
Exeter College

University of Oxford

A thesis submitted for the degree of Masters of Science by Research
Department of Engineering Science

Michaelmas 2011

Statement of Originality

The work presented in this thesis is, to the best of the candidate's knowledge and belief, original and the candidate's own work, except as acknowledged in the text. The material has not been submitted, either in whole or in part, for a degree at this or any other university.

Roni Yadlin

Acknowledgements

This thesis would not have been possible without the help of many individuals to whom I am incredibly thankful. I owe my deepest gratitude to my supervisors Professor Basil Kouvaritakis and Dr Mark Cannon for their devotion to me and my research. More often than not I gave them more trouble than I was worth and I thank them for their dedication to me, their patience with me, and their faith in me. Without their efforts, this thesis would never have been started, let alone completed.

I cannot begin to express the gratitude I have towards Mr Bart Holaday, who has funded my time at Oxford University. I deeply respect Mr Holaday in so many ways and I hope that one day I will make an impact on a student's life in half the way that he has impacted mine. I am eternally grateful to him for the incredible opportunity to study at Oxford and the support he has given me along the way.

I would also not be here without the help of the United States Air Force Academy, in particular the Department of Astronautics. The support provided by the staff there, especially Col Martin France, Dr Scott Dahlke, Captain Luke Sauter, and Professor William Saylor, was invaluable to me and my research.

I would also like to thank the previous Holaday Scholars for their help in navigating the world of Oxford studies. Without the insight and advice of Andrew Sellars and Ian Helms, I would have been completely lost.

I would also like to thank my Oxford family, in particular the members of the Oxford University Women's Association Football Club and OUSD, for their support outside the classroom. I will never forget the encouragement shown me by Neal Wendt, Bonnie van Wilgenburg, Kim Kilmartin, Sarah Campbell, and many others throughout my time here. My experiences in Oxford would not have been the same without your love and support.

Finally, I must thank my family for supporting me, believing me, and standing beside me no matter what. Through the ups and the downs, the good times and the bad, they have been there and have gotten me through. Nothing I do in my life would mean anything without their love.

I am indebted to so many people for their help and assistance with this thesis and with making my time in Oxford incredibly meaningful.

Roni Yadlin

Stochastic Model Predictive Control and its Application for Small Satellite Attitude Control
Roni Yadlin Exeter College MSc by Research Michaelmas Term 2011

Abstract

Model predictive control is an attractive control method applicable to a wide range of real-world processes with the ability to handle systems subject to probabilistic constraints and stochastic disturbances. While many methods exist that handle disturbance effects, there are fewer methods that are equipped to handle systems with measurement errors. Additionally, whereas model predictive control is used in a wide range of engineering processes, its use is limited in space applications. This thesis will investigate the use of model predictive control, in a manner that handles stochastic measurement errors, to control the small satellite FalconSAT-5.

This study focused on model predictive control methods that construct a region of tubes in which the state is required to fall in order to meet the probabilistic constraints. Three such methods were studied. The first method used the probabilistic distributions of the disturbances to tighten the constraints so that, even in the presence of disturbances, the constraints would still be met. This method was then expanded to handle both stochastic disturbances and stochastic measurement errors by also including the distribution of the measurement errors as an additional constraint tightening factor. This method was superior to the first method when the system exhibited both disturbances and measurement errors. The third method used state estimation to avoid the errored measurements. When the disturbances have a greater effect on the system response, the method that considers the measurement errors was more effective than the estimation method. However, if the measurement errors have a greater effect, the estimation method was more effective. The model predictive control method was then applied to the FalconSAT-5 dynamic model for all the control modes necessary for satellite operation and the results of these control simulations were compared to the current satellite control scheme of proportional-derivative control.

The simulations showed that, for FalconSAT-5, the model predictive control method that includes the measurement error effects in the constraint definition was superior to the estimation method. This control method was used to simulate control of the satellite in the initial deployment phase, also called the detumble phase, for pointing control, and for control during a slew manoeuvre. This method was found to be superior to the proportional-derivative control in all three control modes in convergence time,control input required, and cost comparison. This study showed that it is possible to develop model predictive control algorithms that handle measurement errors and are applicable to small satellite control. Model predictive control is a viable alternative to classical control for space applications, providing superior performance and better control.

Nomenclature

Roman

A	state space state matrix
B	state space input matrix
c_k	free control moves on the input
C	coordinate transform
D	state space disturbance matrix
e	control error signal
f	vector used to define input constraints
G	gain for PID control
h	vector used to define constraints
H	angular momentum
I	intertia tensor
J	cost
K	optimal linear quadratic regulator gain
K_d	gain for derivative control
K_i	gain for integral control
K_p	gain for proportional control
L	estimator gain
m	measurement error
N	horizon length
p	probability of constraint satisfaction
Q	weighting matrix for states
R	weighting matrix for inputs
T	torque
u	input
w	disturbance
x	state value
$\hat{x}$	state estimate
y	state measurement

Greek

β	constraint tightening factor used to ensure recursive feasibility
γ	constraint tightening factor used to ensure constraint satisfaction in presence of disturbances
η	constraint tightening factor used to ensure constraint satisfaction in the presence of measurement errors
θ	pitch
$\dot{\theta}$	pitch rate
$\ddot{\theta}$	pitch acceleration
ι	constraint tightening factor used to ensure constraint satisfaction in the presence of measurement errors
μ	constraint tightening factor used to ensure constraint satisfaction in the presence of measurement errors
ϕ	roll position
$\dot{\phi}$	roll rate
$\ddot{\phi}$	roll acceleration
Φ	state transition matrix
ψ	yaw position
$\dot{\psi}$	yaw rate
$\ddot{\psi}$	yaw acceleration
ω	used to ensure constraint satisfaction in presence of measurement errors
ω_o	orbital velocity

Abbreviations

ADCS	Attitude Determination and Control System
ESPA	Evolved Expendable Launch Vehicle Secondary Payload Adapter
iMESA	Integrated Miniaturized Electrostatic Analyser
MPC	Model Predictive Control
PD	Proportional-Derivative Control
PI	Proportional-Integral Control
PID	Proportional-Integral-Derivative Control
SPCS	Space Plasma Characterization Source
WISPERS	Wafer-Integrated Spectometer
USAFA DFAS	United States Air Force Academy Department of Astronautics

Contents

List of Figures

List of Tables

Chapter 1

Literature Review and Introduction

1.1 Classical Control Theory

Control systems are an integral part of everyday life and exist in both the man-made and natural world. A control system is, at a surface level, a system that uses inputs to achieve a desired response, even in the presence of disturbances or uncertainty. Much of the general theory used in classical control today is attributed to Nicholas Minorsky, whose work in the 1900s led to the development of proportional-integral-derivative (PID) control.

In general, control systems are made up of a plant and a controller where the plant is the system being controlled and the controller uses measurements of the system output and a desired reference signal to calculate the inputs necessary to achieve the desired output. Figure 1.1 shows the basic block diagram for a classical control system [Nise, 2003].

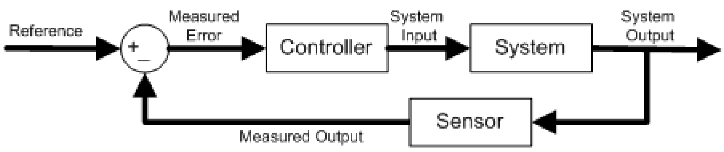

Figure 1.1: Classical control system block diagram

1.1.1 Proportional-Integral-Derivative Control

One set of classical control techniques includes proportional, integral, and derivative control, or any various combinations of the three. These control techniques utilize a feedback control scheme that calculates an error value from the difference between the measured state and the desired state outcome. This error is then manipulated to calculate a control input that will minimize the error and therefore achieve the desired output. Table 1.1 shows the control signals and gains for proportional, integral and derivative control [Nise, 2003].

Table 1.1: Proportional-Integral-Derivative Control

Type	Gain	Control Signal
Proportional	$G_c = K_p$	$u = K_p e$
Integral	$G_c = \frac{K_i}{s}$	$u = K_i \int e$
Derivative	$G_c = K_d s$	$u = K_d \frac{de}{dt}$
PI	$G_c = K_p + \frac{K_i}{s}$	$u = K_p e + K_i \int e$
PD	$G_c = K_p + K_d s$	$u = K_p e + K_d \frac{de}{dt}$
PID	$G_c = K_p + \frac{K_i}{s} + K_d s$	$u = K_p e + K_i \int e + K_d \frac{de}{dt}$

1.1.2 Linear Quadratic Regulator

Linear quadratic regulators are controllers that force a linear system to a final state by minimizing a quadratic cost function. This method is useful in that it obtains an optimal input signal through the use of full state feedback. This optimal signal is found by solving a Ricatti equation associated with the system being controlled and using that solution to calculate the control input $u = Kx$ [Friedland, 1986].

1.1.3 Shortcomings of Classical Control Techniques

While classical control theory has many uses, it exhibits some serious shortfalls. PID controllers fail to guarantee optimal performance or stability and may require extensive tuning to obtain optimal results. Linear quadratic methods fail to take into consideration constraints on the input or states and many classical control techniques are often unable to control constrained systems. By not considering the constraints in the calculation of the control law, input constraints are often violated, causing the controller to become saturated. This input saturation can cause the output of the system to overshoot the desired final state and oscillate until the error signal is driven to zero. This response is demonstrated in Figures 1.2 and 1.3.

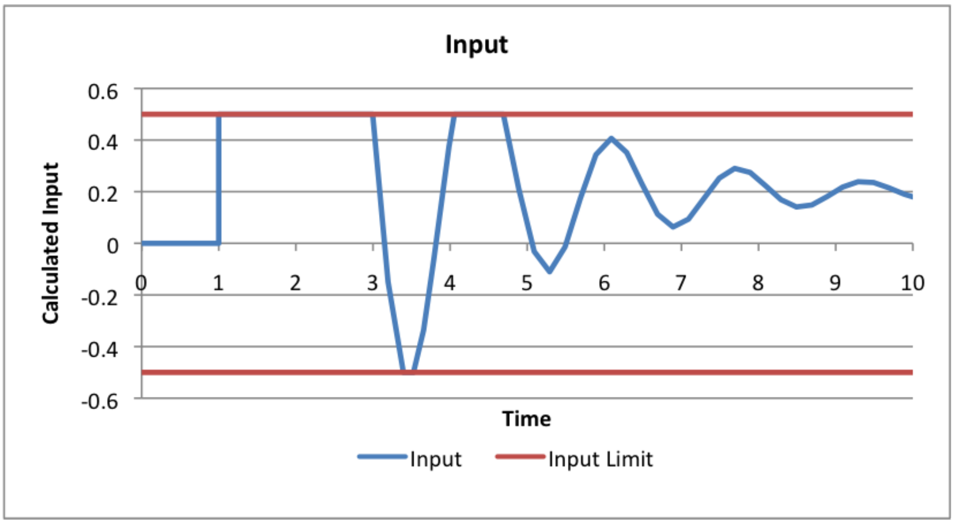

Figure 1.2: Control input saturation

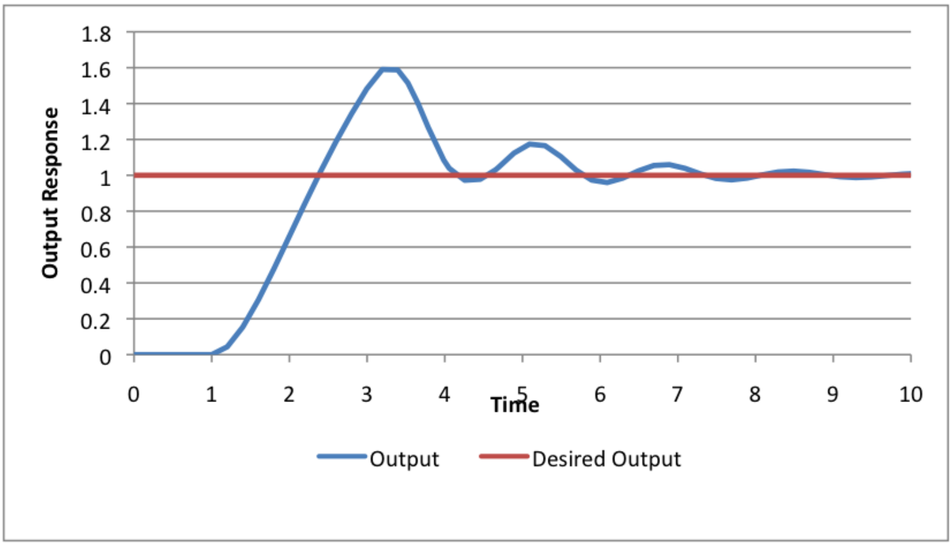

Figure 1.3: Demonstration of effect of controller saturation

The introduction of disturbances into a system further highlights the shortcomings of classical control techniques. Operating in an open loop fashion with no feedback can lead to constraint violation or instability in the presence of uncertainty whereas constrained closed loop control methods can be prohibitively computationally complex. Linear quadratic control methods use an infinite control horizon and can exhibit desired stability characteristics, but solving an infinite horizon open loop problem, in the presence of constraints, can be impractical and difficult to implement in a real world system.

Attempts to minimize or eliminate the previously discussed shortcomings of classical control led to the development of alternative control techniques, including model predictive control (MPC).

1.2 Introduction to Model Predictive Control

In general, model predictive control is a method in which the current control action is obtained by solving, online, at each sampling instance, a finite horizon open loop optimal control problem. The first control input in the calculated control sequence is then implemented and this is repeated in a receding horizon fashion. The basic model predictive control algorithm is as follows:

1. Obtain measurements of the state.

2. Using the system model, predict future state behaviour.

3. Compute an optimal input signal to achieve the predicted state behaviour by minimizing a given cost function over a certain prediction horizon.

4. Implement the first part of the calculated control sequence until new state measurements are available.

5. Repeat process starting with Step 1.

Figure 1.4 shows a block diagram for model predictive control.

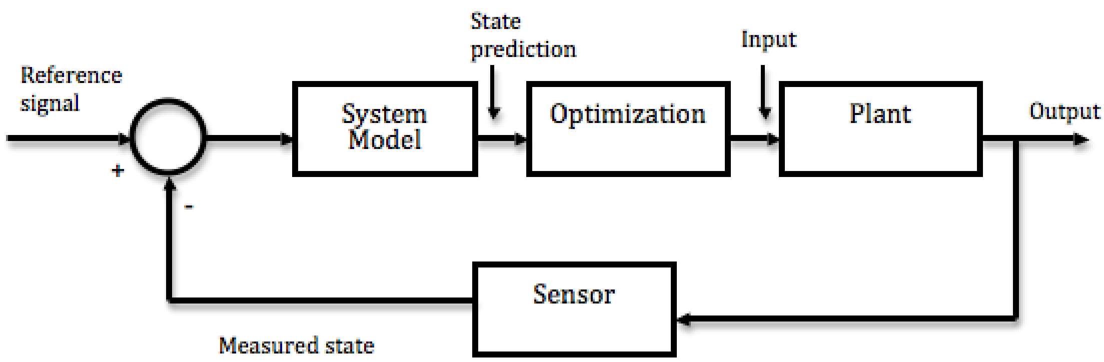

Figure 1.4: Block diagram for model predictive control

There are both advantages and disadvantages to using model predictive control, several of which are outlined in Table 1.2 [Findeisen and Allgower, 2002].

Table 1.2: Advantages and Disadvantages of Model Predictive Control

Advantages	Disadvantages
Can be used to control a wide range of processes	Computationally complex, even for models of relative simplicity
Intrinsically compensates for dead time	Effectiveness of control law is affected by discrepancies between model and actual system
Conceptually simple to implement constraints	Predicted open loop performance can differ significantly from actual closed loop response
Capable of handling systems subject to disturbances	

1.2.1 Traits of Model Predictive Control

Most model predictive control algorithms exhibit the following three traits: a process or system model, a receding horizon, and a minimization of an objective function [Camacho and Bordons, 2004].

1.2.1.1 Process Model

A crucial aspect of model predictive control is the system model itself. In order to predict the future state behaviour, an accurate model of the system dynamics is needed. Model predictive control techniques exist for both discrete and continuous system models. Most systems controlled by model predictive control are described, or approximated, by an ordinary differential equation and modeled by a difference equation. The model must be rich enough to capture the dynamics of the plant, both free and forced response, and must be analysable so that an accurate prediction of future behaviour can be made. The more closely the model matches the actual system, the more effective the control law will be [Clarke, 1994].

1.2.1.2 Receding Horizon

Receding horizon control seeks to mitigate the problems that arise from fixed horizon and infinite horizon control. In receding horizon control, an open loop control sequence is calculated for a finite control horizon. The first control input of this sequence is implemented and then new measurements are taken and a new control sequence is then calculated. Receding horizon control allows for better control authority and better handling of disturbances.

1.2.1.3 Cost Function

Model predictive control relies on the minization of a cost, or objective function. Minimizing the cost function, subject to the constraints, will yield an optimal control sequence. Some model predictive control algorithms solve a least squares optimization problem whereas most algorithms consider a quadratic cost function subject to linear constraints and solve the optimization using quadratic programming. The cost function is often chosen as a Lyapunov function so as to aid in ensuring stability [Mayne et al., 2000].

1.3 Model Introduction

There are many ways to model systems for model predictive control. A common method that will be used for the remainder of this thesis is a state space model. The constrained system takes the following form:

$$\begin{aligned} x_{k+1} &= Ax_k + Bu_k \\ u_k &\in \mathbb{U} \\ x_k &\in \mathbb{X} \end{aligned} \tag{1.1}$$

In this formulation the control inputs $u_k \in \mathbb{R}^l$, and the state $x_k \in \mathbb{R}^n$ are known at time k. $\mathbb{U}$ and $\mathbb{X}$ are sets representing the input and state constraints, respectively. These sets are convex, compact, and contain the origin.

1.3.1 Constraints

One of the benefits of model predictive control is its ability to handle constrained systems. There are two main categories of constraints: state constraints and input constraints. State constraints are informed by the environment in which the system is operating and they ensure that the behaviour of the system and the resulting output stay within an acceptable range. These constraints can either be user defined or environment defined. Input constraints are informed by the limits of the control mechanisms available to the system. Controller hardware has inherent limits and these limits serve as constraints on the control authority available.

1.3.2 Stability

Much of the model predictive control literature focuses on proving and guaranteeing stability for the receding horizon open loop optimization problem. Early model predictive control techniques failed to guarantee stability and instead used stabilizing plants or large prediction horizons to achieve the stabilizing properties of infinite horizon control. Stability can be established by using a Lyapunov function for the value function and making use of the Lyapunov properties to ensure stability; this method is now almost exclusively used. [Chen and Shaw, 1982] [Keerthi and Gilbert, 1988].

Several stabilizing modifications to system models and constraints are available which help ensure stability. These include the use of a terminal equality constraint, a terminal cost function, or a terminal constraint set. Including a terminal equality constraint, where the final state is constrained to the origin, guarantees stability. The use of a terminal cost function was one of the earliest stabilizing proposals and can be used for constrained and non-linear systems. Finally, a terminal constraint set can be used to steer the state into a defined terminal set in a finite time. Once inside that set a local stabilizing controller is used to maintain stability. Often a combination of these methods is used; most model predictive control algorithms use a combination of terminal cost and terminal constraint set [Mayne et al., 2000].

In a survey paper about stability and optimality in constrained model predictive control, Mayne et al (2000) outlined a set of four conditions that, if met, are sufficient for closed loop asymptotic stability. In this paper, the following notation is used. X_f is the terminal constraint set, κ_f is the terminal stabilizing control law, x_{k+1} is a function of x_k and κ_f, F is the terminal cost function which must be positive-definite, and the cost (V) is defined as the sum of the stage costs (ℓ).

The stability conditions are as follows [Mayne et al., 2000]:

A1: $X_f \subset \mathbb{X}$, X_f closed, $0 \in X_f$ (state constraint is satisfied in X_f)

A2: $\kappa_f \in \mathbb{U}$, $\forall x \in X_f$ (input constraint is satisfied in X_f)

A3: $x_{k+1} \in X_f$, $\forall x \in X_f$ (X_f is positivey invariant under κ_f)

A4: $[F^* + \ell](x, \kappa_f(x)) \leq 0$, $\forall x \in X_f$ (F is a local Lyapunov function)

The first three conditions are requirements on the terminal cost, constraint set, and control sequence that are often present in most forms of model predictive control. Condition A1 states that the terminal constraint set X_f must be closed, included in the constraint set for x (which is $\mathbb{X}$), and must contain the origin. If this is the case, then the state constraint is met inside the terminal set X_f. Condition A2 ensures that for all x values in the terminal set, the terminal stabilizing control law κ_f meets the control constraint $\mathbb{U}$. Condition A3 states that, for all $x \in X_f$, the value of the next state (x_{k+1}) is also included in the terminal set. This means the terminal set X_f is positively invariant under the control law κ_f. If conditions A1-A3 are met, there exists a feasible control sequence for the optimal control problem. Condition A4 utilizes a Lyapunov function to ensure stability. F^* is defined as the change in F (the terminal cost) as the state changes from x_k to x_{k+1} and therefore condition A4 says that, for all x included in X_f, the difference between the cost function at each successive time is less than or equal to the opposite of the stage cost. If this is the case, then F is a control Lyapunov function and this, in combination with the requirements on κ and X_f, will ensure that the state of the closed loop system $x_{k+1} = f(x, \kappa_f(x))$ converges to zero as $k \to \infty$ for the set of feasible initial x values. Satisfying these four conditions means that the known stability benefits of infinite horizon control are achieved even though the horizon is finite.

1.3.3 Robustness

Model predictive control is a convenient method because of its ability to be implemented in real world situations. However, real world processes almost always exhibit external disturbances or model uncertainty. When uncertainty is included in the model, Equation (1.1) becomes Equation (1.2):

$$x_{k+1} = Ax_k + Bu_k + Dw_k \tag{1.2}$$

In this formulation, w_k represents additive disturbances where $w \in W_f$.

The introduction of uncertainty into the system brings the problem of maintenance of the properties of stability and performance despite that uncertainty. Furthermore, when constraints are present there is an added level of complexity in ensuring that the disturbances do not cause constraint violations. Early model predictive control methods assumed worst case disturbance and used min-max optimal control, but the results were often conservative. In order to ensure stability in the presence of uncertainty, the four stability conditions must be strengthened in the following way [Mayne et al. [2000]]:

A1: $X_f \subset \mathbb{X}$, X_f closed, $0 \in X_f$ (state constraint is satisfied in X_f)

A2: $\kappa_f \in \mathbb{U}$, $\forall x \in X_f$ (input constraint is satisfied in X_f)

A3: $f(x, \kappa_f(x), w) \in X_f$, $\forall x \in X_f$, $\forall w \in W_f$ (X_f is positivey invariant under κ_f)

A4: $[F^* + \ell](x, \kappa_f(x), w) \leq 0$, $\forall x \in X_f$, $\forall w \in W_f$ (F is a local Lyapunov function)

These conditions are similar to the conditions discussed in Section 1.3.2 except that they are stricter so that, despite the presence of uncertainty, the conditions are still met. These four assumptions ensure monotonicity for all x in an appropriate set and all $w \in W(x, \kappa_N(x))$, thereby implying stability, even in the presence of disturbances.

There are several methods that are being discussed in the current work in the study of robustness. The first utilizes the inherent robustness of the closed loop system to design a control law for the closed loop nominal system, completely ignoring the uncertainty. While this method can result in an asymptotically stable response, it isn't guaranteed to do so and the region of attraction will be much smaller than that for a method that considers the uncertainty. The second option is to consider all possible uncertainty effects, also known as min-max optimal control. This second method considers all possible realizations of the future states based on all possible realizations of the uncertainty to ensure that all possible future states meet the constraints. Because this type of min-max control ignores feedback by solving the optimization in an open loop it can be conservative and, depending on the size of the uncertainty, can diverge. This can result in a region of attraction that is too small to be practical. To remedy this, there are methods that introduce feedback and solve the min-max problem online. In this last method the sequence of calculated control inputs is replaced by a control policy, or a sequence of control laws. While the online min-max method is attractive it can be prohibitively complex and the complexity increases exponentially with the horizon length.

1.4 Thesis Introduction

The purpose of this thesis is to investigate the possibility of implementing model predictive control techniques on a small satellite. The test case used for the implementation of model predictive control for a satellite is a model of FalconSAT-5, a student designed and built small satellite constructed at the United States Air Force Academy [DFAS, 2009]. Several model predictive control techniques are outlined and discussed, each of which can, in theory, be used to control a system that matches FalconSAT-5. The relative merits of these methods are discussed to determine which method is most applicable to FalconSAT-5. FalconSAT-5 is introduced through a description of the environment in which it operates, the mission requirements, the various control modes that must be achieved, and the system model development. The model predictive control method selected for FalconSAT-5 is implemented on the FalconSAT-5 dynamic model for the defined control modes. Finally, the results of the model predictive control are compared with classical control techniques, with a discussion of the relative merits of each.

Chapter 2

Stochastic Tubes for Model Predictive Control

As previously discussed, model predictive control is a convenient control technique because of its ability to consider explicitly constraints in the optimization and its capability of handling systems that are subject to disturbances and uncertainties.

Usually, when handling real world systems, constraints must be considered to be hard and they must never be violated. However, there are instances where constraints can be treated as soft and violation of the constraints is allowed to occur below a predetermined probabilistic threshold. This property is useful in that it can allow for more control authority and a larger feasible region.

Disturbances on a system can take many different forms. One large class of disturbances, which is extremely common in the real world, is that of stochastic, or random, disturbances. By definition, a stochastic disturbance sequence is one in which the values follow some random probability distribution so that their behaviour and effects can by analysed statistically, but not determined precisely.

Because of its similarity to the circumstances in which a small satellite operates, the focus of this research is on controlling systems subject to stochastic disturbances and probabilistic constraints.

The following summarizes a method that explicitly uses the distribution of the disturbances to construct a series of regions, referred to as tubes, in which the predicted state of the system is to lie at a given time. These tubes guarantee satisfaction of the probabilistic constraints and also guarantee feasibility over all times, given feasibility at initial time [Kouvaritakis et al., 2010a].

2.1 System and System Dynamics

The system in question takes the form of Equation (2.1):

$$x_{k+1} = Ax_k + Bu_k + Dw_k \tag{2.1}$$

For the system, $x_k \in \mathbb{R}^n$, $u_k \in \mathbb{R}^l$ and $w_k \in \mathbb{R}^m$. The disturbance sequence is independently and identically distributed with a zero-mean and known probabilistic distribution. The disturbances also lie in the orthotope described by Equation (2.2):

$$w_k \in \Pi_w = \{w : |w| \leq \alpha\} \tag{2.2}$$

The following method can be applied when input and/or state constraints are present and can be expanded to control systems subject to multiple constraints. To maintain consistency with the representation of a small satellite, which will be described in full in Chapter 5, this system will include input constraints in the form of Equation (2.3). These constraints are probabilistic in nature but this framework can also be used to consider hard constraints by using $p = 1$:

$$\Pr(f^T u_k \leq h) \geq p \tag{2.3}$$

Because closed-loop optimization is impractical in the presence of uncertainty and constraints, this method makes use of a manipulation of the closed loop paradigm in which the control input is centred around the unconstrained optimal linear quadratic regulator but includes perturbations on the feedback as degrees of freedom. These are free control moves, c_k, that can be chosen so as to provide optimal control in the presence of constraints. These free control moves are only used to ensure constraint satisfaction and should be kept as small as possible. Equation (2.4) demonstrates this closed-loop paradigm control law:

$$u_k = Kx_k + c_k \tag{2.4}$$

The goal of this model predictive control method is to devise an optimization strategy that minimizes the cost shown in Equation (2.5) where $\mathbb{E}$ denotes expected value. This cost function guarantees that the closed loop system is stable and ensures that the state converges to a neighborhood of the origin:

$$J = \sum_{k=0}^{\infty} \mathbb{E}(x_k^T Q x_k + u_k^T R u_k) \tag{2.5}$$

2.2 Predictions

Model predictive control relies on predicting the future behaviour of the system being controlled. Both the future states and the future constraints must be predicted.

2.2.1 State Predictions

The state predictions are made using the system's dynamic model. Using the closed loop paradigm and $\Phi = A + BK$ the following sequence of equations represents the state predictions:

$$\begin{aligned} x_{k+1} &= Ax_k + Bu_k + Dw_k \\ &= Ax_k + BKx_k + Bc_k + Dw_k \\ &= \Phi x_k + Bc_k + Dw_k \\ &\vdots \\ x_{k+i} &= \Phi^i x_k + \Phi^{i-1} Bc_k + \ldots + Bc_{k+i-1} + \Phi^{i-1} Dw_k + \ldots + Dw_{k+i-1} \end{aligned} \tag{2.6}$$

In order to simplify the predictions it is useful to decompose the state into two parts: one that represents the nominal (disturbance free) dynamics and one that represents the stochastic effects. Because a measurement for the initial state is available, the initial stochastic effect can be taken to be zero, yielding the following decomposition.

$$\begin{aligned} x_{k+i} &= z_{k+i} + e_{k+i} \text{ for all } i > 0 \\ z_k &= x_k \qquad e_k = 0 \end{aligned} \tag{2.7}$$

Using the closed loop paradigm and predicting the nominal dynamics and uncertainy effects yields the following predictions:

$$\begin{aligned} z_{k+1} &= \Phi z_k + Bc_k \\ z_{k+2} &= \Phi z_{k+1} + Bc_{k+1} \\ &= \Phi^2 z_k + \Phi Bc_k + Bc_{k+1} \\ &\vdots \\ z_{k+i} &= \Phi^i z_k + \Phi^{i-1} Bc_k + \ldots + Bc_{k+i-1} \\ \\ e_{k+1} &= \Phi e_k + Dw_k \\ e_{k+2} &= \Phi e_{k+1} + Dw_{k+1} \\ &= \Phi^2 e_k + \Phi Dw_k + Dw_{k+1} \\ &= \Phi Dw_k + Dw_{k+1} \\ &\vdots \\ e_{k+i} &= \Phi^{i-1} Dw_k + \ldots + Dw_{k+i-1} \end{aligned}$$

2.2.2 Constraint Predictions

The constraints (2.3) must be considered over the entire prediction horizon (from k to $k+i$) and therefore take the form of Equation (2.8):

$$\Pr(f^T K(\Phi^i z_k + \Phi^{i-1} Bc_k + \ldots + Bc_{k+i-1}) + f^T K(\Phi^{i-1} Dw_k + \ldots + Dw_{k+i-1}) \leq h) \geq p \tag{2.8}$$

By making use of the knowledge of the probabilistic distribution of the disturbances, an approximation can be made for the distribution of the sequence $f^T K(\Phi^{i-1} Dw_k + \ldots +$

Dw_{k+i-1}). Finding the exact value of this distribution requires summing a large number of independent density functions which requires multiple convolution integrals. This can be computionally impractical but through discretizing the distributions and carrying out discrete convolution, an approximation of the sum of the distribution functions can be obtained with a reasonable computational complexity. A γ_i value is calculated offline and is used to define the constraint tubes for the control law and ensure that the constraints are met, even in the presence of uncertainty. For each $i = 1, 2, \ldots,$ γ_i is defined as the minimum value for which Equation (2.9) is true:

$$\Pr(f^T K(\Phi^{i-1} Dw_k + \ldots + Dw_{k+i-1}) \leq \gamma_i) \geq p \tag{2.9}$$

2.3 Stochastic Tube Definition

The first step in guaranteeing constraint satisfaction in closed loop operation is to ensure that the constraint is met by the prediction dynamics at time instant k. Using the distribution of the disturbance effects described in Equation (2.9), the vector of free control moves $\bar{c_k} = [c_k \quad c_{k+1} \ \ldots c_{k+N-1}]^T$ will satisfy the probabilistic constraints at time k if and only if Equation (2.10) is true:

$$f^T K \Phi^i z_k + f^T K \left[\Phi^{i-1} B \ldots \ B\right] \bar{c_k} \leq h - \gamma_i \tag{2.10}$$

2.3.1 Ensuring Recursive Feasibility

The expression in Equation (2.10), however, only proves the existence of a feasible solution at time k. In order to guarantee a feasible solution at all future prediction times $k + j$ for $j > 1$ the equation must be modified. At time k, looking ahead to time $k + j$, the prediction of the stochastic effects at time $k + j + i$, based on the information available at time $k + j$, is shown in Equation (2.11):

$$e_{k+j+i|k+j} = \Phi^i e_{k+j|k+j} + \Phi^{i-1} Dw_{k+j|k+j} + \cdots + Dw_{k+j+i-1|k+j} \tag{2.11}$$

Equation (2.11) expresses $e_{k+j+i|k+j}$ in terms of $e_{k+j|k+j}$. Because this prediction occurs at time k, no information is yet available about x_{k+j} and therefore the assumption used formerly that $e_k = 0$ does not hold. However when the control input is used, this disturbance will have occured and will have been dependent upon the earlier disturbance values; therefore it will not be a random variable. It is possible that these earlier disturbance values were the worst case values and therefore, in order to account for the unknown disturbance effect of $e_{k+j+i|k+j}$ the entire range of possible disturbances must be considered. The worst case disturbance value must be used to ensure the constraint is satisfied for all future times $k + j$ for $j > 1$. This modification means that the tubes are now defined according to the following set of conditions:

$$f^T K\Phi^i z_k + f^T K\Phi^i e_k + f^T K \left[\Phi^{i-1}B \ldots\ B\right] \bar{c_k} \leq h - \beta_i \tag{2.12}$$

$$\beta = \begin{bmatrix} \gamma_1 & \gamma_2 & \gamma_3 & \gamma_4 & \cdots \\ 0 & \gamma_1 + a_1 & \gamma_2 + a_2 & \gamma_3 + a_3 & \cdots \\ 0 & 0 & \gamma_1 + a_1 + a_2 & \gamma_2 + a_2 + a_3 & \cdots \\ \vdots & \vdots & \vdots & \vdots & \ddots \end{bmatrix}$$

$$\beta_i = \text{maximum element of } i^{\text{th}}\text{column of } \beta$$

$$a_i = |f^T K\Phi^i D| w_{max}$$

2.3.2 Dual Mode Prediction

In order to ensure that the constraints are met over the entirety of the prediction horizon it is useful to use a dual-mode prediction strategy in which the first N control moves are dictated by the control law $u_k = Kx_k + c_k$ whereas in mode 2 the control moves are prescribed by the optimal linear quadratic regulator control law of $u_k = Kx_k$. The linear quadratic regulator does not consider the constraints and therefore a terminal constraint set must be used to ensure constraint satisfaction in mode 2. A maximal admissible set S_∞ is defined as the set of all z_N values so that the following terminal constraint holds for all j values if $z_N \in S_\infty$:

$$f^T K \Phi^j z_N \leq h - \beta_{N+j} \tag{2.13}$$

Because the sequence of β values is monotonically non-decreasing to a limit of $\bar{\beta}$, rather than calculate an infinite number of future β_i values, the limit can be upper bounded and used after a certain number $(\hat{N})$ of prediction instances. Because of the definitions of γ_i and a_i, $\gamma_{i+1} \leq \gamma_i + a_i$. From that, and the definition of β_i it follows that $\beta_i \leq \beta_{i+1}$ for all i. As the β_i value approaches the $\bar{\beta}$, the difference between the effect those two values in the constraint definition will eventually be small enough to be negligible. The use of this $\bar{\beta}$ beyond the $j = \hat{N}$ defines a subset of S_∞ that can be approximated using a finite number of inequalities [Gilbert and Tan, 1991]. Provided n^* is large enough, the set need only be defined by the first $\hat{N} + n^*$ values and once the state has entered the set defined by Equation (2.14), it will remain in that set without the use of additional constraints:

$$S_{\hat{N}} = \{z_N : f^T K \Phi^l z_N \leq h - \bar{\beta},\ \text{for } l = \hat{N} + 1 \ldots \hat{N} + n^*\} \tag{2.14}$$

To find n^*, the first step is to set $n = 0$ and solve the following optimization problem: $\max f^T K \Phi^{n+1} z_N$ subject to the constraints $f^T K \Phi^k z_N \leq h - \bar{\beta}$ for all $k = 0, \ldots, n$. If this optimized value is less than $h - \bar{\beta}$, n^* is set to n and the optimization ends. If not, $n = n + 1$ and the optimization repeats until the maximum value is below $h - \bar{\beta}$ [Gilbert and Tan, 1991].

The $\bar{\beta}$ limit can be bounded using Equation (2.15) [Kouvaritakis et al. [2010a]]:

$$\bar{\beta} \leq \gamma_1 + \sum_{j=1}^{\nu-1} a_j + \frac{\rho^\nu}{1-\rho} ||f^T K||_S \tag{2.15}$$

Equation (2.15) holds for any non-negative integer ν, where the conditions in (2.16) are true:

$$||f^T K||_S = \sqrt{K^T f S f^T K} \tag{2.16a}$$

$$\max_{w \in \Pi} ||Dw||_{S^{-1}} \leq 1 \tag{2.16b}$$

$$\Phi S \Phi^T \leq \rho^2 S, \quad \rho \in (0,1) \tag{2.16c}$$

2.4 Optimization Policy

The parameters that define the constraints are calculated offline and the optimization is then conducted online. Equation (2.17) defines the optimal sequence of control moves $\bar{c_k}$:

$$\bar{c_k} = \underset{\bar{c_k}}{\operatorname{argmin}} \sum_{i=0}^{\infty} \mathbb{E}(x_{k+i}^T Q x_{k+i} + u_{k+i}^T R u_{k+i}) - L_{ss} \tag{2.17}$$

The first value of this optimal sequence of control moves is then used in the closed loop paradigm (2.4) to calculate the control input. After time $k = N$, the c_k value is set to zero. The steady state limit (L_{ss}) is included in the cost function because of the presence of additive disturbance. In the presence of this disturbance the closed loop stage cost will converge to a non-zero limit as defined by Equation (2.18). This limit must therefore be considered in the cost function that defines the optimization [Kouvaritakis et al., 2010a].

$$L_{ss} = \text{trace}(DD^T(Q + K^T RK)) \tag{2.18}$$

Equation (2.19) defines the set of constraints for the optimization:

$$\begin{cases} f^T K \Phi^i z_k + f^T K \left[\Phi^{i-1} B \dots \; B\right] \bar{c_k} \leq h - \beta_i & \text{if } i = 1, \dots, N-1 \\ f^T K \Phi^j z_N \leq h - \beta_{N+j} & \text{if } j = N, \dots, \hat{N} \\ f^T K \Phi^j z_N \leq h - \bar{\beta} & \text{if } j = \hat{N}+1, \dots \hat{N} + n^* \end{cases} \tag{2.19}$$

This cost can be shown to be a Lyapunov function, thereby implying stability. The system (2.1) is augmented to include the state and the calculated control moves:

$$x_{k+i} = \Phi x_k + Bc_k + Dw_k \tag{2.20}$$

$$\chi_k = \begin{bmatrix} x_k \\ \bar{c}_k \\ 1 \end{bmatrix} \tag{2.21}$$

$$\chi_{k+1} = \begin{bmatrix} \Phi & BE & Dw_k \\ 0 & M & 0 \\ 0 & 0 & 1 \end{bmatrix} \chi_k = \Psi \chi_k \tag{2.22}$$

$$\tilde{\Psi} = \begin{bmatrix} \Phi & BE \\ 0 & M \end{bmatrix} \tag{2.23}$$

$$E = \begin{bmatrix} I & 0 & \dots & 0 \end{bmatrix}$$

$$M = \begin{bmatrix} 0 & I & 0 & \dots \\ 0 & 0 & I & \dots \\ \vdots & \vdots & \vdots & \vdots \\ 0 & 0 & \dots & I \\ 0 & 0 & 0 & 0 \end{bmatrix}$$

By using the closed loop paradigm (2.4) in the cost function, the cost function becomes Equation (2.25), where c_i is the i^{th} component of $\bar{c}_k$ and $c_i = 0$ for $i > N$:

$$J = \sum_{i=0}^{\infty} \mathbb{E}(x_i^T(Q + K^T RK)x_i + x_i^T K^T Rc_i + c_i^T RKx_i + c_i^T Rc_i) - L_{ss} \tag{2.25}$$

Using the augmented state representation, the stage cost can be rewritten in quadratic form:

$$l_{k+i} = \mathbb{E}(\chi_{k+i}^T \begin{bmatrix} Q + K^T RK & K^T RE & 0 \\ E^T RK & E^T RE & 0 \\ 0 & 0 & -L_{ss} \end{bmatrix} \chi_{k+i}) = \mathbb{E}(\chi_{k+i}^T \bar{Q} \chi_{k+i}) \tag{2.26}$$

$\tilde{Q}$ is defined as:

$$\tilde{Q} = \begin{bmatrix} Q + K^T RK & K^T RE \\ E^T RK & E^T RE \end{bmatrix} \tag{2.27}$$

Equation (2.28) shows the expected value cost at each time $k, k+1, \dots$ can be written as a quadratic function in terms of χ and P. P is defined by Equation (2.29a) through Equation (2.29d) [Cannon et al., 2009]:

$$\mathbb{E}(V_k) = \chi_k^T P \chi_k \tag{2.28}$$

$$P = \begin{bmatrix} P_{11} & P_{12} \\ P_{21} & P_{22} \end{bmatrix}$$

$$P_{11} - \tilde{\Psi}^T P_{11} \tilde{\Psi} = \tilde{Q} \tag{2.29a}$$

$$P_{12} = P_{21} = 0 \tag{2.29b}$$

$$P_{22} = -\mathrm{tr}(\Theta P_{11}) \tag{2.29c}$$

$$\Theta - \Psi \Theta \Psi^T = D^T D \mathbb{E}(ww^T) = D^T D \Sigma \tag{2.29d}$$

Combining Equation (2.28) and Equation (2.22) gives the expected value cost, in quadratic form, at $k+1$, as:

$$V_{k+1} = (\Psi \chi_k)^T P (\Psi \chi_k) \tag{2.30}$$

Subracting the stage cost at $k+1$ from the cost at k yields the following:

$$\begin{aligned}
\mathbb{E}(V_k) - \mathbb{E}(V_{k+1}) &= \chi_k^T P \chi_k - \chi_k^T \Psi^T P \Psi \chi_k \\
\mathbb{E}(V_k) - \mathbb{E}(V_{k+1}) &= \mathbb{E}(\chi_k^T (P - \Psi^T P \Psi) \chi_k) \\
\mathbb{E}(V_k) - \mathbb{E}(V_{k+1}) &= \mathbb{E}(\chi_k^T \bar{Q} \chi_k) \\
\mathbb{E}(V_k) - \mathbb{E}(V_{k+1}) &= \ell_k
\end{aligned}$$

Continuing this subtraction for all time instants $k+i \geq 0$,and then summing the sequence of differences shows the following:

$$\begin{gathered}
\mathbb{E}(V_k) - \mathbb{E}(V_{k+1}) = \ell_k \\
\mathbb{E}(V_{k+1}) - \mathbb{E}(V_{k+2}) = \ell_{k+1} \\
\mathbb{E}(V_{k+2}) - \mathbb{E}(V_{k+3}) = \ell_{k+2} \\
\vdots \\
\mathbb{E}(V_k) - \mathbb{E}(V_\infty) = \sum_{k=0}^{\infty} \ell_k
\end{gathered}$$

As $i \to \infty$, $\mathbb{E}(V_{k+i}) \to 0$ so therefore, the expected value cost, as written in Equation (2.28), can be shown to equal the sum of the stage costs.

$$\mathbb{E}(V_k) = \sum_{k=0}^{\infty} \ell_k = J \tag{2.31}$$

This chapter describes a method that provides recursive feasibility and guarantees stability for a dynamic system with stochastic disturbances, subject to probabilistic constraints. The offline calculation of the tube tightening factors requires modest and reasonable computation and the results are as tight as possible, within the prediction structure adopted, while maintaining computational practicability [Kouvaritakis et al., 2010a].

2.5 Simulation Results

Using the following model, a simulation of this method was completed to show the ability of this method to control systems subject to probabilistic constraints and stochastic disturbances.

$$A = \begin{bmatrix} 1 & 1 \\ 0 & 1 \end{bmatrix}$$

$$B = \begin{bmatrix} .5 \\ 1 \end{bmatrix}$$

$$D = \begin{bmatrix} .1 & 0 \\ 0 & .1 \end{bmatrix}$$

$$x_0 = \begin{bmatrix} -5 \\ -2 \end{bmatrix}$$

$$|u_k| \leq 2.5 \qquad |w_k| \leq 1 \qquad Q = I \qquad R = .1 \qquad N = 10 \qquad \hat{N} = 6 \qquad n^* = 1 \qquad p = .8$$

In this simulation, the disturbace elements w_k exhibit a truncated normal distribution with a standard deviation $\sigma = \frac{1}{144}$. Figure 2.1 shows the state response of the model predictive control method for the above system, showing the mean state value for 200 realizations of uncertainty. Figure 2.2 shows the convergence of the state towards zero for 10 realizations of uncertainty and also includes the mean response for 200 uncertainty realizations. The state response is shown to converge to, and remain in, the terminal set defined by Equation (2.14). This method will be referred to as “baseline MPC”and this name will be used in all future references to this method.

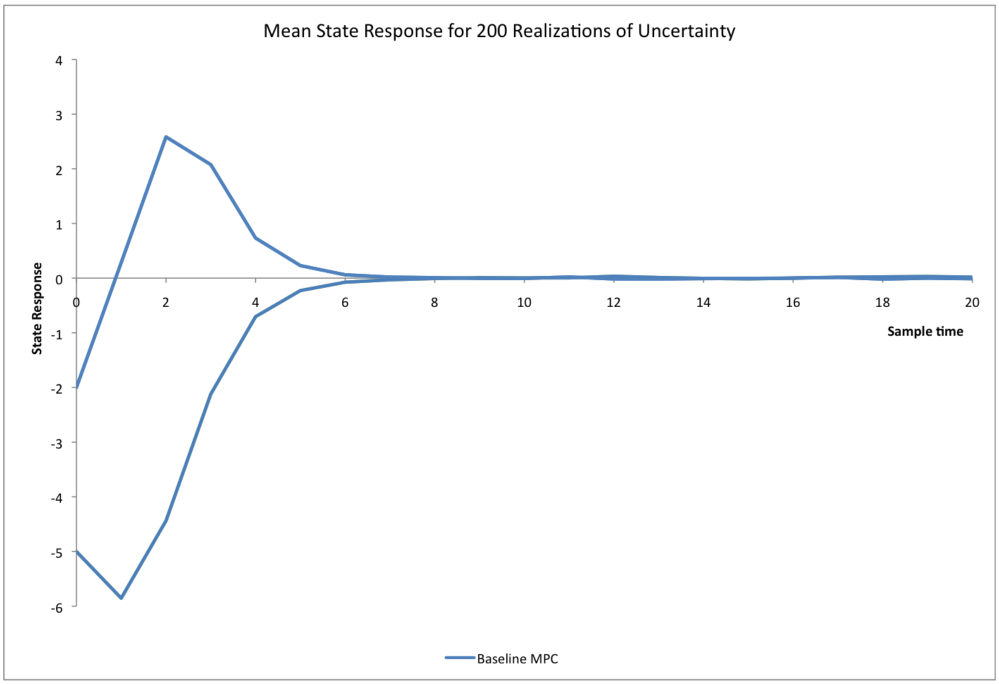

Figure 2.1: Mean state response for 200 realizations of uncertainty for baseline MPC method

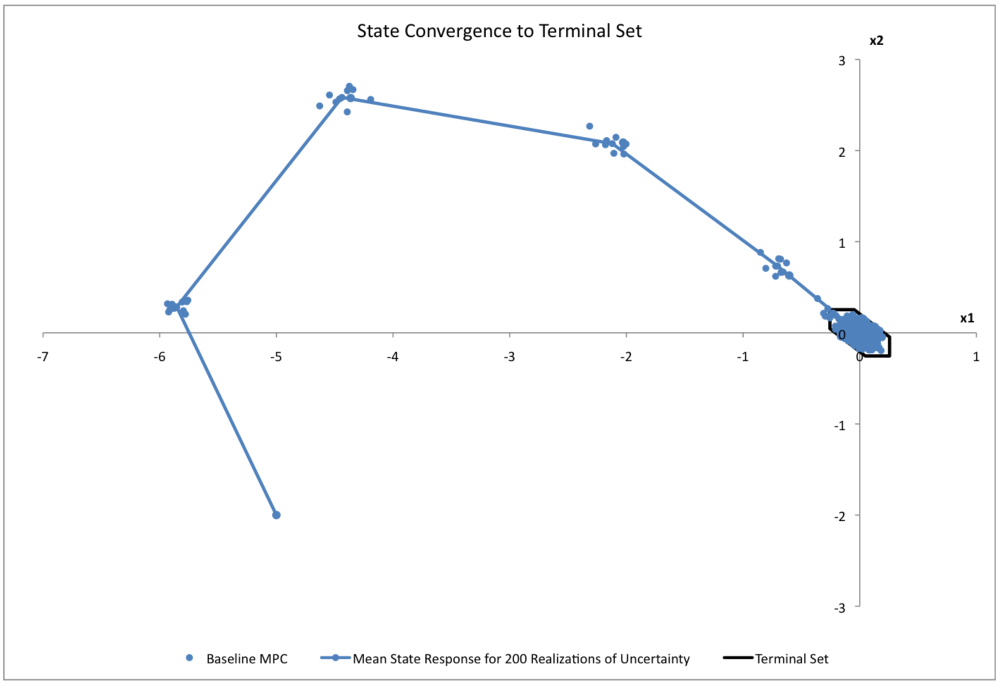

Figure 2.2: State convergence to terminal set for 10 realizations of uncertainty

Table 2.1 shows the average cost, the worst case cost, and the percent of constraint violation for the 200 uncertainty realizations.

Table 2.1: Cost and Percent Constraint Violation for Baseline Model Predictive Control Method for 200 Realizations of Uncertainty

Average Cost	102.1245
Maximum Cost	106.1175
Percent Constraint Violation	20%

2.5.1 Comparison with Linear Quadratic Regulator

As a means of discussing the merits of baseline MPC, a comparison to the optimal linear quadratic regulator was made. The system, including weighting matrices, for the LQR method matches the system defined in Section 2.5. The unconstrained linear quadratic regulator yields a much lower cost of 70.0657 but this method fails to meet the input constraints at time $k = 1$. If a constraint is imposed, after the fact, on the unconstrained linear quadratic regulator by truncating the calculated input value, the input constraint can be met at time $k = 1$, with a higher cost of 95.1275. However, in the presence of uncertainty, the constraints will be violated at time $k + 1$ for all possible values of uncertainty and the input would again need to be truncated in order to meet the constraints. Therefore, without the use of the degrees of freedom included in $\bar{c}$, the presence of uncertainty results in a violation of the constraints. Table 2.2 shows the cost and constraint violation for these three methods. In the table, the first value for constraint violation is for sample time $k = 1$ whereas the second value is for future prediction time $k + 1$.

Table 2.2: Comparison of Cost for 200 Realizations of Uncertainty for LQR, Baseline MPC, and clipped LQR Methods

Method	Average Cost	% Constraint Violation
LQR	70.0657	100% 0%
Baseline MPC	102.1235	0% 20%
Truncated LQR	94.5682	0% 100%

The simulation results, including a graphical representation of the input required for control, for the linear quadratic regulator and truncated linear quadratic regulator are found in Appendix A.

Chapter 3

Stochastic Model Predictive Control with Measurement Error Consideration

3.1 Modified System and System Dynamics

The baseline MPC method discussed in the previous chapter is based on state feedback through the closed loop paradigm. This reliance on feedback presupposes that the state is measurable. However, this may not be the case and, in practice, state measurements may be inaccurate or completely unavailable. For FalconSAT-5, for example, the state measurements provided by the onboard attitude sensors contain an unknown, randomly distributed, error and therefore this error must be considered when developing a stochastic model predictive control algorithm for control of FalconSAT-5. This method that considers the measurement errors will be referred to as "MPC with error consideration."

When including the measurement errors in the system, Equation (2.1) now takes the form of Equations (3.1a) and (3.1b) where x_k is the actual state, y_k is the state measurement, and m_k is the measurement error:

$$x_{k+1} = Ax_k + Bu_k + Dw_k \tag{3.1a}$$

$$y_k = x_k + m_k \tag{3.1b}$$

The same assumptions that were made about the disturbances are made about the measurement errors, namely that the error sequence is independently and identically distributed with a zero-mean and known probabilistic distribution. The measurement errors are described by Equation (3.2):

$$m_k \in \Pi_m = \{m : |m| \leq m_{max}\} \tag{3.2}$$

Because the only information available for use in the state feedback is the inaccurate state measurement, this measurement is used to compute the input using the closed loop paradigm:

$$u_k = Ky_k + c_k \tag{3.3}$$

3.2 Predictions

As with the baseline MPC method, the MPC with error consideration method relies on a prediction of both the states and constraints.

3.2.1 State Predictions

Combining the state prediction equation (3.1a), the measurement error equation (3.1b) and the input equation (3.3) yields the following state predictions:

$$
\begin{aligned}
x_{k+1} &= A(y_k - m_k) + B(Ky_k + c_k) + Dw_k \\
x_{k+1} &= \Phi y_k - Am_k + Bc_k + Dw_k \\
x_{k+2} &= \Phi y_{k+1} - Am_{k+1} + Bc_{k+1} + Dw_{k+1} \\
x_{k+2} &= \Phi^2 y_k - \Phi Am_k - Am_{k+1} + \Phi Bc_k + Bc_{k+1} + \Phi Dw_k + Dw_{k+1} + \Phi m_{k+1} \\
&\vdots \\
x_{k+i} &= \Phi^i y_k - (\Phi^{i-1}Am_k + \ldots + Am_{k+i-1}) + (\Phi^{i-1}Bc_k + \ldots + Bc_{k+i-1}) \\
&\quad + (\Phi^{i-1}Dw_k + \ldots + Dw_{k+i-1}) + (\Phi^{i-1}m_{k+1} + \ldots + \Phi m_{k+i-1}) \\
x_{k+i} &= \Phi^i y_k + (\Phi^{i-1}Bc_k + \ldots + Bc_{k+i-1}) + (\Phi^{i-1}Dw_k + \ldots + Dw_{k+i-1}) \\
&\quad - \Phi^{i-1}Am_k + (\Phi^{i-2}(\Phi - A)m_{k+1} + \ldots + (\Phi - A)m_{k+i-1})
\end{aligned}
\tag{3.4}
$$

This state prediction is similar to the prediction in Equation (2.6) except that there is an additional group of distribution functions m_k to m_{k+i-1} that represent the effects of the measurement error. Whereas in the previous method it was useful to decompose the state into nominal and stochastic components (2.7), that method is not applicable to a system with inaccurate measurements. The decomposition relies on the knowledge of the initial state ($z_k = x_k$), allowing the initial stochastic effects to be zero ($e_k = 0$), and therefore when the exact initial state measurement is unavailable, that assumption cannot be made and this decomposition does not provide any advantages.

3.2.2 Constraint Predictions

Again, the constraints must be taken over the whole of the prediction horizon:

$$
\begin{aligned}
&Pr(f^T u_k \leq h) \geq p \\
&Pr(f^T(Ky_k + c_k) \leq h) \geq p \\
&Pr(f^T(Ky_{k+i} + c_{k+i}) \leq h) \geq p \\
&Pr(f^T K(\Phi^i y_k + (\Phi^{i-1}Bc_k + \ldots + Bc_{k+i-1}) + (\Phi^{i-1}Dw_k + \ldots + Dw_{k+i-1}) \\
&+ (\Phi^{i-2}(\Phi - A)m_{k+1} + \ldots + (\Phi - A)m_{k+i-1}) + m_{k+i} - \Phi^{i-1}Am_k) \leq h) \geq p
\end{aligned}
\tag{3.5}
$$

It is useful to consider the various parts of this constraint definition to determine which parts are known, which are unknown, which can be considered stochastically, and which must be taken as the worst possible disturbance or error value.

The first term in the constraint is the $f^T K \Phi^i y_k$ term. Because y_k is the current measurement value, this is known at all times k. The sequence of disturbance distributions $f^T K(\Phi^{i-1} D w_k + \ldots + D w_{k+i-1})$ is unknown but can be treated the same as outlined in Section 2.2.2, by summing the distributions through the use of discretization and convolution. As in Chapter 2, the sequence of free control moves $f^T K(\Phi^{i-1} B c_k + \ldots + c_{k+i})$ is what informs the optimization. This leaves the effect of the measurement error as described by Expression 3.6:

$$f^T K(-\Phi^{i-1} A m_k + \Phi^{i-2}(\Phi - A) m_{k+1} + \ldots + (\Phi - A) m_{k+i-1} + m_{k+i}) \tag{3.6}$$

In determining how to consider these sequences, it is useful to break this sum into two parts: one part includes the terms that are prior to the implementation time (Expression 3.7a) and the other part includes the term that is current to implementation time (Expression 3.7b):

$$f^T K(-\Phi^{i-1} A m_k + \Phi^{i-2}(\Phi - A) m_{k+1} + \ldots + (\Phi - A) m_{k+i-1}) \tag{3.7a}$$

$$f^T K m_{k+i} \tag{3.7b}$$

In Expression 3.7a all the error terms are future to the prediction time (k) but prior to the time $k + i$ at which the control would be implemented. The prediction used to calculate the control input for time $k + 1$ is dependent upon m_k and m_{k+1}. Similarly, the prediction at $k+2$ is dependent upon m_k, m_{k+1}, and m_{k+2}, and so on. Because these error values will have already happened at the time the calculated control is implemented, it is possible that the measurement error would have been the worst case value. Therefore the maximum possible error must be considered.

Expression 3.7b is future to the prediciton time, but current with the implementation time. Because this term will not have already occured, it can be treated as a random variable rather than having to consider the worst case value.

3.3 Stochastic Tube Definition

The previously discussed treatment of the disturbances and errors will be used to determine their effect on the definition of the stochastic tube.

3.3.1 Disturbance Effects

The effects of the disturbances on the constraint definition are evaluated as described in Section 2.2.2 where, for each $i = 1, 2, \ldots$, γ_i is defined as the minimum value so that the following is true.

$$Pr(f^T K(\Phi^{i-1} D w_k + \ldots + D w_{k+i-1}) \leq \gamma_i) \geq p \tag{3.8}$$

However, as previously discussed, in order to ensure recursive feasibility, the constraint must be defined in terms of β_i where β_i is defined as follows:

$$f^T K \Phi^i z_k + f^T K \Phi^i e_k + f^T K \left[\Phi^{i-1} B \ldots \ B\right] \bar{c_k} \leq h - \beta_i \tag{3.9}$$

$$\beta = \begin{bmatrix} \gamma_1 & \gamma_2 & \gamma_3 & \gamma_4 & \cdots \\ 0 & \gamma_1 + a_1 & \gamma_2 + a_2 & \gamma_3 + a_3 & \cdots \\ 0 & 0 & \gamma_1 + a_1 + a_2 & \gamma_2 + a_2 + a_3 & \cdots \\ \vdots & \vdots & \vdots & \vdots & \ddots \end{bmatrix}$$

$$\beta_i = \text{maximum element of } i^{\text{th}} \text{column of } \beta$$

$$a_i = |f^T K \Phi^i D| w_{max}$$

3.3.2 Measurement Error Effects

The effects of the measurement errors on the constraint tubes, as discussed in Section 3.2.2 are calculated according to Equations (3.10a) - (3.10e). ι_i is defined as the constraint tightening factor that compensates for the measurement error current to the implementation time (m_{k+i}). μ_i and η_i are the constraint tightening factors that take the maximum possible error measurement value into consideration. These terms are combined into the overall constraint tightening factor ω_i which is used to ensure constraint satisfaction in the presence of measurement error for all times k through $k+i$.

$$Pr(f^T K m_{k+i} \leq \iota_i) \geq p \tag{3.10a}$$

$$\mu_i = |-f^T K \Phi^{i-1} A| m_{\max} \tag{3.10b}$$

$$\eta_1 = 0 \tag{3.10c}$$

$$\eta_i = |f^T K \Phi^{i-2}(\Phi - A)| m_{\max} \text{ for all } i > 1 \tag{3.10d}$$

$$\omega_i = \iota_i + \mu_i + \sum_{j=1}^{i} \eta_j \tag{3.10e}$$

These parameters are used to define the stochastic tube for the model predictive control law.

$$Pr(f^T K \Phi^i y_k + f^T K \begin{bmatrix} \Phi^{i-1} B \dots & I \end{bmatrix} \bar{c}_k \leq h - \beta_i - \omega_i) \geq p \tag{3.11}$$

3.3.3 Mode 2 Constraints

Equation (3.11) defines the constraint for mode 1 whereas the constraints in mode 2 are defined as discussed in Section 2.3.2. When considering the error measurement, S_∞ is defined as the set of all y_N so that the terminal constraint in Equation (3.12) holds for all j values if $y_N \in S_\infty$.

$$f^T K \Phi^j y_N \leq \beta_{N+j} \tag{3.12}$$

As described in Section 2.3.2, the β_i values will converge of a $\bar{\beta}$ limit that can be approximated and used to define the terminal constraint with a finite number of inequalities.

$$\bar{\beta} \leq \gamma_1 + \sum_{j=1}^{\nu-1} a_j + \frac{\rho^\nu}{1-\rho}||f^T K||_S \tag{3.13}$$

This holds for any non-negative integer ν, where the conditions in 3.14 hold true.

$$||f^T K||_S = \sqrt{K^T f S f^T K} \tag{3.14a}$$

$$\max_{w \in \Pi} ||Dw||_{S^{-1}} \leq 1 \tag{3.14b}$$

$$\Phi S \Phi^T \leq \rho^2 S, \quad \rho \in (0,1) \tag{3.14c}$$

Similarly to the β_i values, the ω_i values defined in Equation (3.10e) will converge on a limit of $\bar{\omega}$. For $i = 1, \dots, N+j$, ω_i takes the following form:

$$\begin{aligned}
\omega_1 &= (\Phi - A)m_k + m_{k+1} - Am_k \\
\omega_2 &= (\Phi - A)m_{k+1} + m_{k+2} - \Phi A m_k \\
\omega_3 &= \Phi(\Phi - A)m_{k+2} + (\Phi - A)m_{K+1} + m_{k+3} - \Phi^2 A m_k \\
&\vdots \\
\omega_{N+j} &= \sum_{i=2}^{N+j} \Phi^{i-2}(\Phi - A)m_{k+i-1} + m_{k+N+j} - \Phi^{N+j-1} m_k
\end{aligned}$$

The m values are evaluated as previously discussed, where the worst case error value is considered for all but the current m_{k+N+j} value. As $j \to \infty$, $\mu_{N+j} \to \infty$ and therefore, if j is large enough, this term can be eliminated from the definition of ω_{N+j}. Therefore the definition of ω_{N+j} becomes:

$$\omega_{N+j} = \iota_{N+j} + \sum_{i=2}^{N+j} \eta_i \tag{3.15}$$

This value will converge on $\bar{\omega}$ and after $\hat{N}$ this limit can be used to define the constraint:

$$\bar{\omega} \leq \iota_{\hat{N}} + \sum_{j=1}^{\nu_m - 1} \eta_j + \frac{\rho_m^{\nu_m}}{1-\rho_m} ||f^T K||_{Sm} \tag{3.16}$$

Again, ν_m, is any integer number where the conditions in 3.17 hold true:

$$||f^T K||_{S_m} = \sqrt{K^T f S_m f^T K} \tag{3.17a}$$

$$\max_{m \in \Pi} ||(\Phi - A)m||_{S_m^{-1}} \leq 1 \tag{3.17b}$$

$$\Phi S_m \Phi^T \leq \rho_m^2 S_m, \quad \rho_m \in (0,1) \tag{3.17c}$$

The terminal constraint for use in mode 2 takes the form of Equation (3.18):

$$\begin{cases} f^T K \Phi^j y_N \leq h - \beta_{N+j} - \omega_{N+j} & \text{if } j = N, \ldots, \hat{N} \\ f^T K \Phi^j y_N \leq h - \bar{\beta} - \bar{\omega} & \text{if } j = \hat{N}+1, \ldots \hat{N} + n^* \end{cases} \tag{3.18}$$

The constraints for both modes are then defined as seen in Equation (3.19):

$$\begin{cases} f^T K \Phi^i y_k + f^T K \left[\Phi^{i-1} B \ldots \; B\right] \bar{c_k} \leq h - \beta_i - \omega_i & \text{if } i = 1, \ldots, N-1 \\ f^T K \Phi^j y_N \leq h - \beta_{N+j} - \omega_{N+j} & \text{if } j = N, \ldots, \hat{N} \\ f^T K \Phi^j y_N \leq h - \bar{\beta} - \bar{\omega} & \text{if } j = \hat{N}+1, \ldots \hat{N} + n^* \end{cases} \tag{3.19}$$

3.4 Optimization Policy

The cost function that is optimized for this control problem is shown in Equation (3.20):

$$J = \sum_{k=0}^{\infty} \mathbb{E}(x_k^T Q x_k + u_k^T R u_k) \tag{3.20}$$

As was done with the system in Chapter 2, the system with measurement error can take an augmented form:

$$\chi_{k+1} = \begin{bmatrix} \Phi & BE & (\Phi - A)m_k + Dw_k \\ 0 & M & 0 \\ 0 & 0 & 1 \end{bmatrix} \chi_k = \Psi \chi_k \tag{3.21}$$

$$\tilde{\Psi} = \begin{bmatrix} \Phi & BE \\ 0 & M \end{bmatrix} \tag{3.22}$$

Again, the cost can be written in quadratic form in terms of χ and P. However, because of the inlusion of the error measurements, the P_{22} term is defined differently. For baseline MPC, the P_{22} was defined in terms of Θ which was defined as the solution to $\Theta - \tilde{\Psi}\Theta\tilde{\Psi}^T = DD^T\Sigma$. However, with the inclusion of the measurement error, this definition of Θ changes to:

$$\mathbb{E}(V_k) = \chi_k^T P \chi_k \tag{3.23a}$$

$$P_{11} - \tilde{\Psi}^T P_{11} \tilde{\Psi} = \tilde{Q} \tag{3.23b}$$

$$P_{22} = -\mathrm{trace}(\Theta P_{11}) \tag{3.23c}$$

$$\begin{aligned} \Theta - \tilde{\Psi}\Theta\tilde{\Psi}i^T =& ((\Phi^T\Phi - \Phi^T A - A^T\Phi + A^T A)\mathbb{E}(m_i m_i^T) \\ &+ 2(\Phi^T D - A^T D)\mathbb{E}(w_i m_i^T) + D^T D\mathbb{E}(w_i w_i^T) \\ \Theta - \tilde{\Psi}\Theta\tilde{\Psi}^T =& (\Phi^T\Phi - \Phi^T A - A^T\Phi + A^T A)\Sigma + D^T D\Sigma \end{aligned} \tag{3.23d}$$

3.5 Simulation Results

Using the system model described in Section 2.5, simulations were carried out to demonstrate the effectiveness of the modification to the model predictive control law introduced in this chapter. The measurement error now included in the system model is zero mean, standard deviation $\sigma = \frac{1}{100}$, independently and identically distributed, and has a truncated normal distribution where $|m_k| \leq .1$. To provide meaningful comparisons, this method was contrasted with the baseline MPC method described in Chapter 2, with slight modifications. The optimization in Chapter 2 was carrried out under the assumption that the state measurement was reliable. However, this is not the case, and therefore in order to compare this with the MPC with error consideration method, an error was added to the state value used for the optimization and state predictions in the baseline MPC method. This error had the same distribution as the measurement error described in this chapter.

Figure 3.1 shows the mean state response for 200 realizations of disturbances and errors and Figure 3.2 shows the convergence of the states towards the origin.

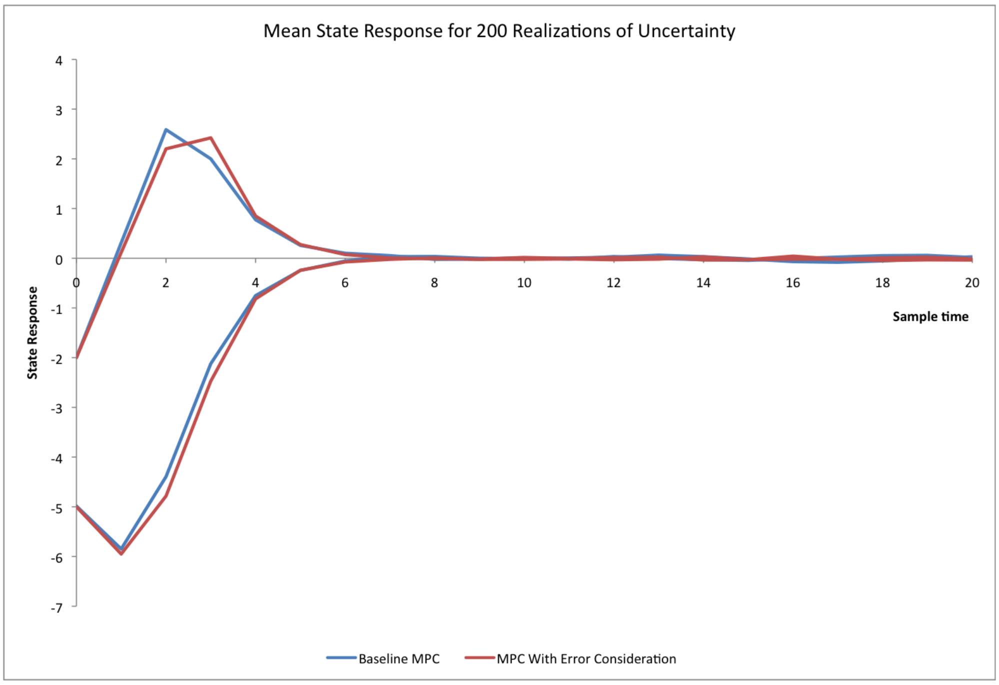

Figure 3.1: Mean state response for 200 realizations of uncertainty for baseline MPC and MPC with error consideration

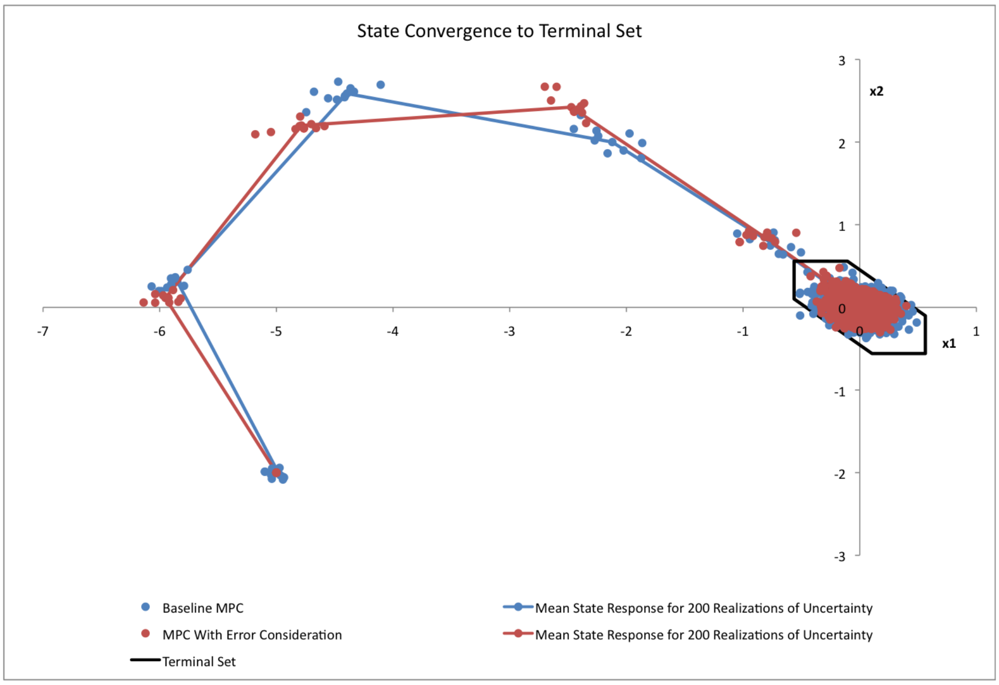

Figure 3.2: State convergence for 10 realizations of uncertainty for baseline MPC and MPC with error consideration

Figure 3.3 shows the mean calculated input for 200 realizations of disturbances and errors.

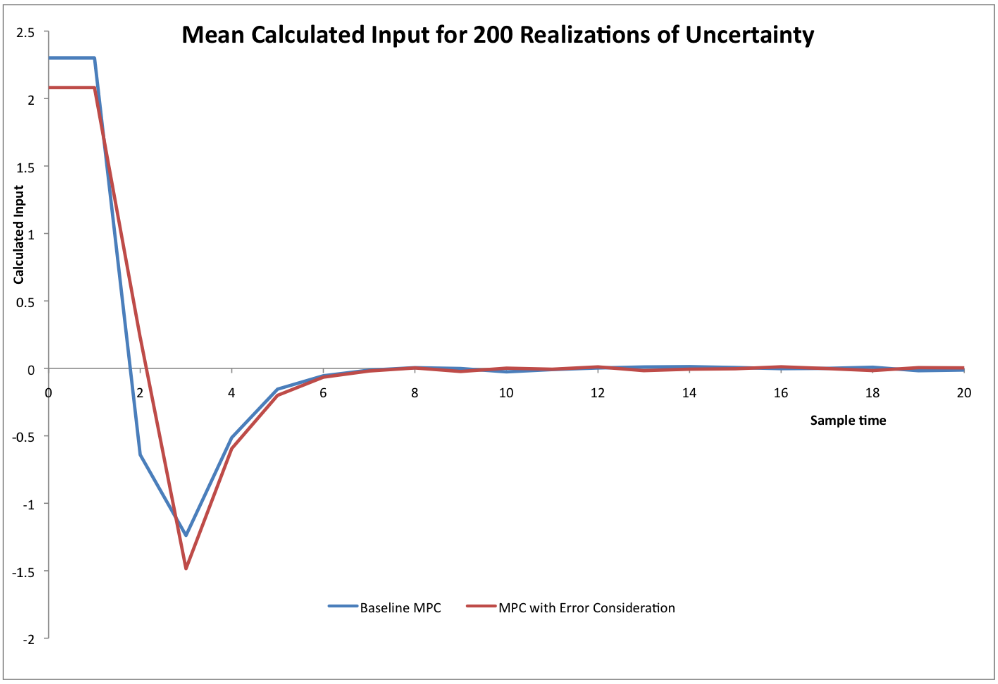

Figure 3.3: Average control input required for 200 realizations of uncertainty for baseline MPC and MPC with error consideration

Because the MPC with error consideration method takes into account the measurement error in the constraint definition, the control authority available is lower. This is demonstrated in Figure 3.3 and allows the baseline MPC control input to converge on zero slightly faster than the MPC with error consideration method.

3.5.1 Cost and Constraint Violation

Table 3.1 shows the comparison between the average costs, the maximum costs, and the percentage of constraint violation for these two methods for 200 realizations of disturbances and measurement error.

Table 3.1: Comparison of Cost for 200 Realizations of Uncertainty for Baseline MPC and MPC with Error Consideration methods

Method	Average Cost	Maximum Cost	% Constraint Violation
Baseline MPC	105.1438	113.1583	34%
MPC with Error Consideration	111.1210	120.4713	20%

These simulation results are as expected. Because the MPC with error consideration includes additional constraint tightening factors related to the measurement error, the constraints are more stringent. The baseline MPC therefore has more control authority available, thereby resulting in a lower cost. Because the error is not considered in the constraint definition for the baseline MPC method, the presence of error in the measurements causes the percentage of constraint violation to increase significantly. While the cost is greater for the MPC with error consideration method, the sacrifice in cost is not excessive, especially when considering the percentage of constraint violation in the baseline MPC method. When both measurement error and disturbances are present in the system, the method of constraint definition described in this chapter should be used to ensure both control and constraint satisfaction.

3.5.2 Response in Mode 2

It is interesting to examine the response of the system in mode 2 to investigate the behaviour of the system under the stabilizing control law. During mode 2 operation, both methods make use of unconstrained linear quadratic regulator control. In the baseline MPC method the state progression takes the following form:

$$x_{k+1} = Ax_k + B(Kx_k) + Dw_k$$

However, while the controller assumes the measurement of x_k used to calculate Kx_k is accurate, it exhibits error, which must be included into the state prediction as follows:

$$x_{k+1} = Ax_k + BK(x_k + m_k) + Dw_k$$
$$x_{k+1} = \Phi x_k + BKm_k + Dw_k$$

For the MPC with error consideration method described in Chapter 3, the state prediction is as follows, using the measurement value y_k to calculate the control input:

$$x_{k+1} = Ax_k + B(Ky_k) + Dw_k$$

$$x_{k+1} = Ax_k + BKx_k + BKm_k + Dw_k$$

$$x_{k+1} = \Phi x_k + BKm_k + Dw_k$$

These methods have the same dynamics in mode 2 and will therefore exhibit the same state response during mode 2 operation.

Chapter 4

Stochastic Model Predictive Control with Estimation

Considering the measurement errors in the construction of the probabilistic tubes for stochastic model predictive control is one way to control systems subject to stochastic disturbances and measurement errors. There also exist methods of control that are used for systems for which a state measurement is unavailable; these methods estimate the state through the use of an observer. It is useful to investigate if state estimation would result in better control of systems with measurement errors than the method introduced in Chapter 3. The following discussion summarizes a method of stochastic tube model predictive control with state estimation described by Cannon et al in [Cannon et al., 2012]. This method will, from hereafter, be referred to as "MPC with estimation."

4.1 System and Observer Dynamics and Predictions

The system takes the form of Equations (4.1a) and (4.1b):

$$x_{k+1} = Ax_k + Bu_k + Dw_k \tag{4.1a}$$

$$y_k = Cx_k + m_k \tag{4.1b}$$

The included linear observer has the dynamics shown in Equations (4.2a) and 4.2b:

$$\hat{x}_{k+1} = A\hat{x}_k + Bu_k + L(y_{k+1} - \hat{y}_{k+1}) \tag{4.2a}$$

$$\hat{y}_k = C\hat{x}_k \tag{4.2b}$$

In Equations (4.2a) and (4.2b), $\hat{x}_k$ is the state estimate and the observer gain L is chosen so that $A - LCA$ is strictly stable. Subtracting Equation (4.2a) from Equation (4.1a) (where $\epsilon = x_k - \hat{x}_k$) yields the following error dynamics:

$$\epsilon_{k+1} = (A - LCA)\epsilon_k + (I - LCA)Dw_k - Lm_{k+1} \tag{4.3}$$

With the estimator it is necessary to predict both the state estimate and the estimation error; the predicted state estimate and error sequences at k are $\{\hat{x}_{k+i|k}, \epsilon_{k+i|k},\ i = 0, 1, \ldots\}$. The closed loop paradigm and an augmented state representation are used for the predictions as per Equations (4.4a) and (4.4b). In these equations, let $\xi_{k+i} = (\hat{x}_{k+i}, \epsilon_{k+i}) \in \mathbb{R}^{2n}$ whereas $\delta_{k+i|k} = (w_{k+i|k}, m_{k+i|k}) \in \mathbb{R}^{n_w+n_m}$ is a stochastic disturbance:

$$\xi_{k+i+1|k} = \Psi\xi_{k+i|k} + \tilde{B}c_{k+i|k} + \tilde{D}\delta_{k+i|k} \tag{4.4a}$$

$$u_{k+i|k} = K\hat{x}_{k+i|k} + c_{k+i|k} \tag{4.4b}$$

$$\Psi = \begin{bmatrix} A + BK & L \\ 0 & A - LCA \end{bmatrix}$$

$$\tilde{B} = \begin{bmatrix} B \\ 0 \end{bmatrix}$$

$$\tilde{D} = \begin{bmatrix} 0 & I - L \\ D & -L \end{bmatrix}$$

In this formulation, the initial estimation error ϵ_0 is assumed to be a random variable with a known and compactly supported distribution. Given the assumptions on the disturbances and estimate errors, the distribution of δ_k is compactly supported and, for all k, $\delta \in \Delta$ where Δ is an orthotope in $\mathbb{R}^{n_w+n_m}$.

As was discussed in Section 2.2.1, the state prediction is split into nominal and uncertain elements. For the initial nominal part the stochastic element is taken to be zero, whereas for the first uncertain element the state estimate is taken as zero. This results in the following series of equations [Cannon et al., 2012]:

$$
\begin{aligned}
\xi_{k+i|k} &= z_{k+i|k} + e_{k+i|k} \\
z_{k+i+1|k} &= \Psi z_{k+i|k} + \tilde{B} c_{k+i|k} \\
e_{k+i+1|k} &= \Psi e_{k+i|k} + \tilde{D} \delta_{k+i|k} \\
z_{k|k} &= (\hat{x}_k, 0) \\
e_{k|k} &= (0, \epsilon_k)
\end{aligned}
$$

4.2 Constraints and Tube Definition

As before, the system is subject to soft input constraints. These constraints take the form of Equation (4.5):

$$\Pr([f^T\ 0]K\xi_{k+i|k} + f^T c_{k+i|k} \leq h) \geq p \tag{4.5}$$

Following the same steps as discussed in Chapter 2, conditions are developed that ensure the constraints are satisfied despite the presence of disturbances and measurement errors. At time k, the constraints are satisfied by the state and error predictions if and only if Equation (4.6) is true, where $\bar{c} = [c_k, c_{k+1}, \ldots, c_{k+N-1}]$:

$$[f^T\ 0]K\Psi^i z_{k|k} + ([f^T\ 0]KH_i + f^T E_i)\bar{c}_k \leq h - \hat{\gamma}_i \tag{4.6}$$

$$
\begin{aligned}
H_i &= \left[\Psi^{i-1}\tilde{B} \ldots\ \tilde{B}\ \ 0 \ldots 0\right] \\
E_i \bar{c}_k &= c_{k+i|k}
\end{aligned}
$$

The sequence of $\hat{\gamma}_{i|k}$ values are defined for each k and $i = 0, 1, \ldots$ as the minimum value such that Equations (4.7a) and (4.7b) are true:

$$\Pr([f^T \ 0]Ke_{k|k} \leq \hat{\gamma}_{0|k}) = p \tag{4.7a}$$

$$\Pr([f^T \ 0]K(\Psi^i e_{k|k} + \Psi^{i-1}\tilde{D}\delta_{k|k} + \ldots + \tilde{D}\delta_{k+i-1|k}) \leq \hat{\gamma}_{i|k}) = p \tag{4.7b}$$

The probability distribution of the sum of the disturbance values in 4.7b can be found as earlier described in Section 2.2.2, by discretizing the distributions of δ and ϵ_0 and approximating the sum by performing discrete convolutions.

4.2.1 Ensuring Recursive Feasibility

As previously discussed in Section 2.3.1, the conditions in Equation (4.6) ensure that the constraints are satisfied over the whole prediction horizon at time k but they do not ensure the existence of a $\bar{c}_{k+1}$ that generates predictions at time $k+1$ that satisfy the constraints. $\hat{\gamma}_{i|k}$ defines the probabilistic bound on the stochastic components for the predictions at time k but the bound for the predictions at time $k+i$, on the basis of information available at time k, could take the maximum possible value for all possible realizations of the estimation error e_k and disturbance δ_k at time k. Therefore, in order to ensure recursive feasibility, the worst case values for e_{k+1} and δ_{k+1} must be included in the definition of the tube. To ensure recursive feasibility, we define γ_i to be the minimum value such that Equation (4.8) holds true:

$$\Pr([f^T \ 0]K(\Psi^{i-1}\tilde{D}\delta_{k|k} + \ldots + \tilde{D}\delta_{k+i-1|k}) \leq \gamma_{i|k}) = p \tag{4.8}$$

We also define the following parameters which factor in the worst possible error and disturbance values and will be used to define the new bounds for the stochastic tube:

$$d_i = \max_{\delta \in \Delta} [f^T \ 0]K\Psi^{i-1}\tilde{D}\delta \tag{4.9a}$$

$$\alpha_{i|k} = \max_{e_{k|k} \in \mathcal{D}} [f^T \ 0]K\Psi^i e_{k|k} \tag{4.9b}$$

Using these parameters, recursive feasibility is ensured if $\bar{c}_k$ satisfies Equation (4.10):

$$[f^T \; 0]K\Psi^i z_{k|k} + ([f^T \; 0]KH_i + f^T E_i)\bar{c_k} \leq h - \beta_{i|k} \tag{4.10}$$

$$\beta_{i|k} = \text{maximum element of}(i+1)^{th}\text{column of}\mathcal{B}_k$$

$$\mathcal{B}_k = \begin{bmatrix} \hat{\gamma}_{0|k} & \hat{\gamma}_{1|k} & \hat{\gamma}_{2|k} & \cdots \\ 0 & \alpha_{1|k} + d_1 + \gamma_0 & \alpha_{2|k} + d_2 + \gamma_1 & \cdots \\ 0 & 0 & \alpha_{2|k} + d_2 + d_1 + \gamma_0 & \cdots \\ \vdots & \vdots & \vdots & \ddots \end{bmatrix}$$

From the above definitions of d_i and $\alpha_{i|k}$ it can be shown that for all $i \geq 1$, $\beta_{i|k} = \alpha_{i|k} + \sum_{j=1}^{i} d_j + \gamma_0$ [Cannon et al., 2012].

4.3 Dual Mode Prediction

As previously, in order to ensure the constraints are met over the entirety of the prediction horizon it is useful to use a dual-mode prediction strategy. A terminal set is again used to ensure constraint satisfaction in Mode 2. Because e_k and $\{\delta_k, \delta_{k+1} \ldots\}$ are bounded and Ψ is strictly stable, the predicted sequence of estimation error $\{e_{k|k}, e_{k+1|k}, \ldots\}$ and $\{\beta_{0|k}, \beta_{1|k}, \ldots\}$ are also bounded. In order to compute the bound of $\beta_{i|k}$ that allows for the use of a finite number of constraints in mode 2, several parameters need to be determined.

First of all, a symmetric positive definite matrix $S \in \mathbb{R}^{2n \times 2n}$ and scalar $\rho \in (0, 1)$ are defined as the solution to the following semidefinite program:

$$(\rho, S) = \arg \min_{\rho > 0 \; S = S^T \geq 0} \rho$$

$$\text{subject to } \Psi S \Psi^T \leq \rho^2 S$$

$$\begin{bmatrix} 1 & \tilde{D}\delta \\ \delta^T \tilde{D} & S \end{bmatrix} \succ 0 \text{ for all } \delta \in \Delta$$

Next, an ellipsoidal set is defined as $\mathcal{E} = \{e : ||e||_{S^{-1}} \leq 1\}$ where $||e||_{S^{-1}} = \sqrt{e^T S^{-1} e}$.

Let $\mathcal{E}_\epsilon$ be the projection of $\mathcal{E}$ onto the subspace $\{e \in \mathbb{R}^{2n} : [I_n 0]e = 0\}$ so that $\mathcal{E}_\epsilon = \{\epsilon : \epsilon^T S_{22}^{-1}\epsilon \leq 1\}$ and S_{22} is the relevant block of $S = \begin{bmatrix} S_{11} & S_{12} \\ S_{21} & S_{22} \end{bmatrix}$.

The next two positive scalars defined are τ and σ:

$$\tau = \max_{e_0 \sim \mathcal{D}_0} \|e_0\|_{S^{-1}} = \max_{\epsilon_0 \in \Pi_0} \left\| \begin{bmatrix} 0 \\ \epsilon \end{bmatrix} \right\|_{S^{-1}} \tag{4.11a}$$

$$\sigma = \max_{\epsilon \in \mathcal{E}} \left\| \begin{bmatrix} 0 \\ \epsilon \end{bmatrix} \right\|_{S^{-1}} = \bar{\lambda}(S_{22}^{1/2}[0\ I]S^{-1}[0\ I]^T S_{22}^{1/2}) \tag{4.11b}$$

Define ν as the positive number of time steps after which the transient response, due to initial estimation error, of the plant and observer is negligible. Using this ν, the following can be said about $\beta_{i|k}$ (where initial estimate error $e_0 \in \mathcal{D}_0$):

$$\beta_{i|k} = \sum_{j=1}^{i} d_j + \sum_{j=1}^{k} b_{ij} + a_{ik} + \gamma_0, \quad 1 \leq i < \nu, \quad k < \nu \tag{4.12a}$$

$$\beta_{i|k} \leq \bar{\beta}_{i|\nu} = \sum_{j=1}^{i} d_j + \sum_{j=1}^{\nu-i} b_{ij} + \bar{\alpha} + \gamma_0, \quad 1 \leq i < \nu, \quad k \geq \nu \tag{4.12b}$$

$$\beta_{i|k} \leq \bar{\beta} = \sum_{j=1}^{\nu} d_j + \bar{\alpha} + \gamma_0, \quad i > \nu \tag{4.12c}$$

$$b_{ij} = \max_{\delta \in \Delta}[f^T\ 0]K\Psi^i G \Psi^{j-1}\tilde{D}\delta$$

$$a_{ik} = \max_{e_0 \in \mathcal{D}_0}[f^T\ 0]K\Psi^i G \Psi^k e_0$$

$$G = \begin{bmatrix} 0 & 0 \\ 0 & I \end{bmatrix}$$

$$\bar{\alpha} = \rho^\nu \sigma(\frac{1}{1-\rho} + \tau)||[f^T\ 0]K||_S$$

The preceding equations and expressions allow for the calculation of the following parameters, all of which can be done offline, and which will be used to define the constraints and stochastic tubes for the stochastic model predictive control:

$$\begin{aligned}&\gamma_0,\ \ \{\hat{\gamma}_{0|k}, k=0,\dots,\nu-1\},\ \ \{d_j,\ \ j=1,\dots,\nu\},\\ &\{b_{ij},\ \ j=1,\dots,\nu-1\},\ \ \{a_{ij},\ \ j=1,\dots,\nu-1\},\ \ \bar{\alpha}\end{aligned} \tag{4.13}$$

4.3.1 Mode 2 Constraint

As described in Chapter 2, the constraints are met in mode 2 through the use of a terminal set. This set $S_{\infty|k}$ is the set of real numbers containing all $z_{k+N|k}$ such that Equation (4.14) is true:

$$[f^T\ 0]K\Psi^j z_{k+N|k} \leq h - \beta_{N+j|k} \tag{4.14}$$

For $k < \nu$ equation 4.15 defines a terminal set $S_{\nu|k}$:

$$S_{\nu|k} = \begin{cases} [f^T\ 0]K\Psi^{i-N}z \leq h - \beta_{i|k} & i = N,\dots,\nu-1 \\ [f^T\ 0]K\Psi^{i-N}z \leq h - \bar{\beta} & i = \nu,\nu+1\dots, \end{cases} \tag{4.15}$$

This set $S_{\nu|k} \subseteq S_{\infty|k}$ and there exists an N_k^* such that $S_{\nu|k}$ can be defined using a finite set of inequalities:

$$S_{\nu|k} = \begin{cases} [f^T\ 0]K\Psi^{i-N}z \leq h - \beta_{i|k} & i = N,\dots,\nu-1 \\ [f^T\ 0]K\Psi^{i-N}z \leq h - \bar{\beta} & i = \nu,\dots,\nu+N_k^* \end{cases} \tag{4.16}$$

For times $k \geq \nu$, Equation (4.17) defines a time invariant set $S_{\nu|k} = S_\nu$:

$$S_{\nu} = \begin{cases} [f^T\ 0]K\Psi^{i-N}z \leq h - \bar{\beta}_{i|\nu} & i = N,\dots,\nu-1 \\ [f^T\ 0]K\Psi^{i-N}z \leq h - \bar{\beta} & i = \nu,\dots,\nu+N_v^* \end{cases} \tag{4.17}$$

Therefore a finite collection of terminal sets $S_{\nu|k}$ for $k = 0,1,\dots,\nu-1$ and S_ν for

$k \geq \nu$ can be used to invoke the constraints in mode 2 [Cannon et al., 2012].

4.4 Optimization Policy

The cost function to be minimized is defined in Equation (4.18):

$$\tilde{J}_k = \sum_{i=1}^{\infty} \mathbb{E}(x_{k+i|k}^T Q x_{k+i|k} + u_{k+i|k}^T R u_{k+i|k}^T) \tag{4.18}$$

However, considering the presence of additive disturbance, this cost will converge on a non-zero limit which must be subtracted from the steady state cost:

$$\tilde{J}_k = \sum_{i=1}^{\infty} \mathbb{E}(x_{k+i|k}^T Q x_{k+i|k} + u_{k+i|k}^T R u_{k+i|k}^T) - l_{ss} \tag{4.19}$$

Given the distribution of δ, the cost can be expressed in quadratic form in $\bar{c}$:

$$\tilde{J}_k(\bar{c}_k) = \bar{c}_k^T P_{cc} \bar{c}_k + 2\hat{x}_k^T P_{xc}^T \bar{c}_k + p_k(\hat{x}_k) \tag{4.20}$$

In Equation (4.20), $P_{cc} \in \mathbb{R}^{Nn_u \times Nn_u}$,$P_{xc} \in \mathbb{R}^{n \times Nn_u}$ are computed offline and $p_k(\hat{x})$ is independent of $\bar{c}_k$.

The algorithm for this estimation method has offline and online requirements. Offline, the distributions of the estimation error and disturbances are used to compute the parameters in Equation (4.13), as well as the parameter N_k^*. Then online, at each time $k = 0, 1, \ldots$, a state estimate $\hat{x}_k$ is computed and then used so that $z_{k|k} = (\hat{x}_k, 0)$. Then, the cost in Equation (4.20) is used to solve the quadratic program in Equation (4.21) to determine the optimal vector of free control moves.

$$\bar{c_k} = \arg\min_{\bar{c}_k} \tilde{J}(\bar{c}_k) \tag{4.21}$$

This is subject to the following constraints:

$$[f^T K\ 0]\Psi^i z_{k|k} + [f^T K\ 0]H_i + f^T E_i \bar{c}_k \leq h - \beta i, \quad i = 0, 1, \ldots, N-1$$
$$z_{k+N|k} \in S_k$$

where $\begin{cases} \beta_i = \beta_{i|k} \text{ and } S_k = S_{\nu|k} & \text{if } k < \nu \\ \beta_i = \bar{\beta}_{i|\nu} \text{ and } S_k = S_\nu & \text{if } k \geq \nu \end{cases}$

Then the optimal input is calculated as $u_k = K\hat{x}_{k+i|k} + c_{k|k}$. This process is then repeated for each time $k \geq 0$ [Cannon et al., 2012].

4.5 Simulation Results

Using the model described for the simulations in Chapter 2 and Chapter 3, and including $C = I$, a simulation of the MPC with estimation method was completed. In this simulation, the initial state estimate is constant at $\hat{x}_0 = [-5; -2]^T$ but the initial state value is taken to be $x_0 = \hat{x}_0 + \epsilon_0$ where the initial state estimate uncertainty has the same distribution as the measurement error described in Chapter 3 and therefore $|\epsilon_0| \leq .1$ and $\sigma = \frac{1}{100}$. Also used for comparison in this simulation is the baseline MPC method described in Chapter 2, but exhibiting the additional uncertainty described in Section 3.5. Figure 4.1 shows the mean state response (again for 200 realizations of uncertainty) of the MPC with estimation method and the baseline MPC method. Figure 4.2 shows the convergence of the states to the region of the origin for both these methods.

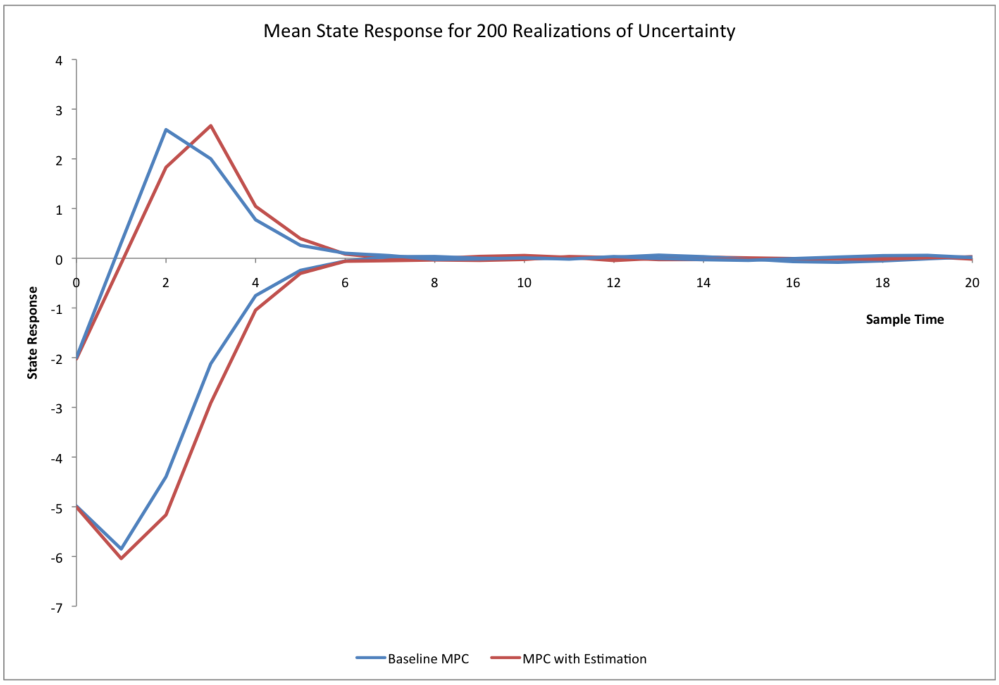

Figure 4.1: Mean state response for 200 realizations of uncertainty for baseline MPC and MPC with estimation

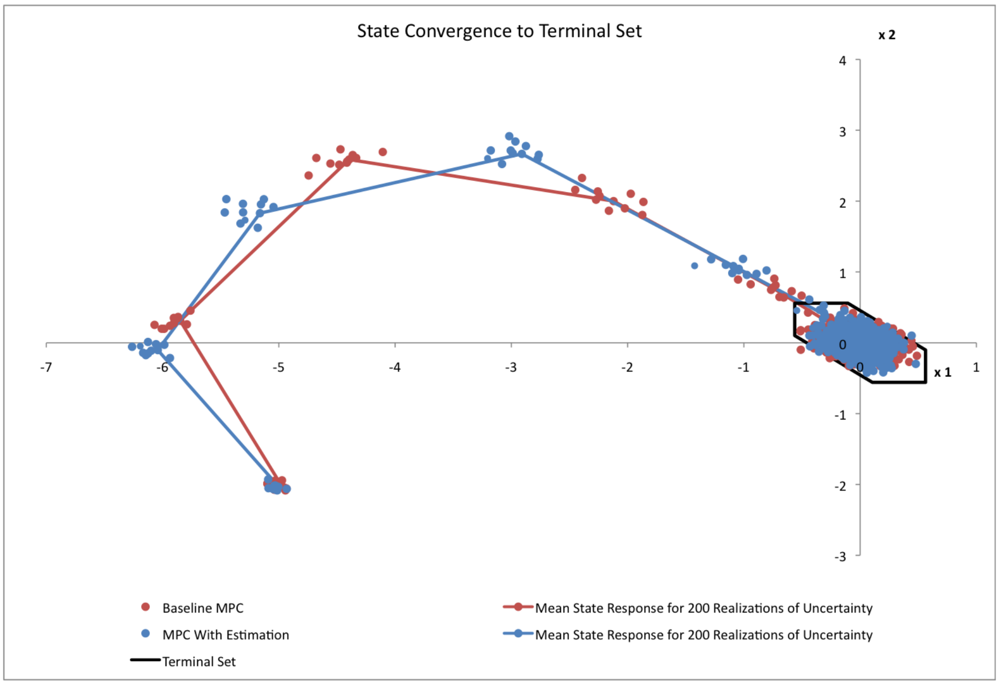

Figure 4.2: State convergence for 10 realizations of uncertainty for baseline MPC and MPC with estimation

Figure 4.3 shows the mean calculated input for 200 realizations of disturbances and errors.

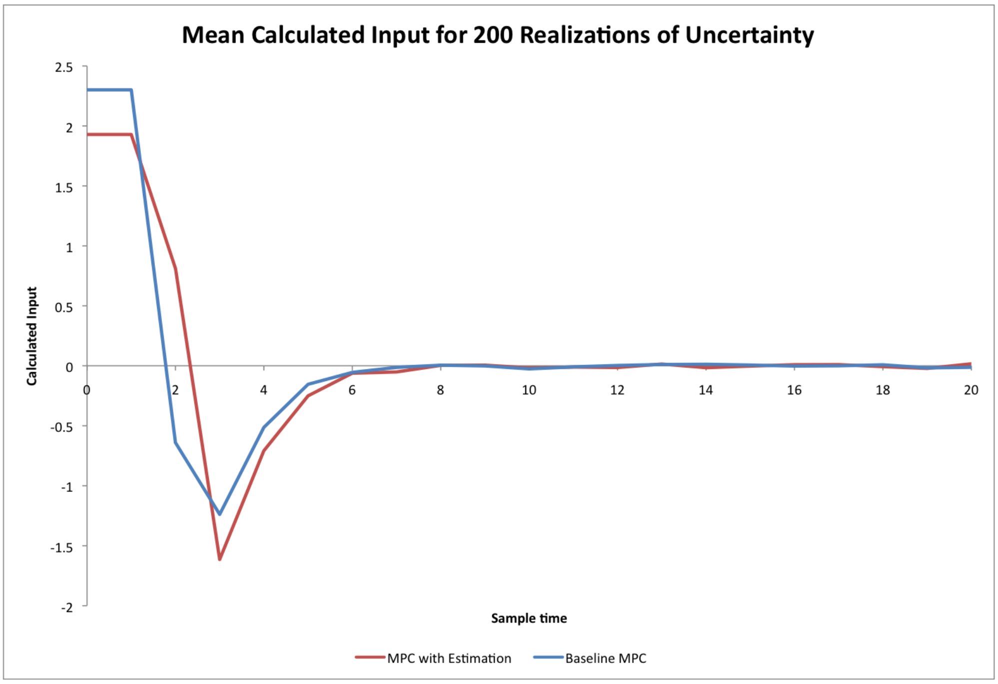

Figure 4.3: Average control input required for 200 realizations of uncertainty for baseline MPC and MPC with estimation

4.5.1 Cost and Constraint Violation

Table 4.1 shows a comparison of the costs of these two methods. While the MPC with estimation method has better convergence properties and constraint satisfaction, the baseline MPC method has a lower cost over the 200 realizations of uncertainty.

Table 4.1: Comparison of Cost for 200 Realizations of Uncertainty for Model Predictive Control and Estimator Methods

Method	Average Cost	Maximum Cost	% Constraint Violation
MPC without Error Consideration	105.1438	113.1583	34%
MPC with State Estimation	118.7211	129.5547	20%

Similar to the comparison in Section 3.5.1, while the MPC with estimation method exhibits a higher cost than the baseline MPC method, the lack of consideration of the measurement errors leads to a constraint violation greater than the required 20% in the latter method. Once again, the increase in cost for the MPC with estimation method is explained by the additional constraint tightening factors used in the tube definition. The increase in cost is offset by the fact that the MPC with estimation method meets the probabilistic constraint whereas the baseline MPC method fails to do so. If measurement errors are present, but not factored into the definition of the constraints in stochastic model predictive control, it is preferable to use estimation in the control scheme.

4.5.2 Response in Mode 2

As was done in Section 3.5.2, the dynamics of two methods in mode 2 were compared. In mode 2, the state prediction for the MPC with estimation method is as follows:

$$x_{k+1} = Ax_k + B(K\hat{x}_k) + Dw_k$$
$$x_{k+1} = Ax_k + BKx_k + BK\epsilon_k + Dw_k$$
$$x_{k+1} = \Phi x_k + BK\epsilon_k + Dw_k$$

If the distribution of the estimation error (ϵ) is the same as the distribution of the measurement errors (m_k), then the state response of the two methods in mode 2 is identical.

4.6 Comparison of MPC with Error Consideration and MPC with Estimation Methods

Now that several methods for handling systems subject to stochastic disturbances and exhibiting stochastic error in the measurements are available, the next step is to compare the results of the methods and determine which method will be the most applicable to control of FalconSAT-5.

The baseline model predictive control method was compared with two methods that attempt to handle the uncertainty and was shown through the simulations results in Sections 3.5 and 4.5 to be have a better cost than the MPC with error consideration and MPC with estimation methods. However, because this method violated the probabilistic constraints, it is not an effective method for control of a system exhibiting measurement errors. The next step is to compare the MPC with error consideration and MPC with estimation methods to determine which is a more effective method for controlling systems with measurement error. Figure 4.4 shows the mean state response for 200 realizations of the uncertainty for the MPC with error consideration and MPC with estimation methods. Figure 4.5 shows the convergence of the state to the terminal set for these two methods. Finally, 4.6 compares the mean calculated input for 200 realizations of disturbances and errors for the MPC with estimation and MPC with error consideration methods.

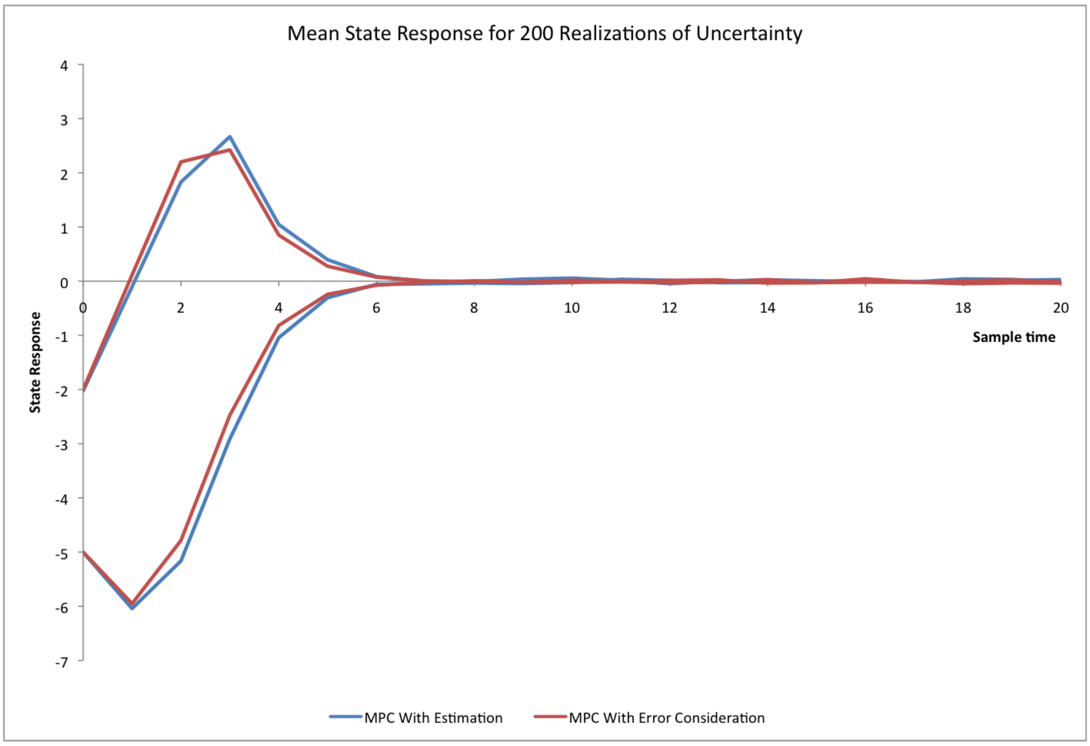

Figure 4.4: Mean state response for 200 realizations of uncertainty for MPC with error consideration and MPC with estimation

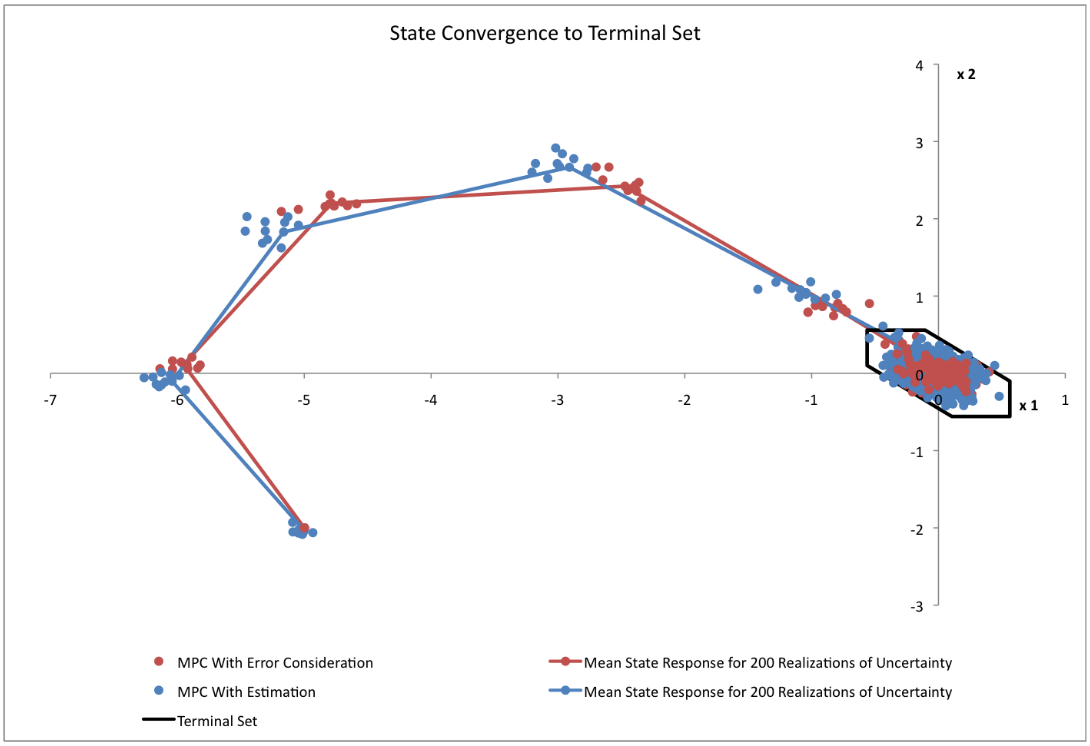

Figure 4.5: State convergence for MPC with error consideration and MPC with estimation

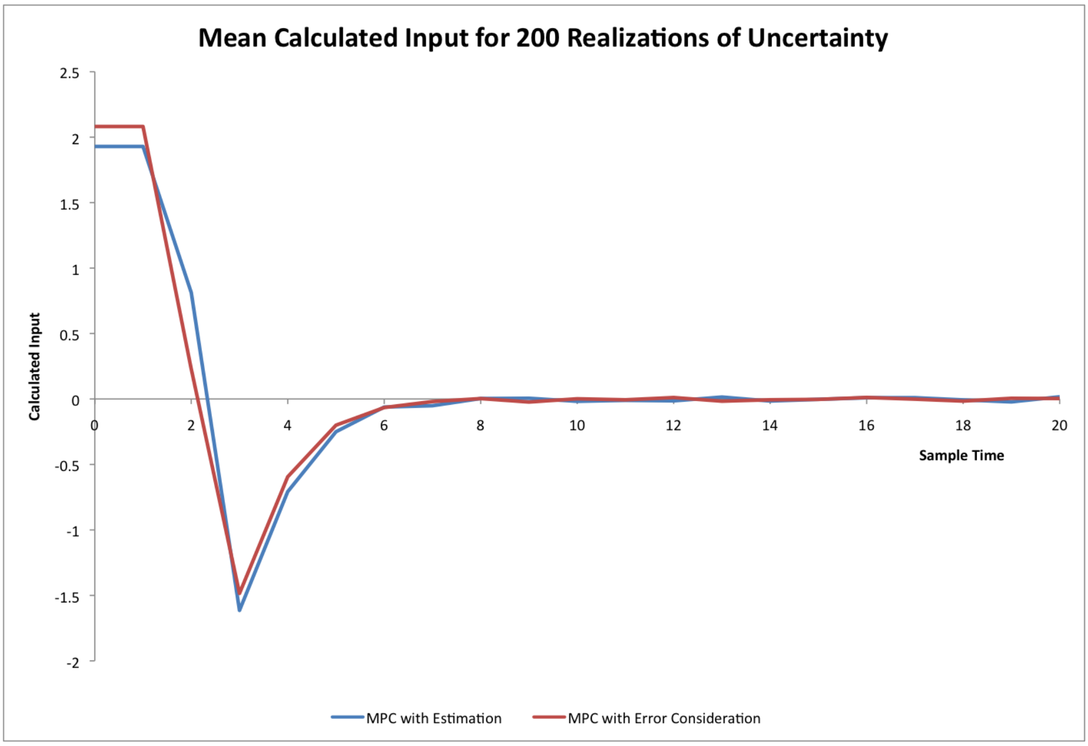

Figure 4.6: Average control input required for 200 realizations of uncertainty for MPC with estimation and MPC withe error consideration

4.6.1 Cost Comparison

Table 4.2 shows a comparison of the costs for these two methods. As seen in the table, the method of measurement error consideration has a lower average cost for 200 realizations of uncertainty.

Table 4.2: Comparison of Cost for 200 Realizations of Uncertainty for MPC with Error Consideration and MPC with Estimation

Control Method	Average Cost	Maximum Cost
MPC with Estimation	118.7211	129.5547
MPC with Error Consideration	111.1210	120.4713

In terms of cost, the MPC with error consideration is superior to the MPC with estimation method. However, this is for the specific example defined in Section 2.5 and it is therefore useful to consider conditions in which the estimator method exhibits superior performance. If the measurement error is sufficiently large, it is possible that the method that considers this error would provide worse performance than the estimator method or may be unable to provide a feasible solution at all.

Table 4.3 shows how changing the relative sizes of the disturbances and measurement errors can change which method will be most effective for controlling systems that exhibit both stochastic disturbances and stochastic measurement error. As demonstrated in the simulations and shown in the table, when the measurement error value is increased, the effect is greater on the cost of the MPC with error consideration method that considers this value in the constraint definition. This is reasonable because, for the MPC with error consideration method, the worst case error value is considered at all times apart from the implementation time. For the MPC with estimation method, the initial estimation error is assumed to be zero and the worst case estimation error is only considered for the implementation time in order to ensure recursive feasibility. Because of this, the estimation error has a greater effect on the performance of the MPC with error consideration and if the measurement errors are significantly larger than the disturbances, the performance of the MPC with error consideration method will be inferior to the MPC with estimation method.

Table 4.3: Cost Comparison Based on Varying Disturbance and Error Values

Dist/Unc Values	MPC with Estimation	MPC with Error Consideration
$\lvert Dw_k \rvert \leq .1$ $\lvert m_k \rvert \leq .1$	118.7211	111.1210
$\lvert Dw_k \rvert \leq .5$ $\lvert m_k \rvert \leq .1$	Infeasible	208.1406
$\lvert Dw_k \rvert \leq .1$ $\lvert m_k \rvert \leq .5$	214.1966	Infeasible
$\lvert Dw_k \rvert \leq .1$ $\lvert m_k \rvert \leq .25$	134.6347	142.0789
$\lvert Dw_k \rvert \leq .25$ $\lvert m_k \rvert \leq .1$	185.4634	127.8467

When considering which method to use for FalconSAT-5 it is necessary to consider the relative effect of the disturbances and the measurement errors in the satellite model to determine which method of control would be more effective. One of these methods will be more applicable to the control of FalconSAT-5 , but the more applicable method will differ for different systems. Therefore, while only one of these methods will be used for the control of FalconSAT-5, the investigation and inclusion of both methods is important for a full understanding of stocahstic model predictive control of systems with stochastic disturbances and measurement errors.

Chapter 5

FalconSAT-5

5.1 Introduction to Small-Satellite Control

The world today is becoming increasingly reliant on satellite technology. There are currently over 900 operational satellites in earth orbit and that number will continue to increase as the ability of private companies to provide adequate launch vehicles continues to rise [Rast et al., 1999]. Accurate control of satellites is crucial for the successful operation of these satellites, both to ensure mission completion and to avoid catastrophic collisions like the one that occurred in February of 2009 between two satellites in low earth orbit [Broad, 2009].

The space environment in which satellites operate presents unique challenges to establishing attitude control. Satellite control is unlike aircraft control in the sense that when aerodynamic forces are available, ailerons, rudders, and elevators can be used for control. However, in the vacuum of space, these types of control mechanisms are ineffective. To remedy this, spacecrafts use alternate control methods, including angular momentum exchange. By applying a specific torque to a spinning body, the angular momentum vector of the body changes in a predictable manner.

There are several commonly used methods for satellite attitude control, including both passive and active control. Passive control techniques include spin stabilization and gravity gradient stabilization. Active control techniques allow for more exact control and are consequently more widely used in satellite operation. The most common active control actuators onboard commercial satellites today include reaction wheels, control moment gyroscopes, magnetic torque rods, and thrusters [Kaplan, 1976].

5.2 FalconSAT-5

FalconSAT-5 is a small satellite designed, built, tested, and operated by fourth year undergraduates at the United States Air Force Academy in Colorado Springs, CO. Figure 5.1 shows the external and internal configuration of FalconSAT-5.

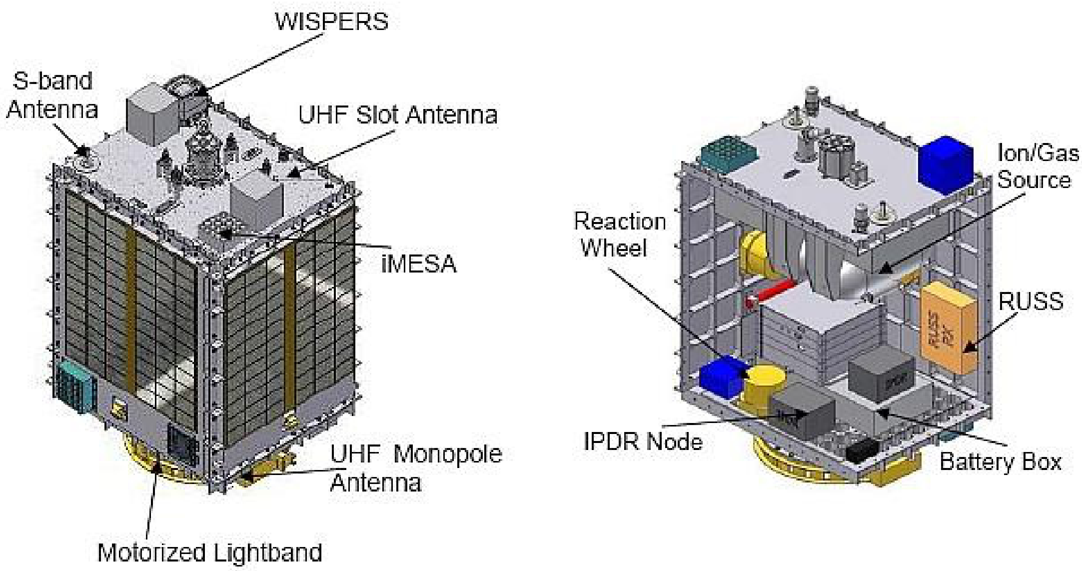

Figure 5.1: Internal and external configuration of FalconSAT-5

FalconSAT-5 serves both an educational and functional purpose. While students working on FalconSAT-5 gain knowledge about and the experience of working on a professional and fully functional spacecraft, the Department of Defense receives data from the satellite and uses the onboard payloads to carry out several Space Experiments Review Board (SERB) approved experiments. The requirements of these payloads motivate the control requirements of FalconSAT-5 and make effective control essential to mission success. Table 5.1 describes the payload control requirements necessary for successful payload implementation for the payloads onboard FalconSAT-5.

Table 5.1: FalconSAT-5 Payload Control Requirements

Payload	Threshold	Objective
Space Plasma Characterization Source (SPCS)	$\pm 4°$	$\pm 1°$
Wafer-Integrated Spectrometer (WISPERS)	$\pm 2.5°$	$\pm 1°$
Integrated Miniaturized ElectroStatic Analyzer (iMESA)	$\pm 4°$	$\pm 1°$

Control of FalconSAT-5 is accomplished using three single-axis reaction wheels. Reaction wheels are small electrical motors that are usually mounted along all three satellite axes. Reaction wheels are spun and when energy is added or removed from the wheels, by changing the wheels spin rate, torque is applied to a single axis of the spacecraft, causing a rotation about that axis. Over time, energy can build up in the wheels, and through the use of the magnetic torque rods, that energy can be transfered, using the earth's magnetic field, to the earth itself, allowing for the excess energy to be removed from the satellite system and allowing for satellite stabilization and control. Table 5.2 shows the specifications of the VECTRONICS VRW-1 reaction wheels used onboard FalconSAT-5 [GmbH].

Table 5.2: Reaction Wheel Specifications

Mass	1.708kg
Maximum wheel speed	5000.05rpm
Maximum angular momentum	1.101Nm-s
Maximum torque	.0245Nm

5.3 FalconSAT-5 Control Modes

There are three major control modes that must be accomplished for succesful mission completion and payload implementation of FalconSAT-5. These three modes include the detumble phase, pointing control, and slew control.

5.3.1 Detumble Phase

The first control mode, the detumble phase, occurs upon initial satellite deployment. When the satellite separates from the launch vehicle it has an inital angular velocity and the goal of the detumble mode is to bring that angular velocity of the satellite to zero and to return the satellite to its original angular position. The actual position the satellite is irrelevant; the purpose is solely three axis stabilization. Therefore the angular position is more accurately refered to, in this control mode, as angular displacement and the goal of the control mode is to bring this angular displacement to zero.

5.3.2 Pointing Control

The second control mode is used to point the satellite from an initial position and velocity to some reference position vector. This mode is used both for payload implementation and to point the satellite towards the sun so as to maximize solar panel exposure. The pointing control must be possible from both a stationary initial position and velocity and from non-zero initial conditions. This control mode must implement control that meets the payload requirements seen in Table 5.1.

5.3.3 Slew Manoeuvre

The final control mode needed for mission completion is a slew manoeuvre. The requirements state that the satellite must be able to complete a slew over 90° in 10 minutes. The slew manoeuvre allows for downlink with the ground station when the satellite is in view of the station as well as the ability to track the position of the sun so as to provide maximum solar panel exposure. The control system must be capable of completing a slew in one, two, or all three axes. The control requirements as presented in the FalconSAT-5 Program Status Review in December of 2008 are attached in Appendix B.

5.4 Stochastic Model Predictive Control for FalconSAT-5

The current control scheme for FalconSAT-5 utilizes classical control techniques, in the form of PD control, to achieve the pointing accuracy described in Table 5.1, but various aspects of the satellite and the environment in which it operates make it useful to investigate the possibility of using stochastic model predictive control techniques for the attitude control of FalconSAT-5.

There are several aspects of FalconSAT-5 that are stochastic. First of all, satellites are subject to external disturbances. These disturbances are difficult to characterize but can be calculated to a degree of certainty by using probabilistic distributions. FalconSAT-5 is subject to both internal and external disturbances. The internal disturbances include gravity gradient torque and the torque generated by the SPCS payload. The external disturbances that have the most effect on FalconSAT-5 are solar radiation, magnetic field torque, aerodynamic torque, and micrometeorite strikes.

Due to unexpected changes in solar pressure, magnetic field fluctuations, and orbital decay, as well the expected external disturbances that come from attitude manoeuvres, the external disturbances on the satellite, and therefore the system, are not constant. The disturbance value is bounded, and the disturbances are more likely to be in the middle of those bounds than on the outer edges, giving the disturbances a distribution that can be represented by a truncated normal distribution. Table 5.3 describes the disturbances on the satellite in all three axes [Larson and Wertz, 1999]. The calculations for these disturbance values are found in Appendix C.

Table 5.3: External Disturbances in Nm

Axis	Minimum	Maximum	Mean	Standard Deviation
Roll	-1.8621×10^{-5}	1.8621×10^{-5}	0	6.21×10^{-6}
Pitch	-2.3247×10^{-5}	2.3247×10^{-5}	0	1.11×10^{-5}
Yaw	-1.1735×10^{-5}	1.1735×10^{-5}	0	3.91×10^{-6}

Not only is the satellite subject to external disturbances, but the attitude sensors that provide the state measurement of the satellite's attitude also exhibit error which contributes uncertainty to the satellite model. The errors in the attitude measurements are twofold: in the sun sensor measurements and the rate sensor measurements. These errors are additive and the error in each sun sensor is independent of the other sensor's errors and therefore the elements of the uncertainty vector are independent of one another. The rate sensor measurements are highly influenced by temperature; when the temperature changes the sensor will be affected and therefore the sensor bias is not constant. The manufacturers of the sensors, SpaceQuest Inc., provided information on the distribution of the sensor errors. The attitude determination algorithm used onboard FalconSAT-5 provides a state measurement with the approximate error distribution seen in Table 5.4.

Table 5.4: Distribution of Measurement Errors in Radians and Radians per second

Minimum	Maximum	Mean	Standard Deviation
-8.988×10^{-6}	8.988×10^{-6}	0	2.909×10^{-6}

5.5 FalconSAT-5 Power Considerations

Apart from the input constraints inherent in the reaction wheels, the most significant operating constraint under which FalconSAT-5 operates is a shortage of available power onboard the satellite. The total power provided by the solar panels and battery array on FalconSAT-5 is approximately 800W at the beginning of life. Nominal satellite performance, which includes general housekeeping and maintenance without any active control or payload implementation, uses roughly 123W. The greatest drain on the power supply is the SPCS payload which includes a Hall-Effect thruster that is propelled by xenon and ammonia cold gas. SPCS requires 100W to heat up and another 500W to fire the thruster, creating a significant drain on the power suppy. In total, when the SPCS thruster is operating, the power required for operation is 649.25W. Each reaction wheel, when operating at 100%, uses 25W, meaning that operating each wheel at maximum power to achieve maximum torque could create a nearly catastrophic drain on the power supply. However, to help mitigate this power shortage, probabilistic constraints can be implemented on the control input provided by the reaction wheels. Imposing a constraint on the torque available from the reactions wheels that is lower than the actual maximum available torque allows for a decrease in the power supply needed to operate the wheels. Making this a soft constraint would allow for violation of the constraints under a certain probability, which would help ensure the reaction wheels provide enough torque to adequately control the satellite without completely draining the power and forcing the satellite to shut down to recharge the batteries.

5.6 FalconSAT-5 Separation Velocity

To determine the initial conditions for control of FalconSAT-5 in the detumble mode, it is important to consider the initial state of the satellite upon separation from the launch vehicle. The following table shows the separation velocity analysis following separation from the Evolved Expendable Launch Vehicle Secondary Payload Adapter (ESPA) to which the satellite is connected during launch.

Table 5.5: Separation Velocity in Degrees per Second

Axis	Maximum Velocity	Minimum Velocity
Roll	$-.515$	$-.66$
Pitch	$.639$	$.15$
Yaw	$-.422$	$-.555$

5.7 Modeling FalconSAT-5

In order to implement stochastic model predictive control, a model of the satellite dynamics is needed. In the satellite model, the following subscripts are used:

I-Inertial reference frame B-Body reference frame sat-Satellite

w-Reaction Wheel C-Control (torque) D-Disturbance (torque)

Euler's moment equations provide the starting point for the derivation of the satellite's equations of motion in all three axes. These equations relate the combined torques ($\bar{T}$) on the satellite to the satellite change in angular momentum ($\frac{dH}{dt}$) in the intertial, earth-centred, reference frame (5.1) [Kaplan, 1976]:

$$\sum \bar{T} = \frac{dH}{dt}_I \tag{5.1}$$

To calculate the change in angular momentum in the satellite body reference frame, the Coriolis operator is used. In order to have a constant, rather than variable, inertia tensor for the satellite, it is convenient to use the satellite body frame as the reference frame. In Equation (5.2), $\bar{\omega}_{B/I}$ refers to the angular velocity of the body frame relative to the intertial frame, or the angular velocity of the satellite around the earth:

$$\sum \bar{T} = \sum \bar{T}_c - \bar{T}_d = \frac{dH}{dt}_B + \bar{\omega}_{B/I} \times \bar{H} \tag{5.2}$$

The angular momentum referenced in Equations (5.1) and (5.2) combines the angular momentum of the satellite body and the momentum of the reaction wheels. The momentum of each reaction wheel is defined relative to an axis system in the centre of the wheel with the principal axis aligned perpedicular to the rotation of the wheel. The axis system of each wheel must be aligned with the satellite axis system and therefore coordinate transformations are necessary to align the wheels reference frames with that of the satellite:

$$\sum \bar{T} = \frac{dH}{dt}_B + \bar{\omega}_{B/I} \times (\bar{H}_{sat} + C_1\bar{H}_{w1} + C_2\bar{H}_{w2} + C_3\bar{H}_{w3}) \tag{5.3}$$

Because angular momentum is the product of the body's moment of inertia and its angular velocity, Equation (5.3) can be written as:

$$\sum \bar{T} = I_{sat}\dot{\bar{\omega}}_{sat} + \bar{\omega}_{B/I} \times (I_{sat}\omega_{sat} + C_1 I_{w1}\omega_{w1} + C_2 I_{w2}\omega_{w2} + C_3 I_{w3}\omega_{w3}) \tag{5.4}$$

The angular velocity of the satellite can be rewritten in terms of the satellite's Euler angles. The Euler angles represent rotations of the satellite around each axis that are used to define the orientation of the satellite body with respect to a reference frame. The angular velocity (and derivative angular acceleration) of the satellite can be written as a function of the satellite euler angles and orbital velocity:

$$\omega = \begin{bmatrix} \dot{\phi} + \psi\omega_o \\ \dot{\theta} + \omega_o \\ \dot{\psi} + \phi\omega_o \end{bmatrix}$$
$$\dot{\omega} = \begin{bmatrix} \ddot{\phi} + \dot{\psi}\omega_o \\ \ddot{\theta} \\ \ddot{\psi} + \dot{\phi}\omega_o \end{bmatrix} \tag{5.5}$$

Using these equations, and the known values for the various moments of inertia, the satellite's angular velocity, and the maximum reaction wheel speed, Equations (5.6), (5.7), and (5.8) define the equations of motion for the satellite in each of the three axes as:

$$\ddot{\phi} = -6.402 \times 10^{-7}\phi - 7.728 \times 10^{-4}\dot{\psi} + .2788\dot{\psi}\dot{\theta} + 2.987 \times 10^{-4}\dot{\theta}\phi - .1158\dot{\theta} - 1.235 \times 10^{-4} - \frac{\sum \bar{T}_\phi}{12.77} \tag{5.6}$$

$$\ddot{\theta} = -1.600 \times 10^{-6}\theta - 4.978 \times 10^{-4}\phi\dot{\phi} - 5.335 \times 10^{-7}\phi\psi - .465\dot{\phi}\dot{\psi} - 4.978 \times 10^{-4}\psi\dot{\psi} + .132\dot{\phi} + 1.414 \times 10^{-4}\psi - \frac{\sum \bar{T}_\theta}{11.15} \tag{5.7}$$

$$\ddot{\psi} = -8.429 \times 10^{-4}\dot{\phi} + 9.803 \times 10^{-7}\psi + .213\dot{\theta}\dot{\phi} + 2.287 \times 10^{-4}\psi\dot{\theta} - \frac{\sum \bar{T}_\phi}{7.59} \tag{5.8}$$

In order to linearize the equations and eliminate the coupled terms, several assumptions and simplifications are necessary. A Simulink model of the satellite was created to simulate the satellite's uncontrolled motion. The results of this simulation were then used to determine which angles and angular rates were the least variable so as to provide an appropriate reference point around which to linearize the equations. Any constant terms were removed from the state space model, but were then compensated for in the control law with an additional constant control torque. The following values were used to linearize the system of equations of motion:

$$\dot{\psi} = 3.19 \times 10^{-4}\tfrac{\text{rad}}{\text{s}} \qquad \dot{\theta} = -2.81 \times 10^{-4}\tfrac{\text{rad}}{\text{s}} \qquad \phi = -.113\text{rad}$$

Using these values, Equations (5.6) -(5.8) now take the linearized form of Equations (5.9) - (5.11):

$$\ddot{\phi} = -6.881 \times 10^{-7}\phi - 8.511 \times 10^{-4}\dot{\psi} - .1152\dot{\theta} - \frac{\sum \bar{T}_\phi}{12.77} \tag{5.9}$$

$$\ddot{\theta} = -1.600 \times 10^{-6}\theta + .1319\dot{\phi} + 1.4184 \times 10^{-4}\psi - \frac{\sum \bar{T}_\theta}{11.15} \tag{5.10}$$

$$\ddot{\psi} = -9.0275 \times 10^{-4}\dot{\phi} + 9.160 \times 10^{-7}\psi - \frac{\sum \bar{T}_\phi}{7.59} \tag{5.11}$$

Now that the equations of motion for the satellite are defined, the state space definition follows logically. The state vector is made up of the angular position and the angular rate in all three axes. The inputs include the control torques in all three axes whereas the disturbances are the disturbance torques in each axis:

$$x = \begin{bmatrix} \phi \\ \theta \\ \psi \\ \dot{\phi} \\ \dot{\theta} \\ \dot{\psi} \end{bmatrix}$$

$$u = \begin{bmatrix} T_{c\phi} \\ T_{c\theta} \\ T_{c\psi} \end{bmatrix}$$

$$w = \begin{bmatrix} T_{d\phi} \\ T_{d\theta} \\ T_{d\psi} \end{bmatrix}$$

These state, input, and distrubance vectors lend themselves to the following state space representation where A is a 6×6 matrix, and B and D are both 6×3:

$$\dot{\bar{x}} = A\bar{x} + B\bar{u} + D\bar{w}$$

$$A = \begin{bmatrix} 0 & 0 & 0 & 1 & 0 & 0 \\ 0 & 0 & 0 & 0 & 1 & 0 \\ 0 & 0 & 0 & 0 & 0 & 1 \\ -6.881 \times 10^{-7} & 0 & 0 & 0 & -.1152 & -8.511 \times 10^{-4} \\ 0 & -1.600 \times 10^{-6} & 0 & .1319 & 0 & 1.4184 \times 10^{-4} \\ 0 & 0 & 9.16 \times 10^{-7} & -9.028 \times 10^{-4} & 0 & 0 \end{bmatrix}$$

$$B = \begin{bmatrix} 0 & 0 & 0 \\ 0 & 0 & 0 \\ 0 & 0 & 0 \\ -\frac{1}{12.77} & 0 & 0 \\ 0 & -\frac{1}{11.15} & 0 \\ 0 & 0 & -\frac{1}{7.59} \end{bmatrix}$$

$$D = -B \tag{5.12}$$

Finally, the system must be converted from the continuous to the discrete time domain, assuming a zero-hold on the input in between the sampling times. Equation (5.13) shows the matrices that make up the discrete time state space model of FalconSAT-5:

$$A = \begin{bmatrix} 1 & 3.070\times10^{-8} & -6.23\times10^{-13} & .9975 & -.05753 & -2.721\times10^{-6} \\ -1.511\times10^{-8} & 1 & 2.164\times10^{-11} & .06587 & .9975 & 7.083\times10^{-5} \\ 1.0345\times10^{-10} & -6.930\times10^{-12} & 1 & -4.508\times10^{-3} & -1.732\times10^{-5} & 1 \\ -6.864\times10^{-7} & 9.204\times10^{-8} & -2.493\times10^{-12} & .9924 & -.1149 & -8.160\times10^{-6} \\ -4.532\times10^{-8} & -1.596\times10^{-6} & 6.488\times10^{-11} & .1316 & .9924 & 1.415\times10^{-4} \\ 3.102\times10^{-10} & -2.771\times10^{-11} & 9.160\times10^{-7} & -9.005\times10^{-4} & 5.193\times10^{-5} & 1 \end{bmatrix}$$

$$B = \begin{bmatrix} -.0391 & .001721 & 8.966\times10^{-8} \\ -.001720 & -.04479 & -3.112\times10^{-6} \\ 1.177\times10^{-5} & -3.884\times10^{-7} & -.06588 \\ -.07811 & 5.159\times10^{-3} & 3.585\times10^{-7} \\ -.005158 & -.08946 & -9.332\times10^{-6} \\ 3.530\times10^{-5} & -1.553\times10^{-6} & -.1318 \end{bmatrix}$$

$$D = -B \tag{5.13}$$

Figures 5.2 and 5.3 show the uncontrolled motion of the satellite for initial condition $x_0 = [0^\circ\ 0^\circ\ -0^\circ\ -.66\frac{^\circ}{s}\ .639\frac{^\circ}{s}\ -.555\frac{^\circ}{s}]^T$. This initial condition was obtained from the worst case separation velocity, as seen in Table 5.5. Figure 5.2 shows that, without active control, the satellite will rotate around the yaw axis while nutating in the roll and pitch axes. This is consistent with the angular velocity seen in Figure 5.3.

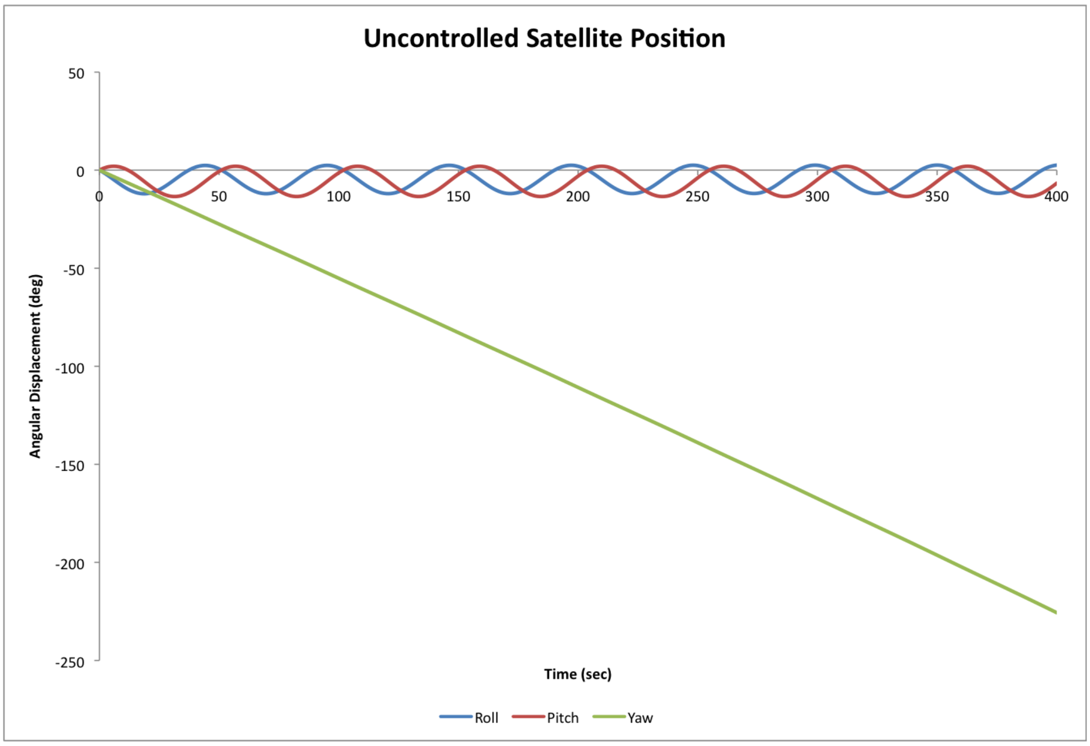

Figure 5.2: Uncontrolled angular position response of FalconSAT-5

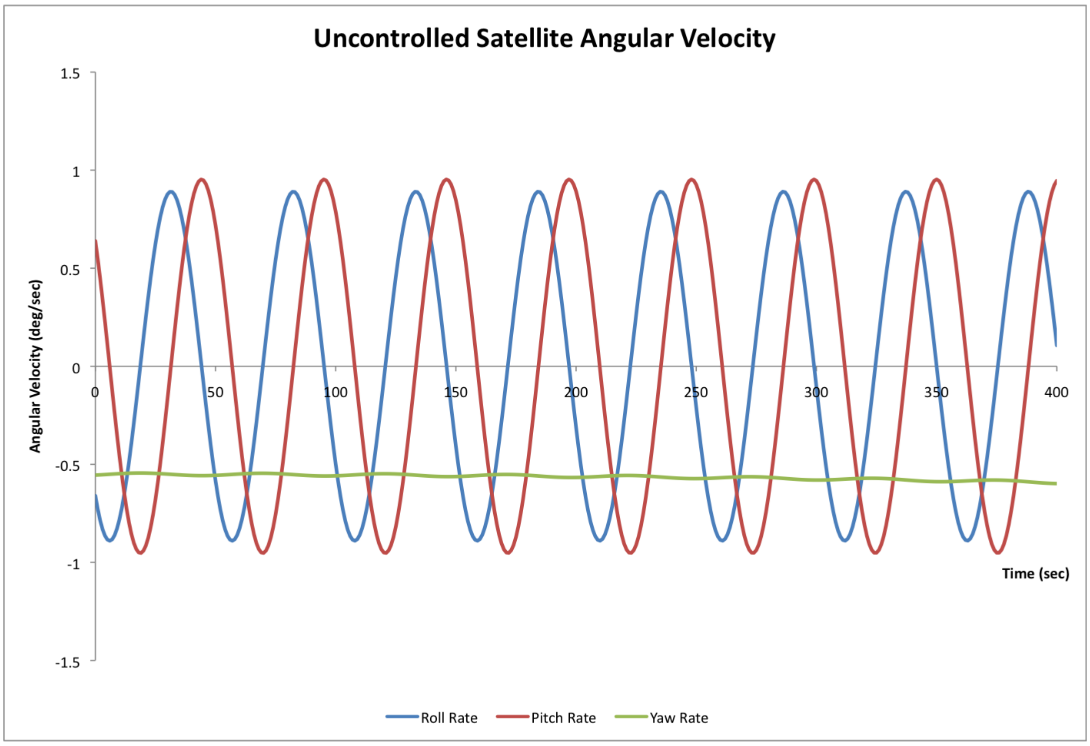

Figure 5.3: Uncontrolled angular velocity response of FalconSAT-5

Chapter 6

Implementation of Stochastic Model Predictive Control for FalconSAT-5

6.1 Control Method

The first step in implementing model predictive control for FalconSAT-5 is to determine which of the three previously discussed control methods is most applicable. The baseline MPC method in Chapter 2 fails to take into account the measurement errors and, when they are included, that method violates the probabilistic constraints, rendering it unsuitable. Therefore it is necessary to use either the MPC with error consideration method described in Chapter 3 or the MPC with estimation method in Chapter 4. As discussed in the comparison in Chapter 4, it is necessary to consider the values and relative effects of the disturbances and the errors on the system response. As seen in Tables 5.3 and 5.4, the disturbances on FalconSAT-5 are an order of magnitude greater than the measurement errors and they have a greater effect on the response of the system. As demonstrated in the comparison in Section 4.6.1, when the values of the disturbances are larger than the measurement errors, the MPC with error consideration method is more suitable than the MPC with estimation method. Therefore the method described in Chapter 3, in which the measurement errors are used in the definition of the constraints, will be used to determine if stochastic model predictive control can be used to control FalconSAT-5.

6.2 System and Parameters

The system developed in Chapter 5 will be used for the implementation of model predictive control for FalconSAT-5.

$$A = \begin{bmatrix} 1 & 3.070\times10^{-8} & -6.23\times10^{-13} & .9975 & -.05753 & -2.721\times10^{-6} \\ -1.511\times10^{-8} & 1 & 2.164\times10^{-11} & .06587 & .9975 & 7.083\times10^{-5} \\ 1.0345\times10^{-10} & -6.930\times10^{-12} & 1 & -4.508\times10^{-3} & -1.732\times10^{-5} & 1 \\ -6.864\times10^{-7} & 9.204\times10^{-8} & -2.493\times10^{-12} & .9924 & -.1149 & -8.160\times10^{-6} \\ -4.532\times10^{-8} & -1.596\times10^{-6} & 6.488\times10^{-11} & .1316 & .9924 & 1.415\times10^{-4} \\ 3.102\times10^{-10} & -2.771\times10^{-11} & 9.160\times10^{-7} & -9.005\times10^{-4} & 5.193\times10^{-5} & 1 \end{bmatrix}$$

$$B = \begin{bmatrix} -.0391 & .001721 & 8.966\times10^{-8} \\ -.001720 & -.04479 & -3.112\times10^{-6} \\ 1.177\times10^{-5} & -3.884\times10^{-7} & -.06588 \\ -.07811 & 5.159\times10^{-3} & 3.585\times10^{-7} \\ -.005158 & -.08946 & -9.332\times10^{-6} \\ 3.530\times10^{-5} & -1.553\times10^{-6} & -.1318 \end{bmatrix}$$

$$D = -B$$

$$|w_k| \leq 2.3247\times10^{-5} \qquad |m_k| \leq -8.988\times10^{-6}$$

$$\sigma_w = 1.11\times10^{-5} \qquad \sigma_m = 2.909\times10^{-6}$$

The weighting matrices Q and R can be chosen to weight the effect of the state response and the input on the cost. Additionally, these matrices can be used to make a particular axis more influential in the cost value. The Q matrix weights the state response, or state convergence, while the R matrix weights the input required. While both the state response and the input are important in the control of FalconSAT-5, the state convergence is a more important consideration in performance and the state response will therefore weigh more heavily in the cost function than the input. Because the goal of the control scheme is to achieve the desired steady state in all three axes, the weighting matrices will weight all three axes the same.

$$Q = I_{6\times6} \qquad R = .1I_{3\times3} \qquad N = 20 \qquad \hat{N} = 6 \qquad n^* = 1$$

6.2.1 Input Constraints

While Table 5.2 gives the maximum torque available for each reaction wheel as .0245 Nm, this value will not be used for the input constraint. By imposing a soft constraint, the power draw of the reaction wheels can be decreased so as to better protect the limited power supply onboard FalconSAT-5. The following simulations will be performed by constraining the reaction wheels to taking 80% of maximum power, with a constraint satisfaction rate of 80%. By constraining to 80% power, the power drain of the reaction wheels can be decreased by up to 1.405 MWhr over the lifetime of the satellite, which equates to an average of 10.69 W less for each orbit. The calculations for these values are found in Appendix D. These values, however, can be changed based on the environment in which the satellite operates. When the satellite is operating in eclipse, it would be useful to impose a tighter constraint on the input so as to minimize the power when less is available, whereas in a sunpointing orbit, the increase in power available for the satellite could lead to a loosening of the constraints. The following simulations use the following values for $\bar{u}_k$ and p.

$$|u_k| \leq .02\text{Nm} \qquad p = .8$$

6.3 Detumble Mode Control

As mentioned in Section 5.3, the detumble mode is used upon the initial deployment of the satellite to drive all states of the satellite to zero. The separation velocity shown in Table 5.5 is used for the initial angular velocity, resulting in the following initial condition.

$$x_0 = [0^\circ\ 0^\circ\ 0^\circ\ \ -.66\frac{\circ}{\text{s}}\ .639\frac{\circ}{\text{s}}\ \ -.555\frac{\circ}{\text{s}}]^T$$

For all simulations in this and the following chapters, the response shown will be an average over 200 possible realizations of disturbances and measurement errors.

6.3.1 Detumble Results

Using the method described in Chapter 3, the following figures show that the model predictive control method that considers the measurement error in the constraint definition is capable of controlling FalconSAT-5 in the detumble mode. Figures 6.1 and 6.2 show the angular position and angular velocity response relative to time.

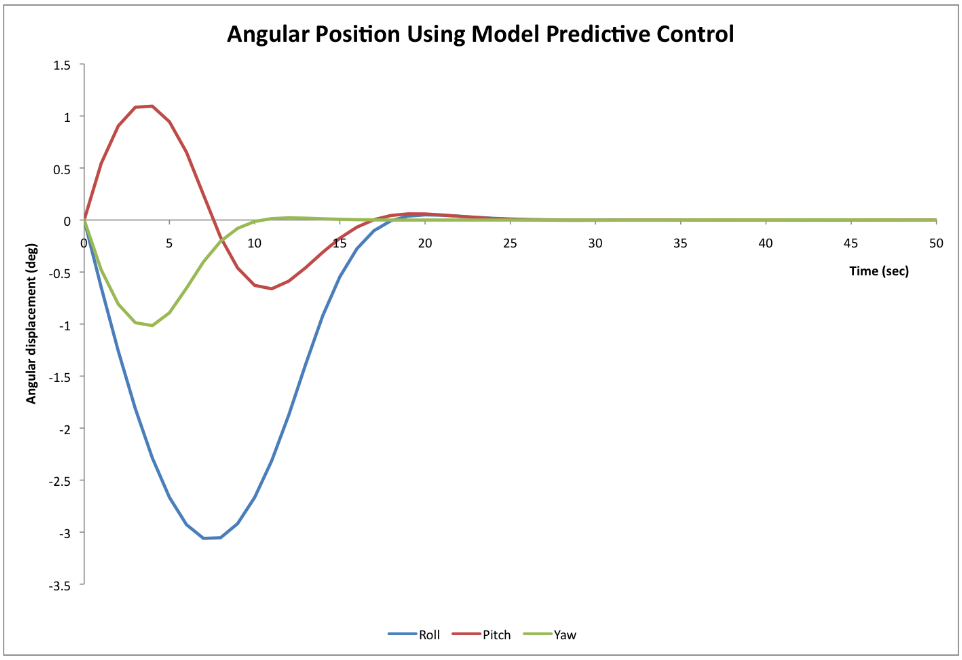

Figure 6.1: Angular position response for detumble mode using model predictive control

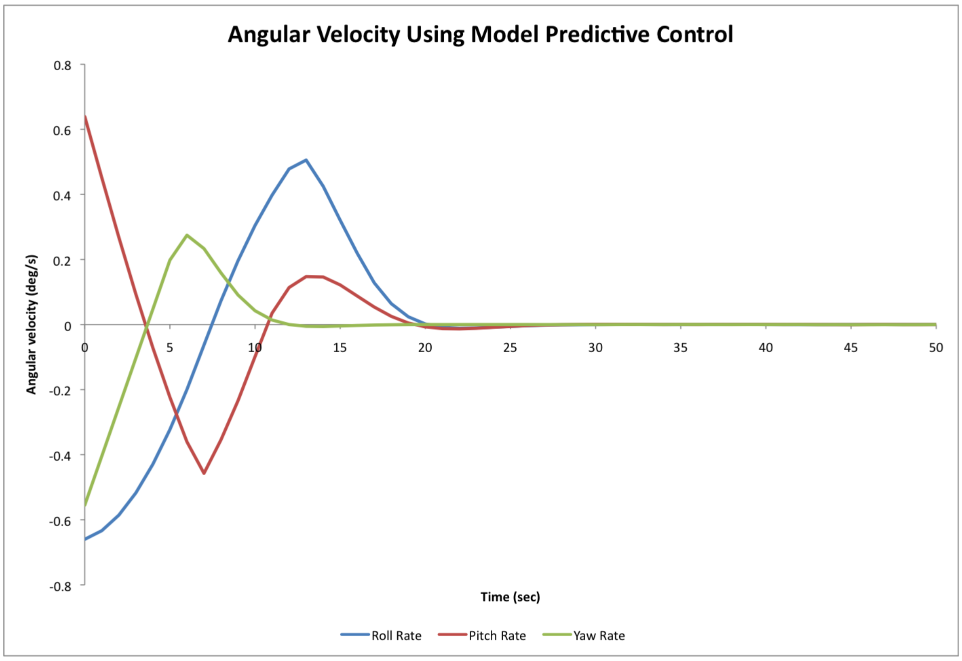

Figure 6.2: Angular velocity response for detumble mode using model predictive control

Figures 6.3 and 6.4 show the convergence of the angular displacement and angular velocity to zero.

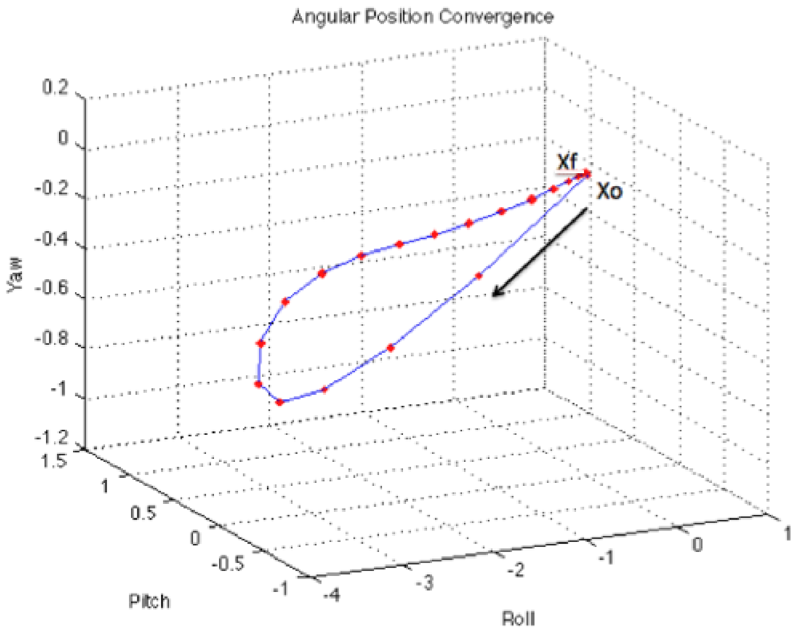

Figure 6.3: Convergence of angular position for detumble mode using model predictive control

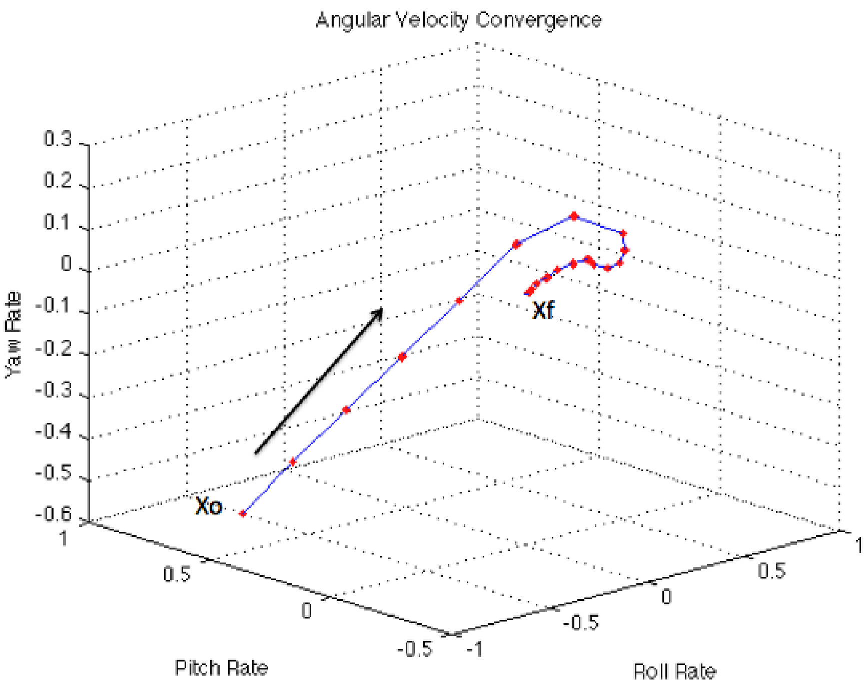

Figure 6.4: Convergence of angular velocity for detumble mode using model predictive control

6.4 Pointing Mode Control

6.4.1 Pointing Control from Stationary

When considering the pointing mode control, the first step is to investigate if model predictive control can be used to acheive a desired angular position from a stationary starting point. This simulates control following the detumbling phase of the satellite where the initial position and initial velocity are equal to zero, thereby using the following initial condition (x_0) and final reference state (x_f).

$$x_0 = [0^\circ\ 0^\circ\ 0^\circ\ 0\tfrac{^\circ}{\mathrm{s}}\ 0\tfrac{^\circ}{\mathrm{s}}\ 0\tfrac{^\circ}{\mathrm{s}}]^T \qquad x_f = [-4^\circ\ 5^\circ\ 3^\circ\ 0\tfrac{^\circ}{\mathrm{s}}\ 0\tfrac{^\circ}{\mathrm{s}}\ 0\tfrac{^\circ}{\mathrm{s}}]^T$$

6.4.1.1 Results

Figure 6.5 shows the ability of the model predictive control algorithm, described in Appendix E, to track to a final state which matches the desired set point.

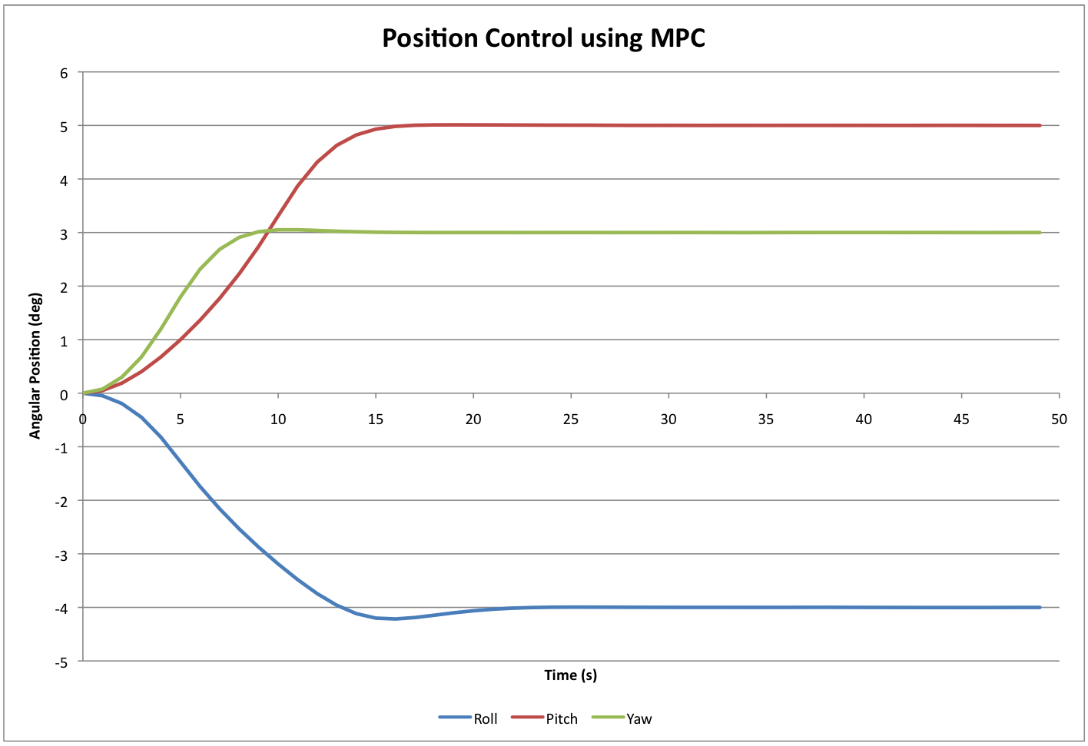

Figure 6.5: Angular position response for pointing control from stationary using model predictive control

6.4.2 Pointing Control from Non-zero Initial Conditions

The next step is to investigate if control is still achievable when the satellite has some initial position and velocity. The following are the initial state and desired final state for this example.

$$x_0 = [-.75^\circ \; 1^\circ \; 2^\circ \; -.35\tfrac{\circ}{\mathrm{s}} \; .4\tfrac{\circ}{\mathrm{s}} \; -.25\tfrac{\circ}{\mathrm{s}}]^T \qquad x_f = [.75^\circ \; -1^\circ \; -.5^\circ \; 0\tfrac{\circ}{\mathrm{s}} \; 0\tfrac{\circ}{\mathrm{s}} \; 0\tfrac{\circ}{\mathrm{s}}]^T$$

6.4.2.1 Results

The following figure shows that, using model predictive control, the position goes to the desired final position from the non-zero initial condition.

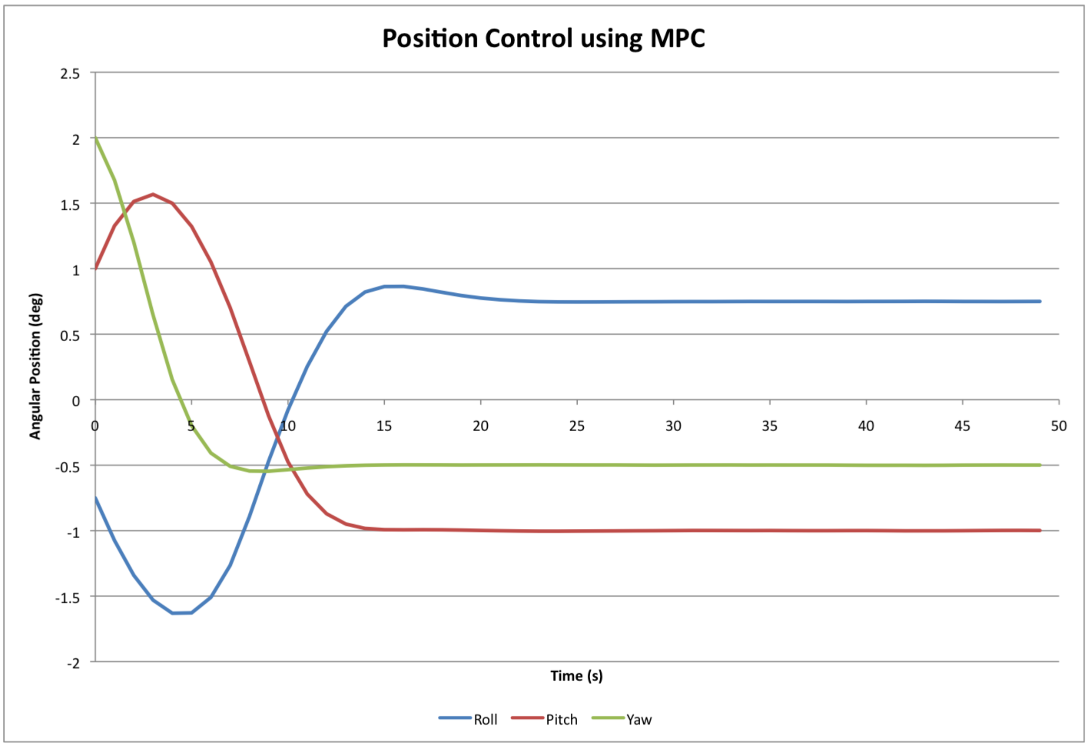

Figure 6.6: Angular position response for pointing control from non-zero initial conditions using model predictive control

The plots of the angular velocity response can be found in Appendix F.

6.5 Slew Manoeuvre

Because the requirements state that the satellite must be able to execute a 90° slew in 10 minutes, the rate at which the satellite must slew is $0.15\frac{\circ}{\mathrm{s}}$. The initial conditions for all three slew manoeuvres will be $x_0 = [0° \ 0° \ 0° \ 0\frac{°}{s} \ 0\frac{°}{s} \ 0\frac{°}{s}]^T$. The initial position is take to be zero because, regardless of the initial position vector, the goal is to slew 90° from that initial position and therefore the angular position again becomes an angular displacement.

The following figures show the position response of the satellite during the slew manoeuvre. Whereas the first figure in each pair (Figures 6.7, 6.9, 6.11) shows the ability of the method to achieve the necessary slew manoeuvre, the second in each pair (Figures 6.8, 6.10, 6.12) show the response of the state before the angular rate reaches the desired slew rate. Because the angular position and velocity begins at zero and the magnitude of the disturbance effects are small, the transient response in the axes in which the slew is not being executed is minimal and difficult to discern in these figures. However, the angular velocity plots that will be described in Chapter 9 show the transient response of the angular velocity for all three axes.

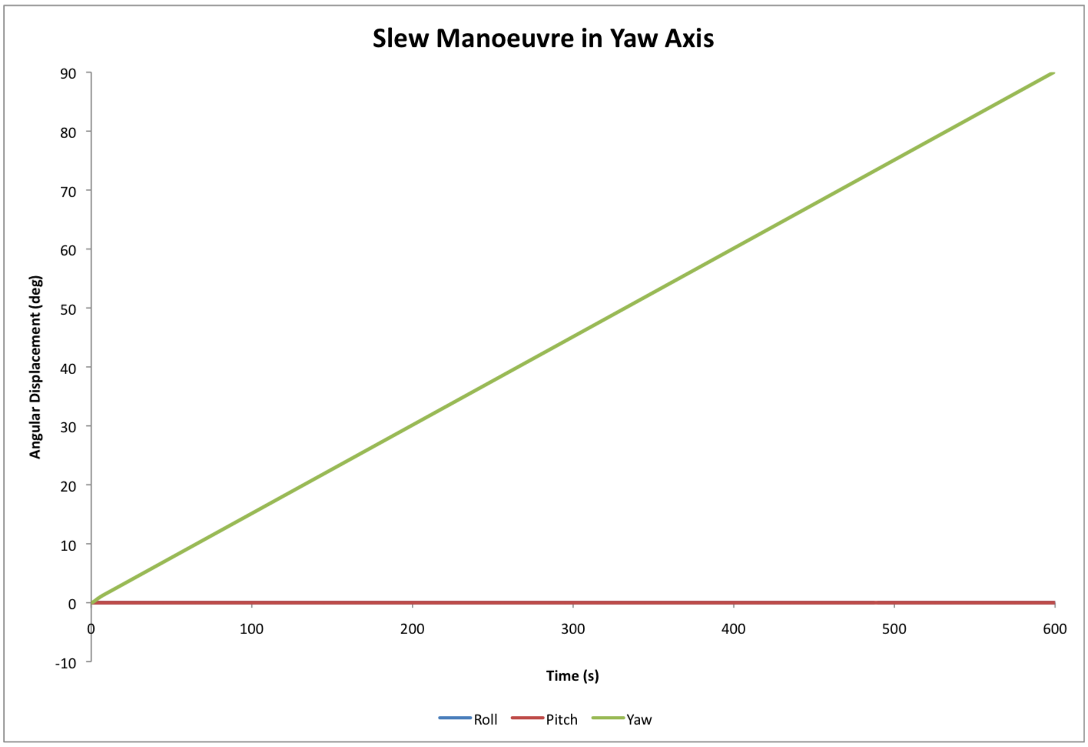

Figure 6.7: Slew manoeuvre in yaw axis using model predictive control

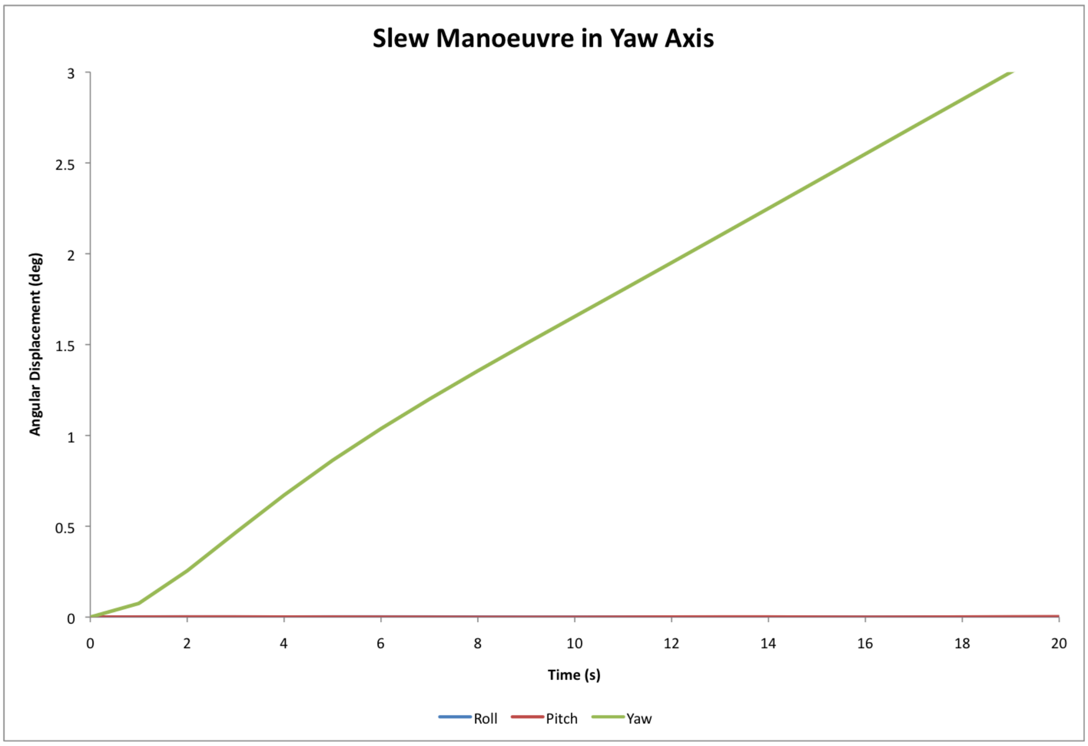

Figure 6.8: Slew manoeuvre in yaw axis using model predictive control

Figure 6.9: Slew manoeuvre in pitch and yaw axes using model predictive control

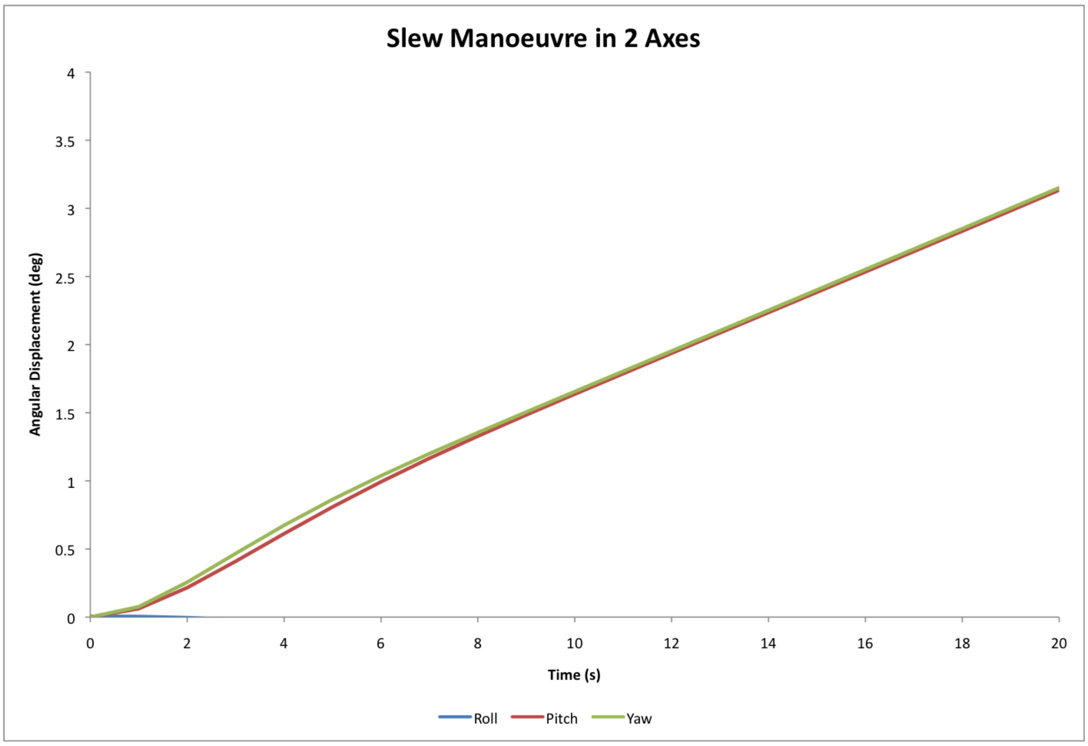

Figure 6.10: Slew manoeuvre in pitch and yaw axis using model predictive control

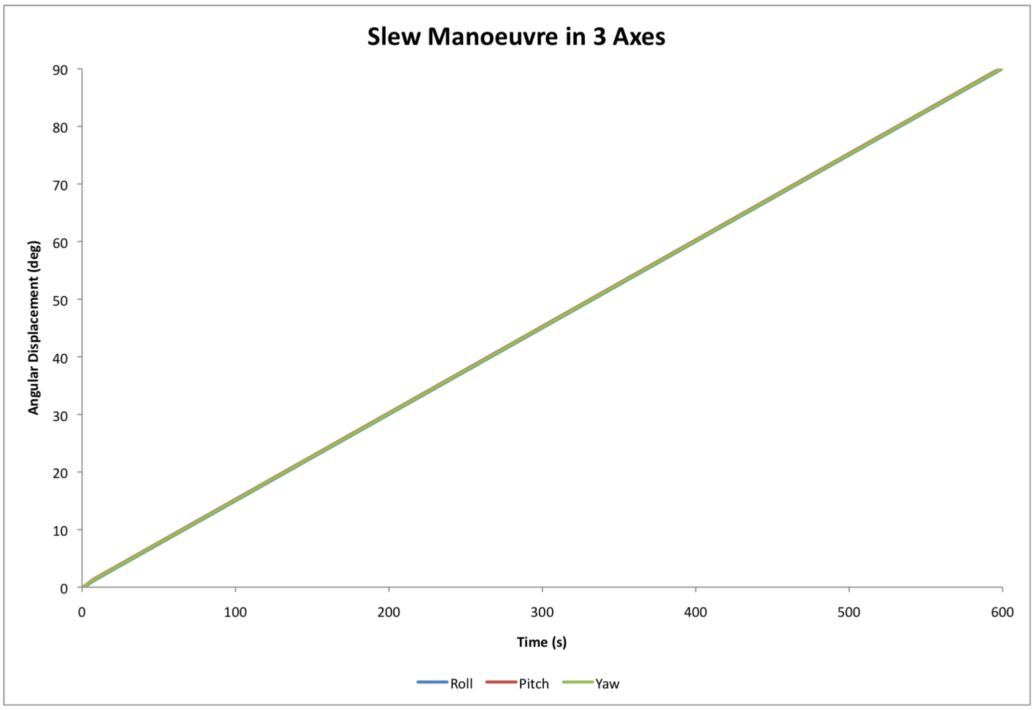

Figure 6.11: Slew manoeuvre in all 3 axes using model predictive control

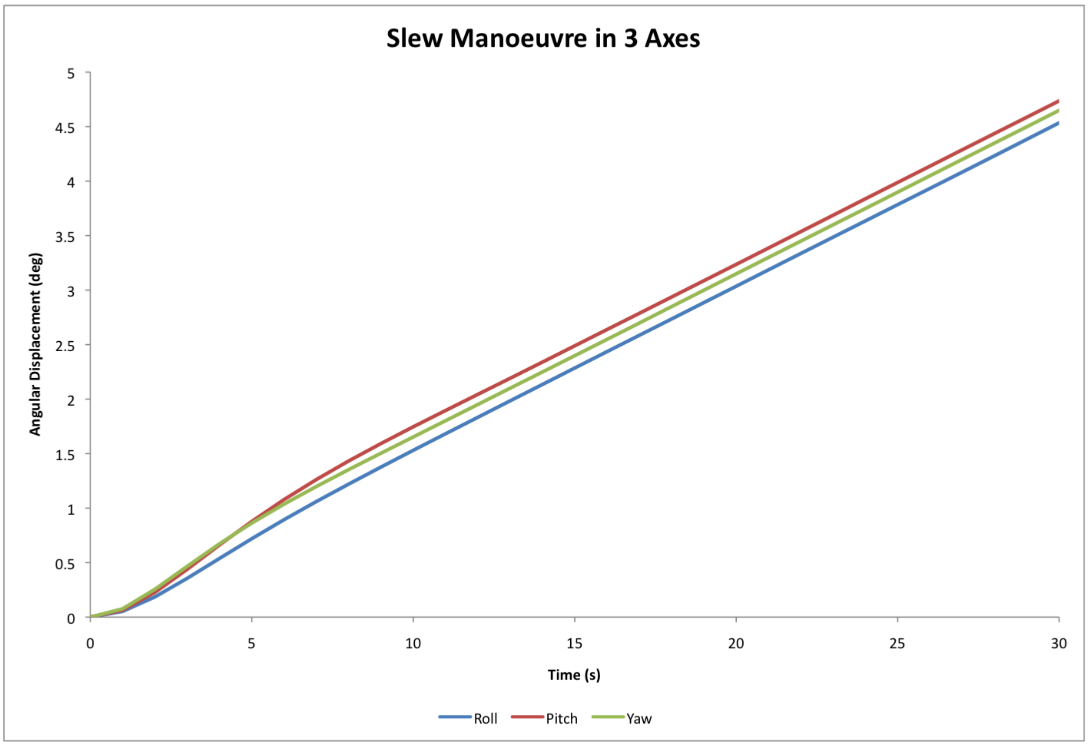

Figure 6.12: Slew manoeuvre in all 3 axes using model predictive control

The results shown in this chapter demonstrate the ability of the model predictive control method that considers the measurement errors in the constraint definition to control FalconSAT-5 for all the necessary control modes. For each of these control modes, the necessary performance is achieved and the probabilistic constraints are met.

Chapter 7

Classical Control Techniques for FalconSAT-5

7.1 Classical Control for FalconSAT-5

The initial control plan for FalconSAT-5 utilized PD methods to achieve satellite control. An initial control analysis was conducted as part of the undergraduate capstone course at the United States Air Force Academy which used a combination of proportional and derivative control for FalconSAT-5. This control scheme was created based off a Simulink model of the satellite dynamics that failed to take into consideration the stochastic disturbances and measurement errors.

Because the Simulink control analysis failed to consider the disturbances and measurement errors, further analysis was completed, this time on the state space model for FalconSAT-5 developed in Chapter 5. As with the model predictive control methods, the PD control methods must be capable of controlling in the detumble, pointing control, and slew modes.

7.1.1 Introducing Probabilistic Constraints for Proportional-Derivative Control

Usually, when PD control is used for systems with an input constraint, the input is clipped post calculation so that the constraint is met for all times. However, because the stochastic model predictive control deals with probabilistic constraints, in order to provide a meaningful comparison, probabilistic constraints need to be introduced to the PD control scheme.

There is no prediction in PD control and the control input is calculated based entirely on current and past state measurements. Therefore, the calculated input will only be dependent upon the measurement errors and will be independent of the external disturbances. Equation (7.1) shows the input for discrete PD control at time i.

$$u_i = K_P(x_i - x_g) + K_D((x_i - x_g) - (x_{i-1} - x_g)) \tag{7.1}$$

In the above equation, x_g is defined as the desired final state of the system. This x_g is constant relative to the satellite body frame for each of the satellite control modes.

Factoring measurement errors into Equation (7.1), results in Equation (7.2).

$$\begin{aligned}
u_i &= K_P(x_i - x_g) + K_D((x_i - x_g) - (x_{i-1} - x_g)) \\
u_i &= (K_P + K_D)(y_i - m_i) - K_P x_g - K_D(y_{i-1} - m_{i-1}) \\
u_i &= (K_P + K_D)y_i - K_P x_g - K_P y_{i-1} - (K_P + K_D)m_i + K_D m_{i-1}
\end{aligned} \tag{7.2}$$

If this input is used in the probabilistic constraint ($\Pr(f^T u_k \leq h) \geq p$) then the constraint becomes:

$$\Pr(f^T((K_P + K_D)y_i - K_P x_g - K_P y_{i-1} - (K_P + K_D)m_i + K_D m_{i-1}) \leq h) \geq p \tag{7.3}$$

Because m_i and m_{i-1} are random variables and are independent of each other, their effect on the constraint can be determined and used to tighten the constraint so that, even in the presence of uncertainty, the constraints are met. The effect of $(K_P + K_D)m_i$ and $K_D m_{i-1}$ can be found by finding the minimum values of θ_i and θ_{i-1} for which the following expressions are true:

$$Pr(f^T(K_P + K_D)m_i \leq \theta_i) \geq p$$
$$Pr(f^T K_D m_{i-1} \leq \theta_{i-1}) \geq p$$

Equation (7.4) shows the constraint using these parameters. Now, when the PD input is calculated it is clipped at a value of $h - (\theta_i + \theta_{i-1})$ so as to provide meaningful comparison to stochastic model predictive control.

$$\Pr(f^T((K_P + K_D)y_i - K_P x_g - K_P y_{i-1} \leq h - (\theta_i + \theta_{i-1})) \geq p \tag{7.4}$$

7.1.2 Detumble Mode

The following gains were used to achieve the detumbling performance seen in Figure 7.1 and Figure 7.2. Because the response doesn't exhibit steady state error, there is no reason to introduce integral control and PD control is sufficient. The PD control gains were designed to minimize the cost function described in Equation (2.5), which results in an equivalent control scheme to an optimal LQR control scheme.

$$K_P = \begin{bmatrix} 5 & 0 & 0 & 10 & 0 & 0 \\ 0 & 7 & 0 & 0 & 10 & 0 \\ 0 & 0 & 3 & 0 & 0 & 5 \end{bmatrix}$$
$$K_D = \begin{bmatrix} 7 & 0 & 0 & 5 & 0 & 0 \\ 0 & 7 & 0 & 0 & 5 & 0 \\ 0 & 0 & 5 & 0 & 0 & 1 \end{bmatrix}$$

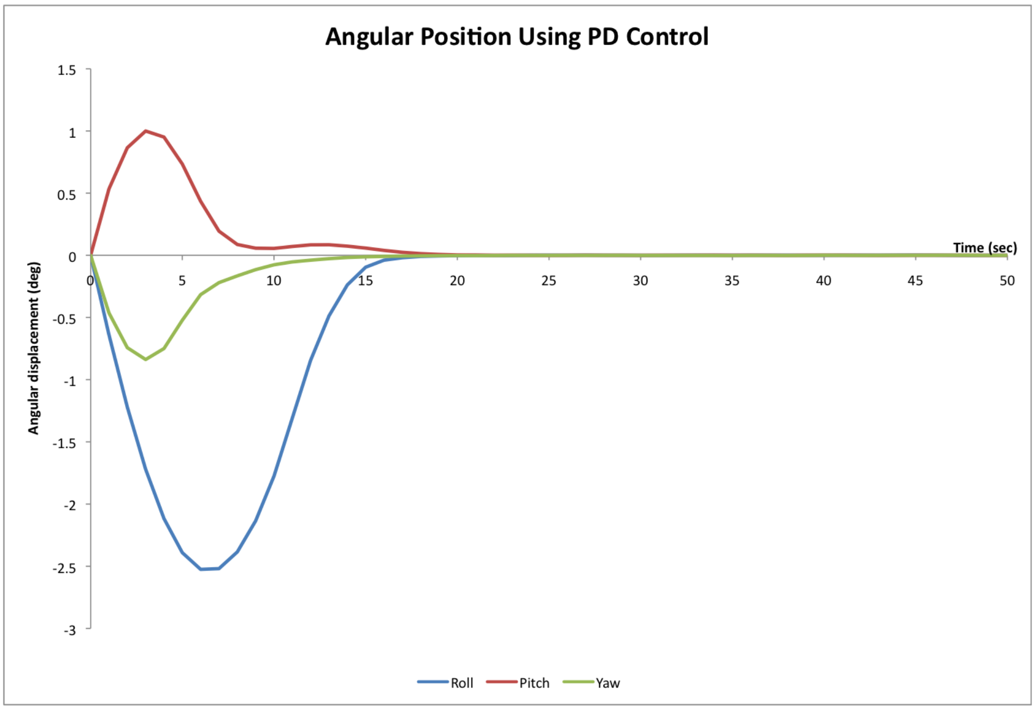

Figure 7.1: Angular position response for detumble mode using PD control

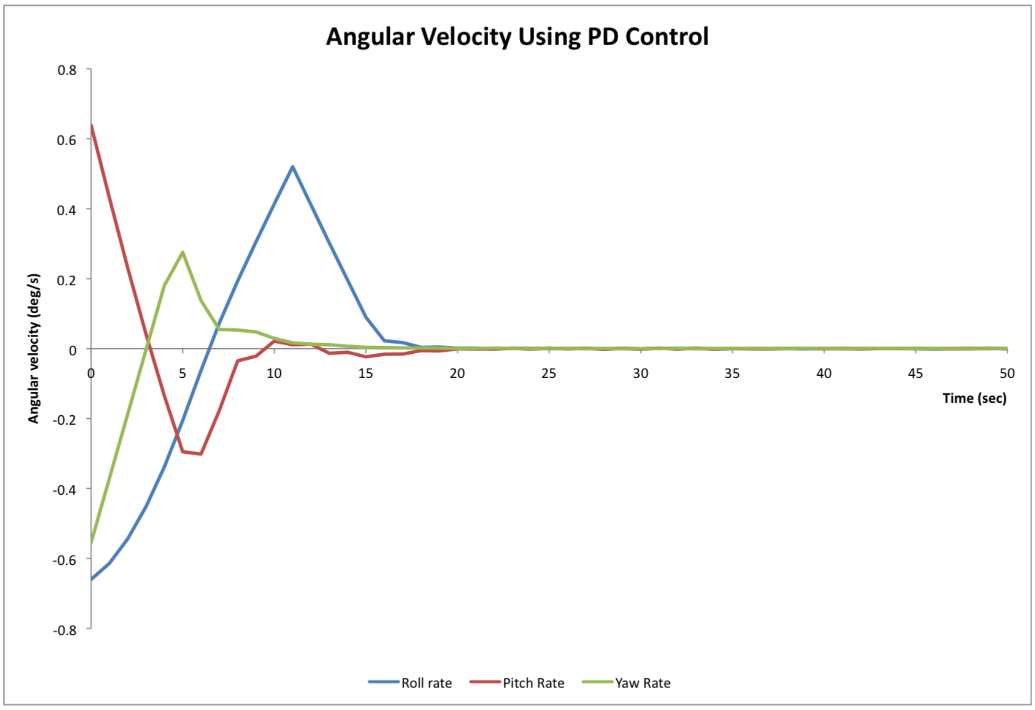

Figure 7.2: Angular velocity response for detumble mode using PD control

7.1.3 Pointing Control from Stationary

The following gains were used to simulate the first of the two pointing control examples in Section 6.4.

$$K_P = \begin{bmatrix} 2 & 0 & 0 & 10 & 0 & 0 \\ 0 & 6 & 0 & 0 & 10 & 0 \\ 0 & 0 & 3 & 0 & 0 & 5 \end{bmatrix}$$

$$K_D = \begin{bmatrix} 3 & 0 & 0 & 5 & 0 & 0 \\ 0 & 8 & 0 & 0 & 5 & 0 \\ 0 & 0 & 5 & 0 & 0 & 1 \end{bmatrix}$$

Figure 7.3 shows the response of the position, going from zero to the desired final state. The velocity response for this and the following example are found in Appendix F.

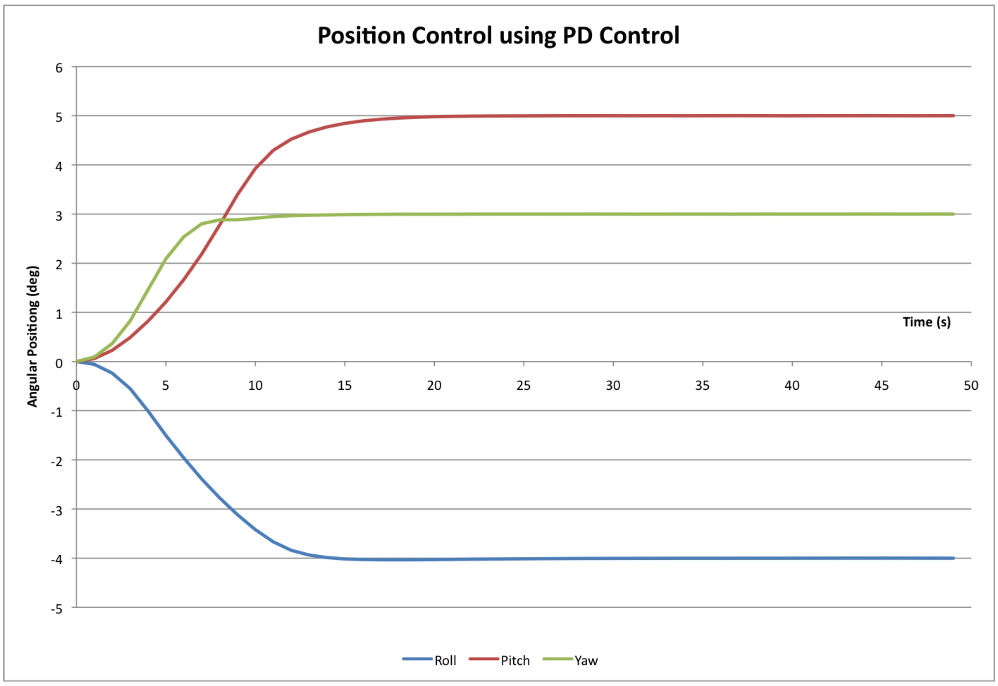

Figure 7.3: Angular position response for pointing control from stationary using PD control

7.1.4 Pointing Control from Non-zero Initial Conditions

The following gains were used for the second pointing example in Section 6.4, resulting in the state response seen in Figure 7.4.

$$K_P = \begin{bmatrix} 3 & 0 & 0 & 10 & 0 & 0 \\ 0 & 9 & 0 & 0 & 10 & 0 \\ 0 & 0 & 4 & 0 & 0 & 5 \end{bmatrix}$$

$$K_D = \begin{bmatrix} 3 & 0 & 0 & 5 & 0 & 0 \\ 0 & 9 & 0 & 0 & 5 & 0 \\ 0 & 0 & 5 & 0 & 0 & 1 \end{bmatrix}$$

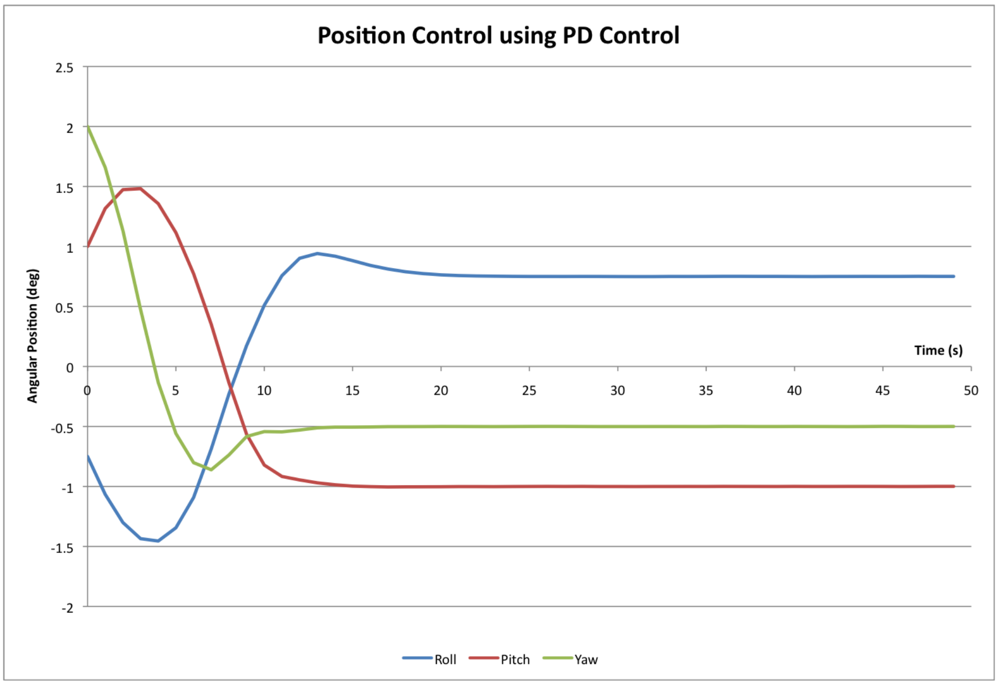

Figure 7.4: Angular position response for pointing control from non-zero initial conditions using PD control

7.1.5 Slew Manoeuvre

The following gains were used for the PD control of the satellite for a slew manoeuvre in the yaw axis.

$$K_P = \begin{bmatrix} 3 & 0 & 0 & 10 & 0 & 0 \\ 0 & 3 & 0 & 0 & 10 & 0 \\ 0 & 0 & 3 & 0 & 0 & 5 \end{bmatrix}$$

$$K_D = \begin{bmatrix} 3 & 0 & 0 & 5 & 0 & 0 \\ 0 & 5 & 0 & 0 & 5 & 0 \\ 0 & 0 & 5 & 0 & 0 & 1 \end{bmatrix}$$

As seen in Figure 7.5, classical control techniques can be used to accomplish a 90° slew in the yaw axis. Figure 7.6 shows the transient response of the yaw axis before the angular velocity reaches the necessary slew rate.

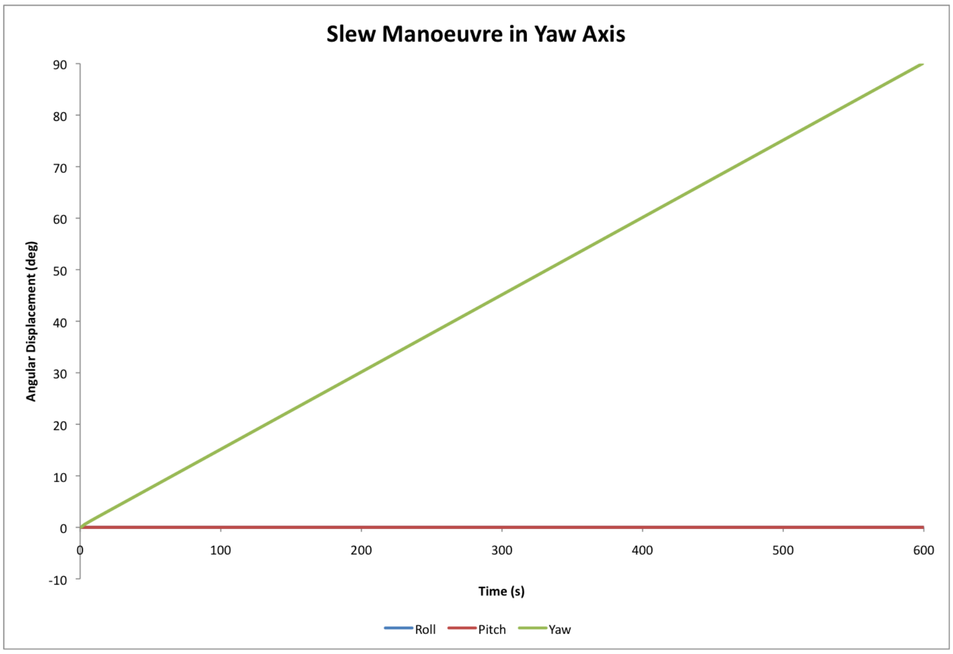

Figure 7.5: Slew manoeuvre in yaw axis using PD control

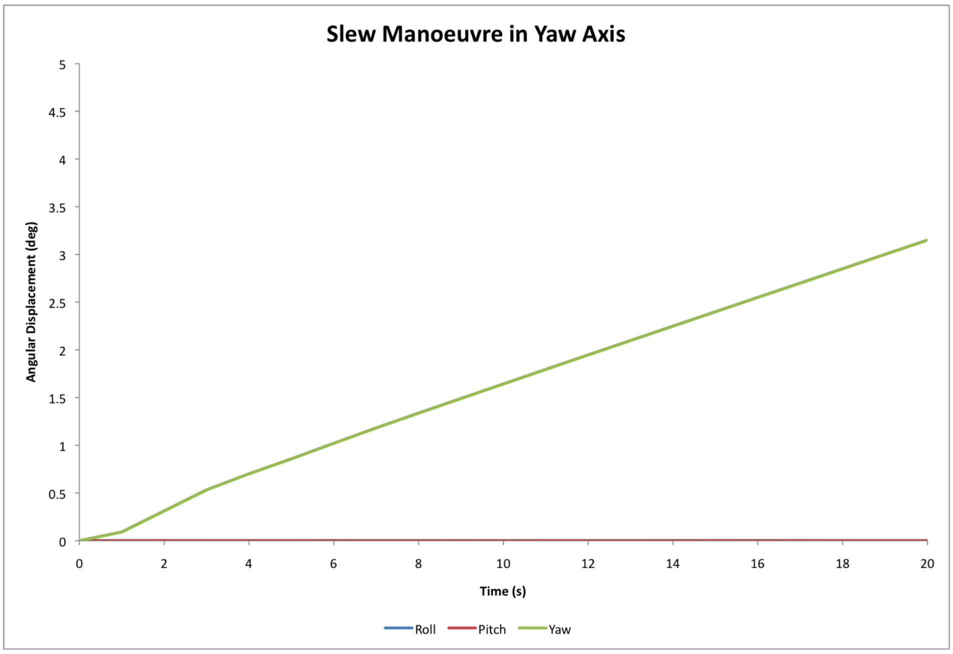

Figure 7.6: Slew manoeuvre in yaw axis using PD control

The following gains were used for the PD control of the satellite needed to accomplish a slew manoeuvre in the pitch and yaw axes.

$$K_P = \begin{bmatrix} 3 & 0 & 0 & 10 & 0 & 0 \\ 0 & 4 & 0 & 0 & 10 & 0 \\ 0 & 0 & 3 & 0 & 0 & 5 \end{bmatrix}$$

$$K_D = \begin{bmatrix} 3 & 0 & 0 & 5 & 0 & 0 \\ 0 & 4 & 0 & 0 & 5 & 0 \\ 0 & 0 & 5 & 0 & 0 & 1 \end{bmatrix}$$

Figure 7.7 shows that classical control techniques can be used to accomplish a 90° slew in both the pitch and the yaw axes whereas Figure 7.8 again shows the transient response.

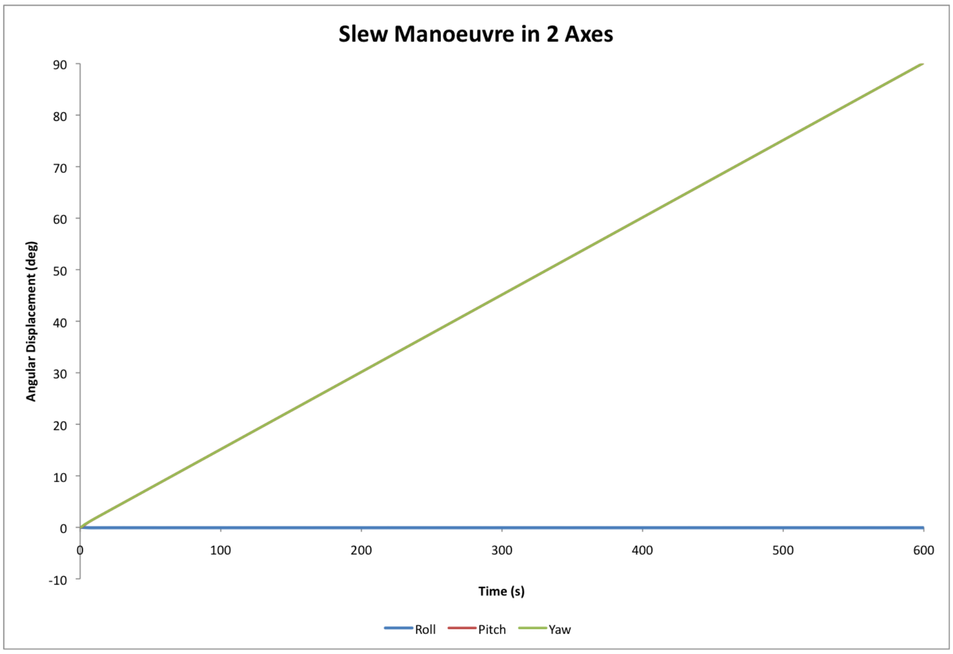

Figure 7.7: Slew manoeuvre in pitch and yaw axes using PD control

Figure 7.8: Slew manoeuvre in pitch and yaw axes using PD control

Finally, the following gains were used for a slew manoeuvre in all three axes using PD control.

$$K_P = \begin{bmatrix} 4 & 0 & 0 & 8 & 0 & 0 \\ 0 & 4 & 0 & 0 & 8 & 0 \\ 0 & 0 & 5 & 0 & 0 & 5 \end{bmatrix}$$

$$K_D = \begin{bmatrix} 3 & 0 & 0 & 5 & 0 & 0 \\ 0 & 4 & 0 & 0 & 5 & 0 \\ 0 & 0 & 5 & 0 & 0 & 1 \end{bmatrix}$$

Figure 7.9 shows the position response of the satellite, demonstrating the ability to compete a slew in all three axes using PD control. Figure 7.10 again shows the transient response in all three axes.

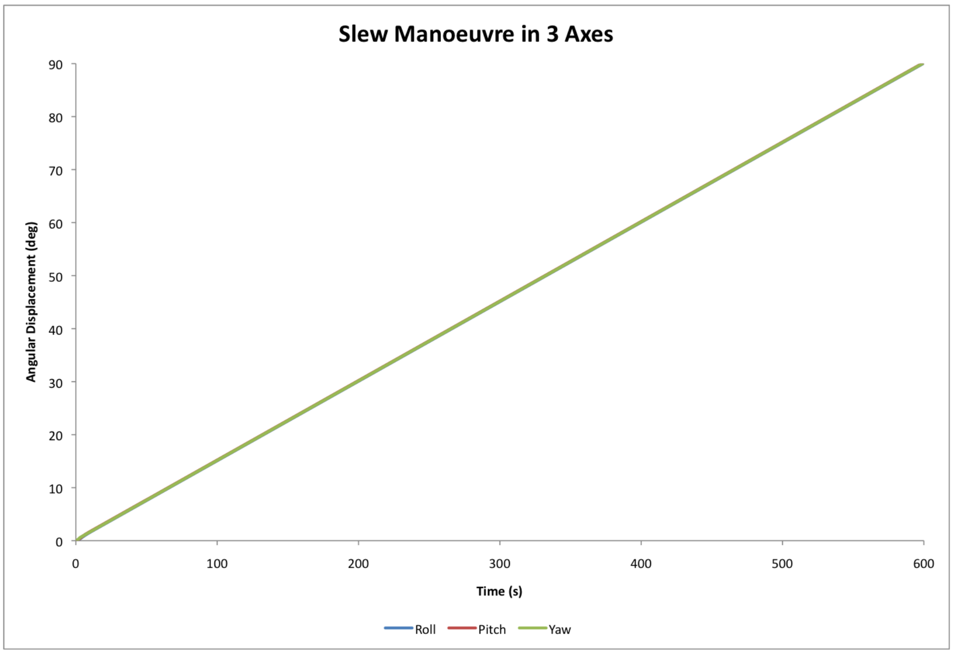

Figure 7.9: Slew manoeuvre in all three axes using PD control

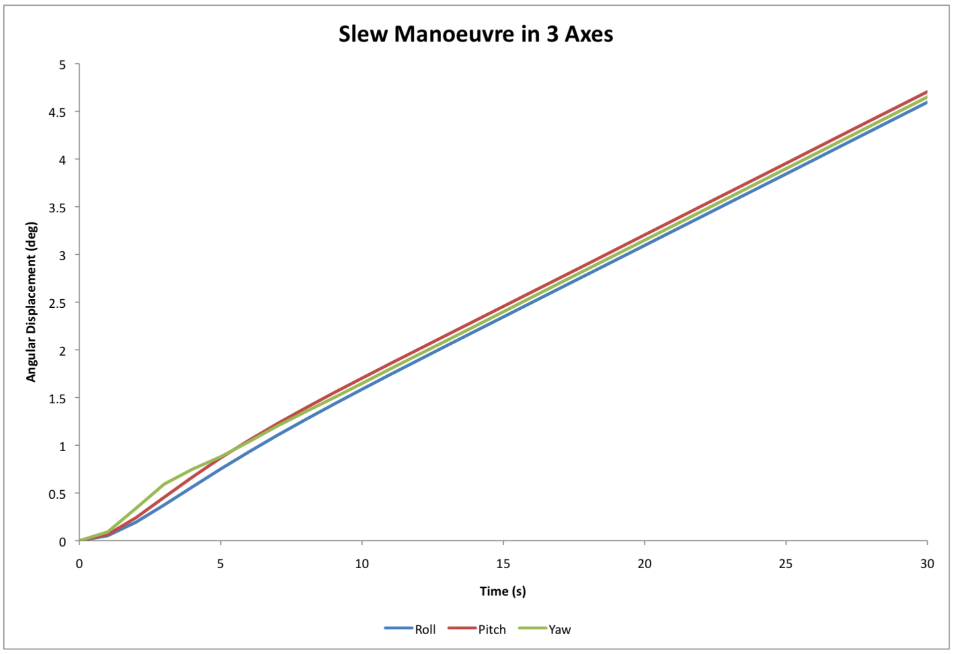

Figure 7.10: Slew manoeuvre in all three axes using PD control

The above simulation results show that PD control, with the introduction of probabilistic constraints, can control FalconSAT-5 for all the necessary control modes.

Chapter 8

Comparison Between Classical Control and Model Predictive Control for FalconSAT-5

The simulations in Chapter 6 showed that FalconSAT-5 can be controlled through the use of model predictive control methods, whereas those in Chapter 7 showed the ability to control the satellite using PD control. The following chapter compares the performance of the classical control techniques and model predictive control for all three control modes. As before, all of these results are the mean response over 200 realizations of disturbances and uncertainties.

8.1 Means of Comparison

When determining which method is superior, it is necessary to consider what criteria are important for satellite control. For control of FalconSAT-5 the two most important criteria are convergence time, the time it takes for the state to reach the final desired state, and control input required. Because the control input is directly proportional to the power required for control, the control input is used as a comparison for power required. Therefore it is these two categories that will be used to compare the performance of the control of FalconSAT-5 using model predictive control and PD control.

The cost of control for each method provides another means of comparison. For the pointing and slew examples, the state does not converge to zero and therefore the stage cost will settle on a non-zero value. Because of this, the cost will not be calculated over the entirety of the time control is operated, but only over the time it takes for the system to reach steady state. If i_{ss} is defined as the time at which the system reaches within 2% of steady state, the cost is calculated as follows:

$$J = \sum_{t=0}^{i_{ss}} (x_i^T Q x_i + u_i^T R u_i) \tag{8.1}$$

8.2 Detumble Control

Figures 8.1 and 8.2 show the angular position and angular velocity response for control in the detumble mode.

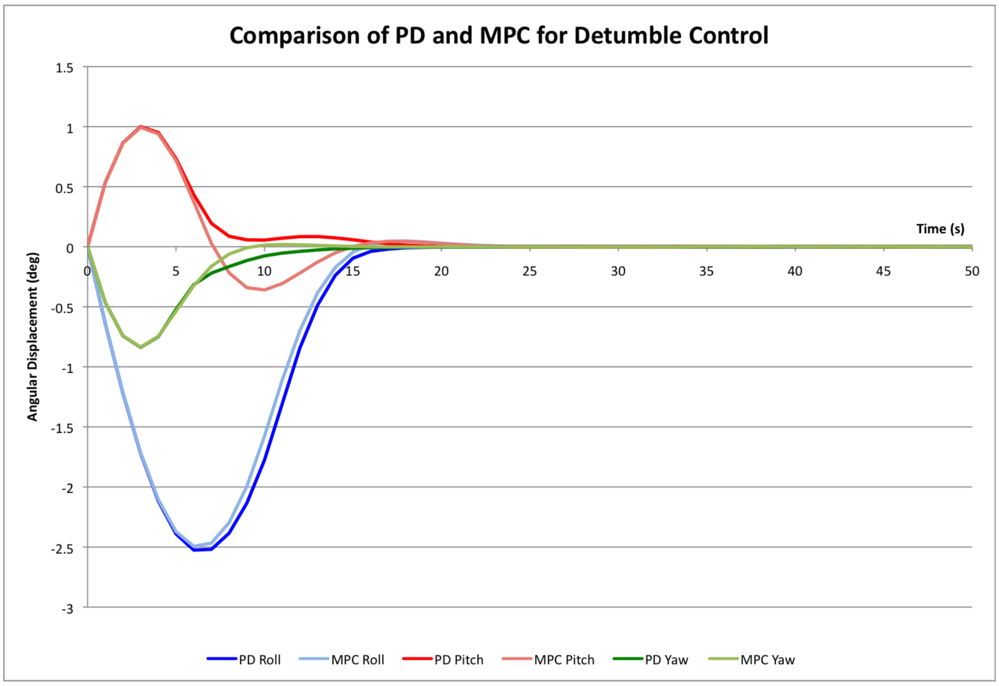

Figure 8.1: Comparison of angular displacement for detumble mode for PD and MPC methods

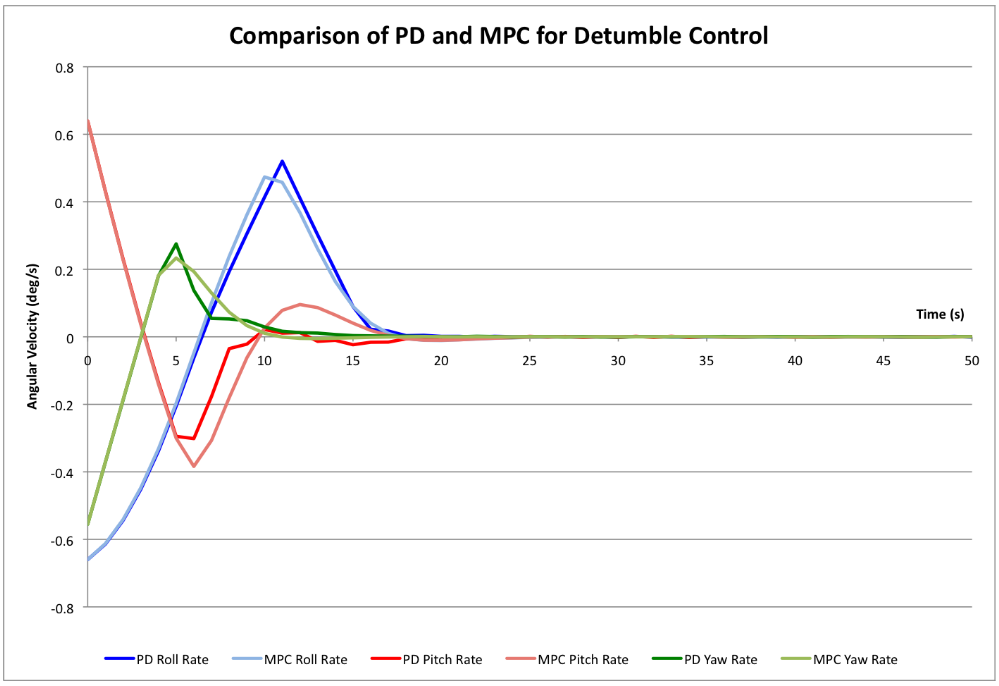

Figure 8.2: Comparison of angular velocity for detumble mode for PD and MPC methods

The presence of uncertainty means that the system will not achieve the desired steady state exactly. Therefore, time of convergence will be defined as time it takes for the state to reach within 2% of the desired steady state. In the roll and yaw axes, the model predictive control method converges faster than the PD method. In the pitch axis, however, the PD method converges faster than the model predictive control method. While the PD method does converge faster in one single axis, the entire state converges to within 2% of the desired zero final state faster for the model predictive control method than for the PD control. This convergence is demonstrated in Figures 8.3 and 8.4. Figure 8.5 shows the input required for the detumble phase for both model predictive control and PD control.

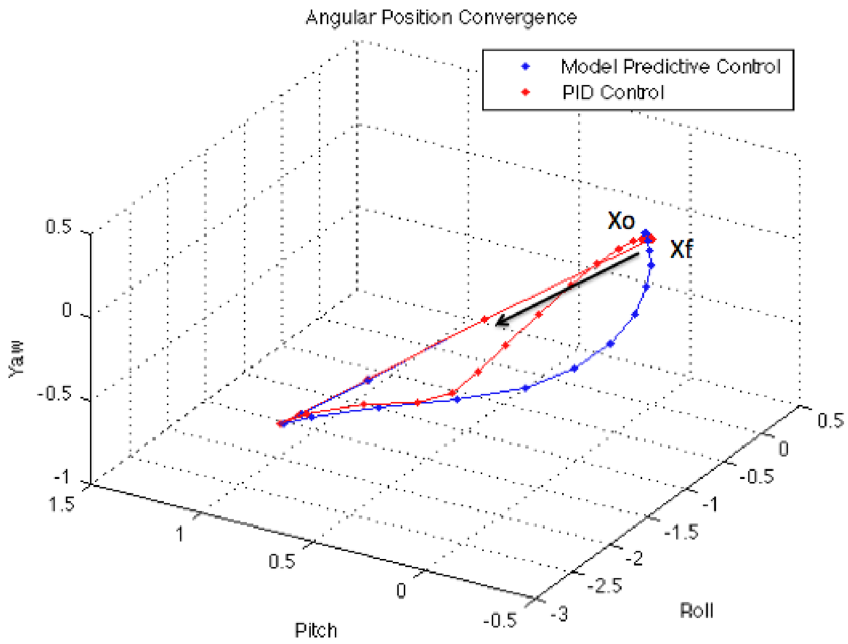

Figure 8.3: Angular position convergence for detumble mode for PD and MPC methods

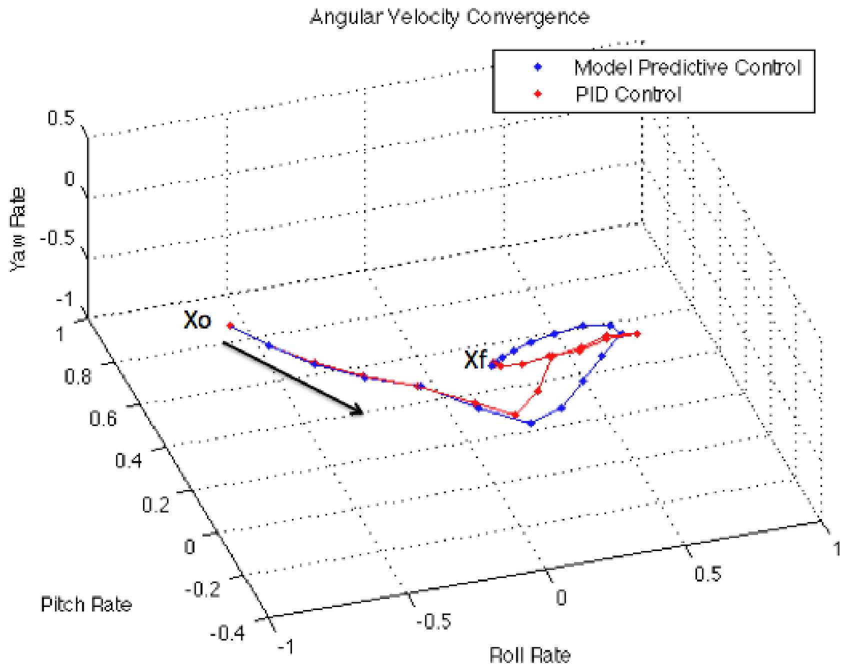

Figure 8.4: Angular velocity convergence for detumble mode for PD and MPC methods

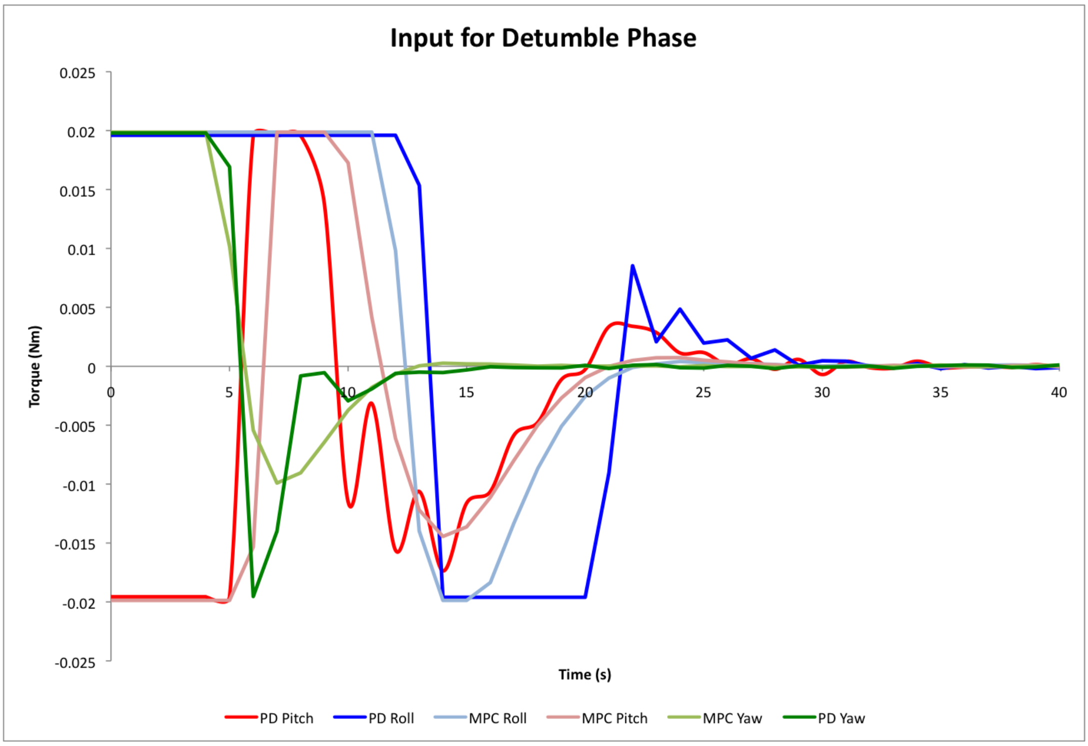

Figure 8.5: Control input required for detumble mode for PD and MPC methods

Table 8.1 shows the average total control input required to control the system for 200 realizations of uncertainty. Less control is needed for the model predictive control method than is needed for the PD control method.

Table 8.1: Comparison of Control Input Required for 200 Realizations of Uncertainty for Model Predictive Control and PD Control for Detumble Mode

Method	Average Total Control Input Required
Model Predictive Control	.7960 Nm
PD Control	.8999 Nm

Table 8.2 shows the average cost over 200 realizations of disturbances and uncertainties. The cost for the model predictive control method is slightly lower than the PD control method. This is reasonable because the model predictive control method is superior in both convergence time and total control input required.

Table 8.2: Comparison of Cost for 200 Realizations of Uncertainty for Model Predictive Control and PD Control for Detumble Mode

Method	Average Cost
Model Predictive Control	50.6532
PD Control	52.4839

8.3 Pointing Control

A comparison of the model predictive control and PD control methods for pointing control from a stationary initial state is shown in Figure 8.6. For this first pointing example the model predictive control algorithm settles on the desired final state faster than the PD control in the pitch and yaw axes. Once again, the response of the whole system converges faster on the desired final state using model predictive control than it does using PD control. This convergence is demonstrated in Figure 8.7. Figure F.5, in Appendix F, shows the comparison of the angular velocity response.

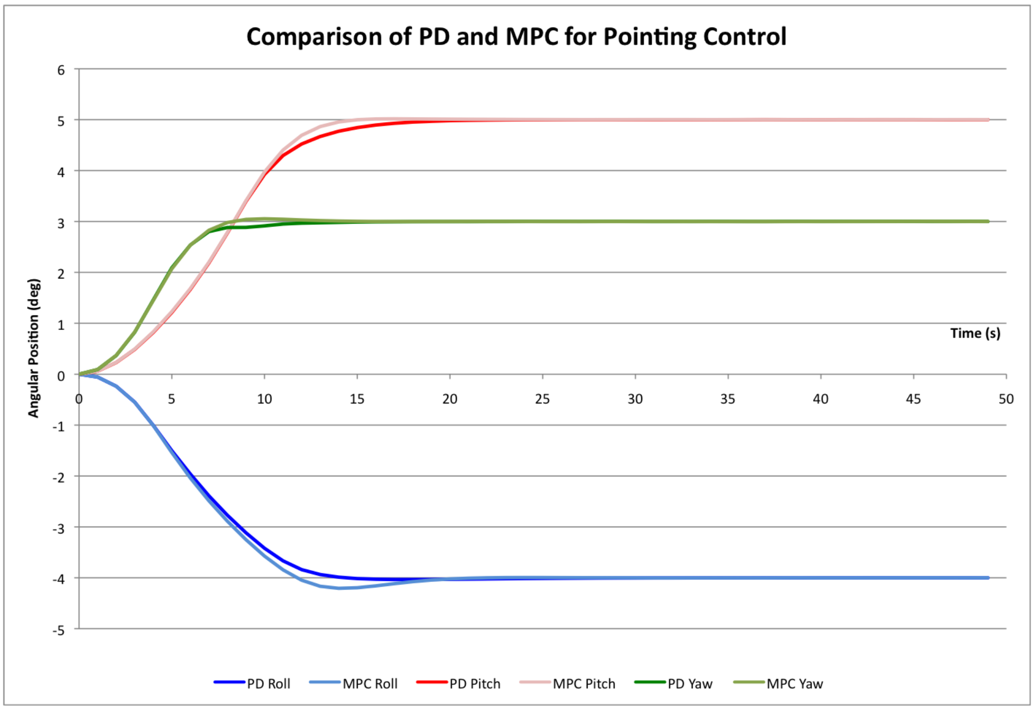

Figure 8.6: Comparison of pointing control from stationary for PD and MPC methods

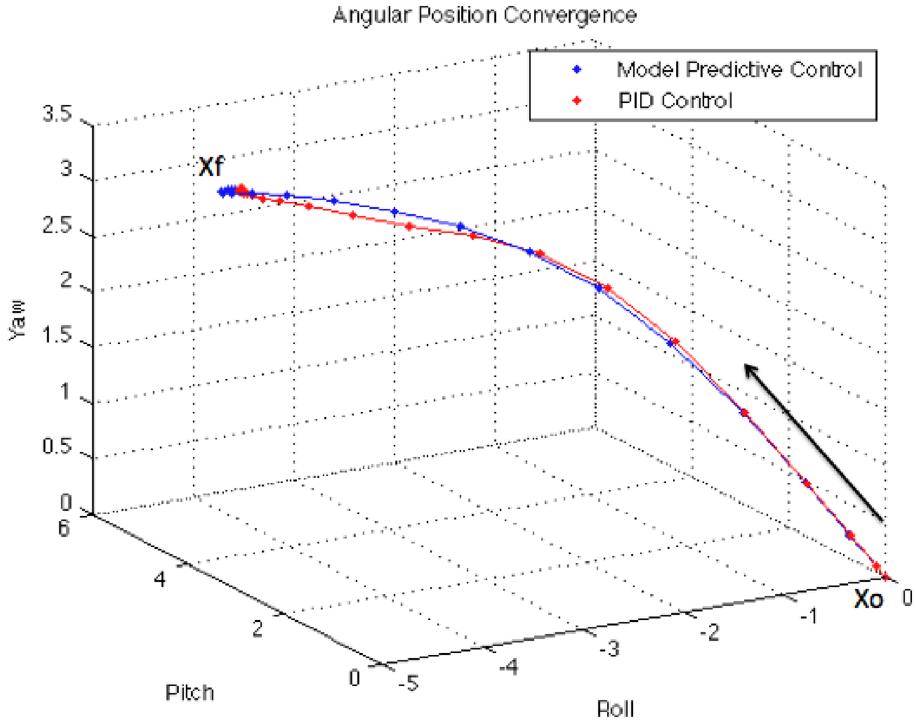

Figure 8.7: Convergence for pointing control from stationary for PD and MPC methods

Again, the model predictive control method requires less control input than the PD control. The control input required is seen in Table 8.3. In terms of cost, the model predictive control method has a lower cost than the PD control. The costs are compared in Table 8.4.

Table 8.3: Comparison of Control Input Required for 200 Realizations of Uncertainty for Model Predictive Control and PD Control for Pointing Control from Stationary

Method	Average Total Control Input Required
Model Predictive Control	.7768 Nm
PD Control	.8160 Nm

Table 8.4: Comparison of Cost for 200 Realizations of Uncertainty for Model Predictive Control and PD Control for Pointing Control from Stationary

Method	Average Cost
Model Predictive Control	492.1022
PD Control	513.9080

For the second pointing example, the model predictive control method converges faster in the roll and yaw axes and exhibits a smaller overshoot in both of those axes. In the pitch axis the PD method converges faster but neither response exhibits any overshoot. The state response is shown in Figures 8.8 and 8.9. Figure F.6, in Appendix F, shows the comparison between the angular velocity response using model predictive control and PD control for the second pointing example.

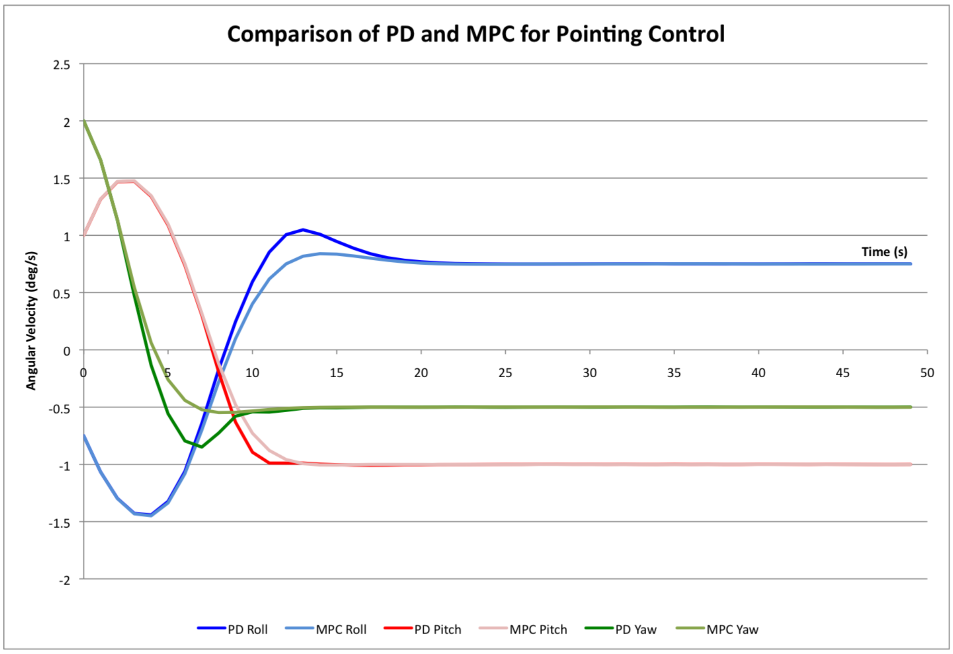

Figure 8.8: Comparison of pointing control from non-zero initial conditions for PD and MPC methods

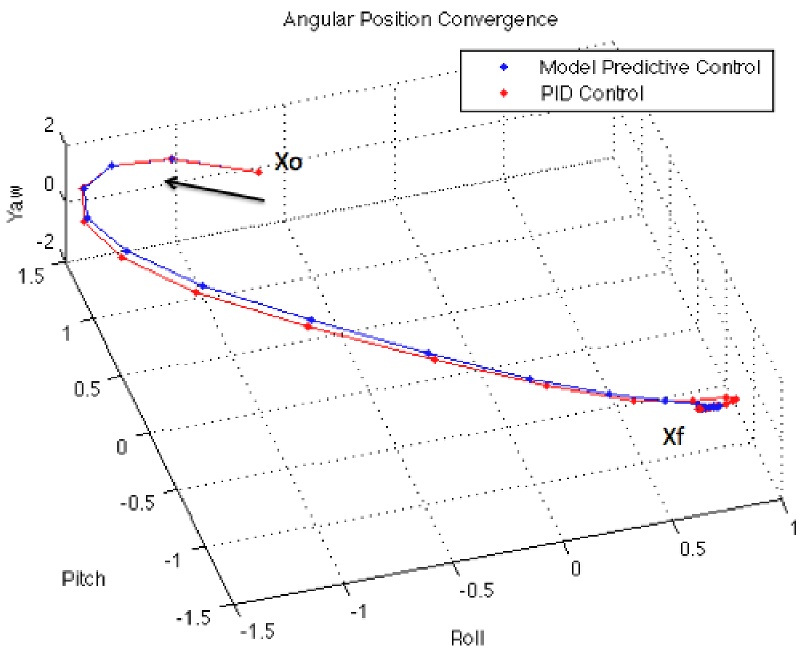

Figure 8.9: Convergence for pointing control from non-zero initial conditions for PD and MPC methods

Again, for this example, the model predictive control method requires less control input than the PD control method. This control input comparison is seen in Table 8.5.

Table 8.5: Comparison of Control Input Required for 200 Realizations of Uncertainty for Model Predictive Control and PD Control for Pointing Control from Non-zero Initial Conditions

Method	Average Total Control Input Required
Model Predictive Control	.6320 Nm
PD Control	.7501 Nm

Just as is seen with the previous examples, the superior convergence and control input required for the model predictive control method results is a lower cost than for the PD control. These values are shown in Table 8.6.

Table 8.6: Comparison of Cost for 200 Realizations of Uncertainty for Model Predictive Control and PD Control for Pointing Control from Non-zero Initial Conditions

Method	Average Cost
Model Predictive Control	50.3173
PD Control	53.9817

8.4 Control Input and Cost Comparison

Because the values of the control input required and the costs differ for each method, a comparison of just the values for the model predictive control and PD control methods does not provide a complete analysis of the difference in performance for the two methods. Tables 8.7 and 8.8 show the percent increase in the control input required and the cost between the model predictive control and PD control methods for the detumble mode and both pointing examples. This comparison of the percent increases shows that, for these examples, the model predictive control performs better than the PD control in terms of control input required and cost.

Table 8.7: Percent Increase in Control Input Required Between Model Predictive Control and PD Control

Control Mode	MPC Input	PD Input	% Increase
Detumble	.7960	.8999	13.02%
Pointing 1	.7769	.8160	5.03 %
Pointing 2	.6320	.7501	18.69 %

Table 8.8: Percent Increase in Cost Between Model Predictive Control and PD Control

Control Mode	MPC Cost	PD Cost	% Increase
Detumble	50.6532	52.4839	3.53%
Pointing 1	492.1022	513.9080	4.43 %
Pointing 2	50.3173	53.9817	7.28 %

8.5 Slew manoeuvre

The simulations in Chapters 6 and 7 demonstrated that both control methods are capable of executing a slew manoeuvre in one, two, or all three axes. While the position response for both methods is virtually indistinguishable, the time it takes for the angular velocity to settle on the desired slew rate differs between the model predictive control and PD control methods. For the slew manoeuvre in one axis (Figure 8.10), the model predictive control method settles on the desired slew rate faster, and has less overshoot, than the PD control method. For the two-axis slew manoeuvre (Figure 8.11), the yaw rate again settles faster for the model predictive control method whereas, in both the pitch and yaw axes, the PD control response undulates while trying to reach the steady state. The PD control method does keep the roll rate closer to the desired zero than the model predictive control method but, as seen with the previous examples, the angular velocity settles on the desired state in all three axes faster for the model predictive control method than the PD control method. Finally, for the three-axis slew manoeuvre (Figure 8.12), the response of the model predictive control method converges faster than the PD response in both the roll and yaw axes. While the pitch axis converges slightly faster for the PD method, it exhibits oscillation before settling that is not seen in the model predictive control method. Additionally, the PD response exhibits more overshoot and oscillation than the model predictive control response in all three axes.

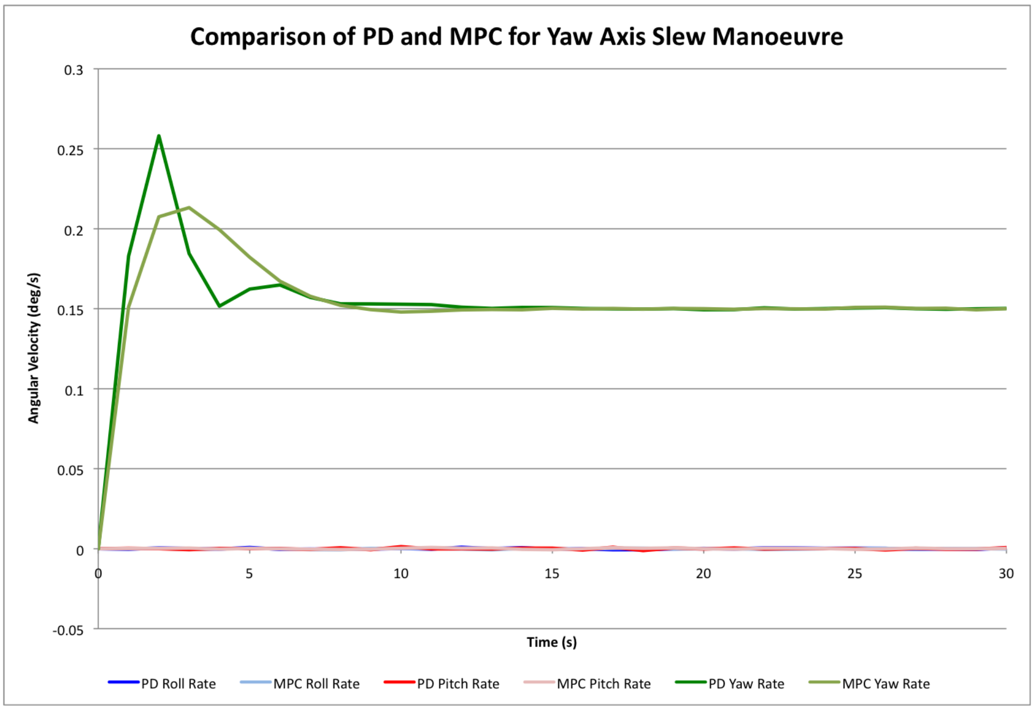

Figure 8.10: Comparison of angular velocity for yaw slew manoeuvre for PD and MPC methods

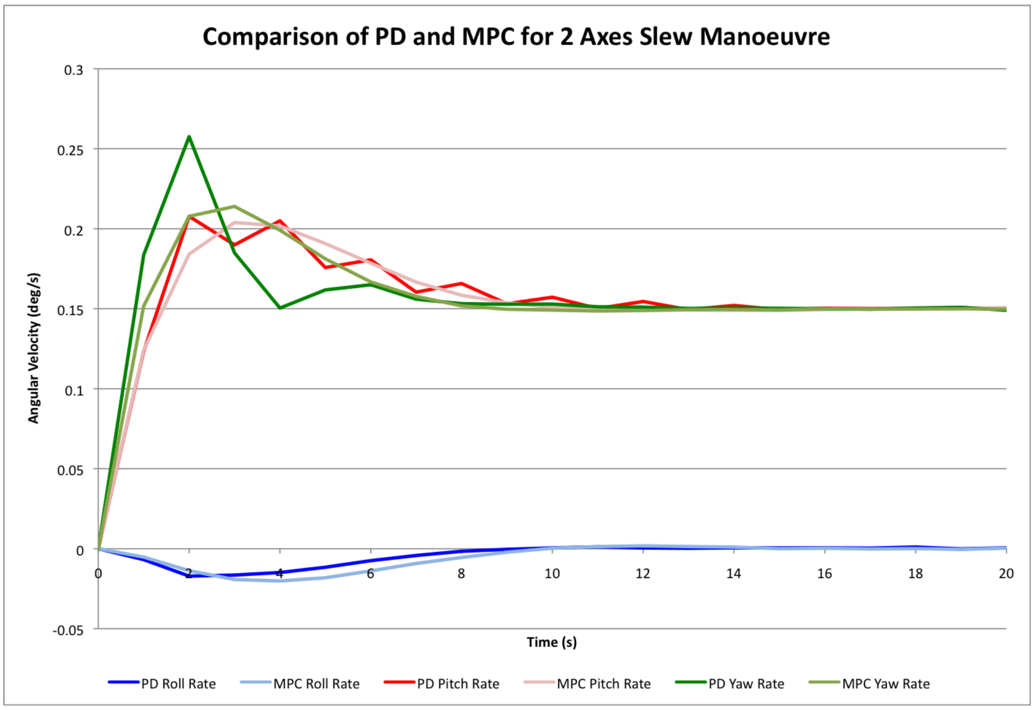

Figure 8.11: Comparison of angular velocity for 2-axis slew manoeuvre for PD and MPC methods

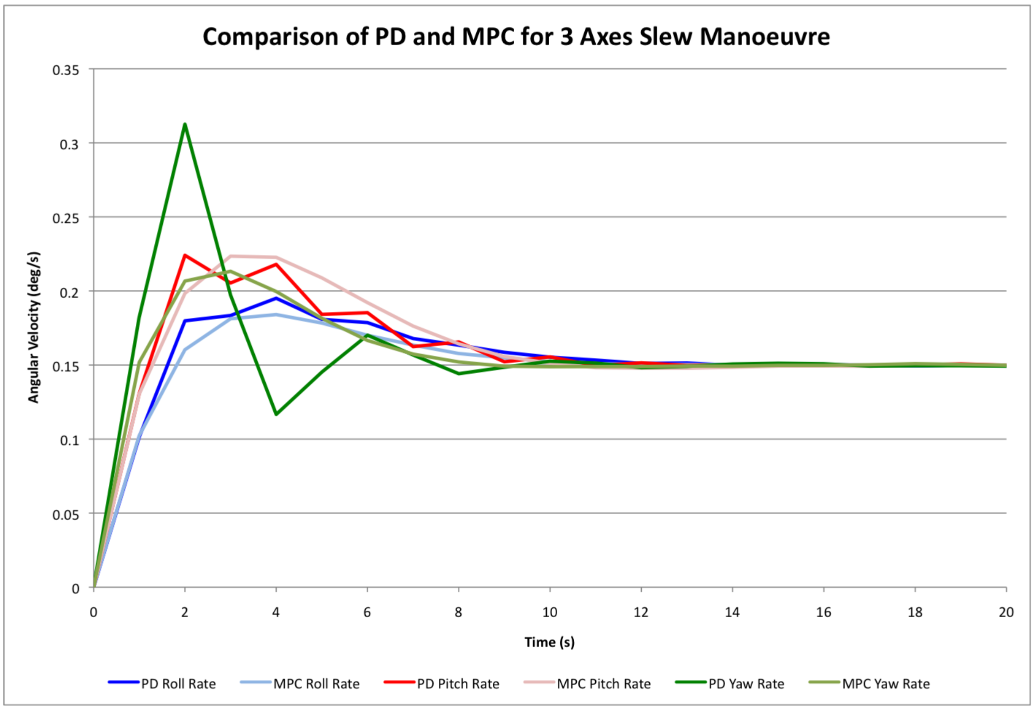

Figure 8.12: Comparison of angular velocity for 3-axis slew manoeuvre for PD and MPC methods

8.5.1 Control Input and Cost Comparison

Table 8.9 shows the control input required, as well as the percent increase, for the slew manoeuvres in all three axes.

Table 8.9: Control Input Required and Percent Increase in Control Input Between Model Predictive Control and PD Control for Slew Manuevers

Control Mode	MPC Input	PD INput	% Increase
1 Axis Slew	.0379 Nm	.0475 Nm	25.33%
2 Axes Slew	.1416 Nm	.1698 Nm	16.22%
3 Axes Slew	.2124 Nm	.2521 Nm	18.69%

Table 8.10 shows the cost of the three slew manoeuvres for both model predictive control and PD control as well as the percent increase between the two methods. Rather than using the cost over the entire 600 seconds, the cost is calculated for the time that it takes for the angular velocity to reach steady state.

Table 8.10: Costs and Percent Increase in Cost Between Model Predictive Control and PD Control for Slew Manuevers

Control Mode	MPC Cost	PD Cost	% Increase
1 Axis Slew	8.3871	11.0825	37.16%
2 Axes Slew	21.7382	28.2065	29.76%
3 Axes Slew	32.1982	42.4938	31.98%

The cost of the model predictive control method is lower than the PD control method for all three slew manoeuvres. The percent increase is significantly higher for the slew manoeuvres than for the other control modes. This is because of the fact that the angular velocity of the system does not converge to zero and therefore the stage cost does not converge. If the PD method takes even one time step more to converge to within 2% of steady state for the angular velocity, the change in the state value in that time results in a greater difference in cost between the model predictive control and PD control methods than in the examples in which the final angular velocity is zero.

8.6 Additional Comparisons

8.6.1 Tightened Constraints

Simulations with the current constraint settings demonstrate the superiority of the model predictive control method over the PD method for all the prescribed control modes. If the constraints are tightened, the superiority increases and the system response for the PD control fails to meet the requirements. Using a control limit of $u = .018$ N and a probability $p = .9$, the model predictive control law is able to control the satellite in the detumble phase whereas the PD control is not. Figures 8.13 and 8.14 show the response for this example and demonstrate how the model predictive control method is able to control the system in instances where the PD control method is not.

Figure 8.13: Comparison of position response for detumble for PD and MPC methods

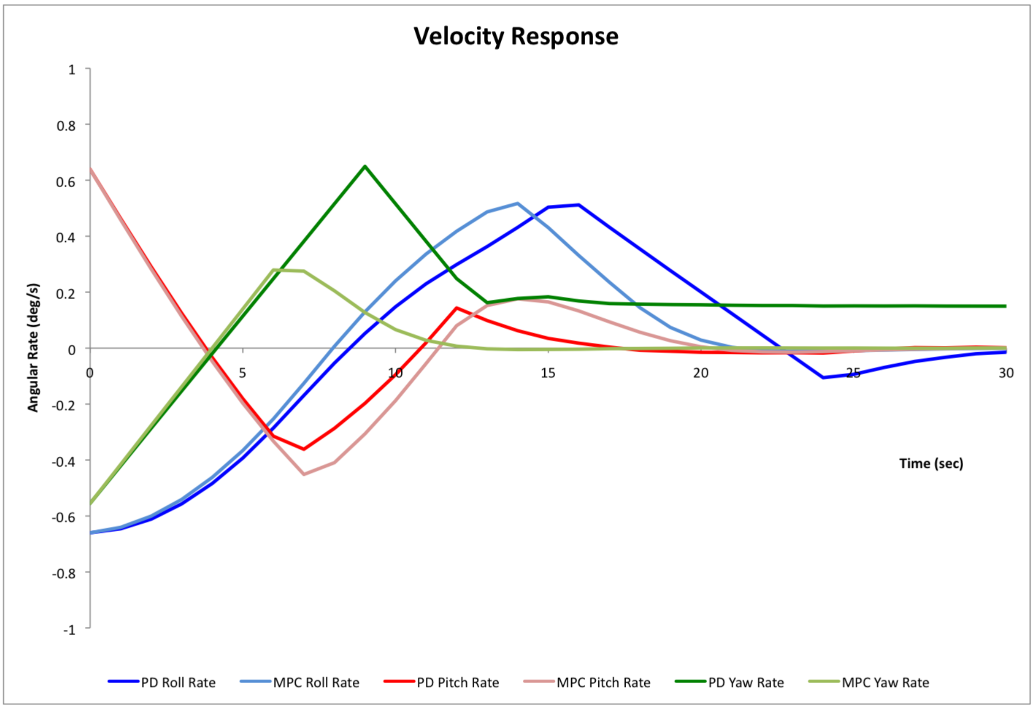

Figure 8.14: Comparison of velocity response for detumble for PD and MPC methods

8.6.2 Computational Complexity

While the model predictive control method is superior to the PD method in terms of performance, model predictive control is computationally complex and requires an online optimization at each time. The PD method is less computationally complex but requires significant tuning to acheive optimal results. While the complexity of the model predictive control method is greater than that of the PD method, the majority of the calculations can be completed offline, thereby causing only a minimal increase in the computational complexity.

Chapter 9

Thesis Review and Conclusions

This thesis outlined several different model predictive control techniques as an introduction to the implementation of model predictive control for the control of a small satellite, FalconSAT-5. Chapter 2 described a method of model predictive control that uses the distribution of the stochastic disturbances to construct a series of probabilistic tubes in which the future states of the system must lie in order to meet the constraints [Kouvaritakis et al., 2010a]. The results of this method were compared to the unconstrained linear quadratic regulator method and a clipped linear quadratic regulator. While these linear quadratic methods had lower costs than the model predictive control method, they violated the probabilistic constraints.

Chapter 3 built on the method in Chapter 2 to handle systems that exhibit both disturbances and measurement errors by considering the measurement errors in the construction of the constraints. Comparisons with the baseline MPC method used in Chapter 2 showed that while the cost of the MPC with error consideration was higher than the baseline MPC method, the probabilistic constraint was violated for the baseline MPC method in the presence of measurement uncertainty. Therefore, when the system exhibits measurement error, it is necessary to consider those errors in the constraint definition.

Chapter 4 attempted to avoid the problem of measurement errors by using an estimator for the states rather than a state measurement [Cannon et al., 2012]. This MPC with estimation method was compared to the MPC with error consideration method. These comparisons showed that the relative effectiveness of the two methods was dependent upon the relative effects of the disturbances and measurement errors. If the effect of the disturbances was greater than the effect of the measurement errors, the MPC with error consideration method was the better control technique. However, if the measurement errors had a greater effect on the system response than the disturbances, the MPC with estimation method was a more effective method of control.

Chapter 5 introduced FalconSAT-5 and discussed the aspects of the satellite that made it ideal for stochastic model predictive control. It described the various control modes needed for succesful satellite operation and described the disturbances and measurement errors present in the system. Chapter 5 also described the development of the FalconSAT-5 dynamic model used for the implementation of the control techniques.

Simulations in Chapter 6 and Chapter 7 showed that both model predictive control and classical control techniques can be used to control FalconSAT-5. The simulations in Chapter 6 showed that stochastic model predictive control methods can meet all the control requirements prescribed for succesful payload implementation and satellite operation for all three control modes. Chapter 7 showed that classical control techniques in the form of proportional-derivative (PD) control can be used to accomplish control of the satellite in all three control modes. The simulations in this chapter introduced the concept of probabilistic constraints to PD control and clipped the input post-calculation to ensure those constraints were met.

9.1 Conclusion

The comparison between the stochastic model predictive control and the PD control in Chapter 8 showed that for the control of FalconSAT-5, model predictive control is superior to PD control. In general, the model predictive control method considers the constraints when calculating the control law, thus providing optimal results. The PD controller ignores the constraints and calculates a control input which is constrained after the fact in order to meet the prescribed constraints. This leads to a sacrifice in performance and results in suboptimal control. This was demonstrated through simulations of all three control modes.

For the detumble phase, the model predictive control method settled on the desired final state faster than the PD control method. For the pointing control examples, the model predictive control method again converged on the desired final position faster than the PD control. Finally, whereas the position performance of the slew manoeuvres was comparable, and each method was capable of completing the necessary slew manoeuvres, the angular velocity response of the model predictive control method converged on the necessary slew rate faster than the PD control method. By using model predictive control, the satellite control system is able to acheive control at a faster rate than the current PD control scheme. This leads to more time for payload implementation, solar panel exposure, or other general housekeeping operations. Furthermore, the less time the reaction wheels are operating, the more power is saved, resulting in more managable power consumption.

In terms of the total control input required, the model predictive control method is superior to the PD control method for all the control modes simulated. The lower control input required leads to a lower power drain from the reaction wheels, thereby helping with the overall power budget.

A comparison of the costs of the model predictive control and PD control techniques also demonstrated the superiority of the model predictive control methods. For all the control modes simulated, the model predictive control method had a lower cost. A further simulation was included which demonstrated that there are instances in which the PD control is unable to meet the prescribed control requirements whereas the model predictive control was able to control the system. While model predictive control is computationally more complex than the classical control techniques, the majority of the model predictive control calculations can be completed offline, thereby keeping the additional computational cost at a minimum.

The simulations showed that, not only can stochastic model predictive control techniques be used to control the small satellite FalconSAT-5, but they can provide a more effective means of control than classical control techniques.

9.2 Future Research

There is current research being conducted in model predictive control that deals with the introduction of the knowledge of future disturbances into the development of the model predictive control law [Kouvaritakis et al., 2010b] [Kouvaritakis et al., 2011]. While the future disturbances are unknown at the prediction times, they will be measurable by the time the control is implemented and therefore those known disturbance values can be factored into the calculation of the constraints. A vein of future research would be to examine ways in which this method could be implemented even in the presence of measurement errors.

Appendix A

Linear Quadratic Regulator Simulation Results

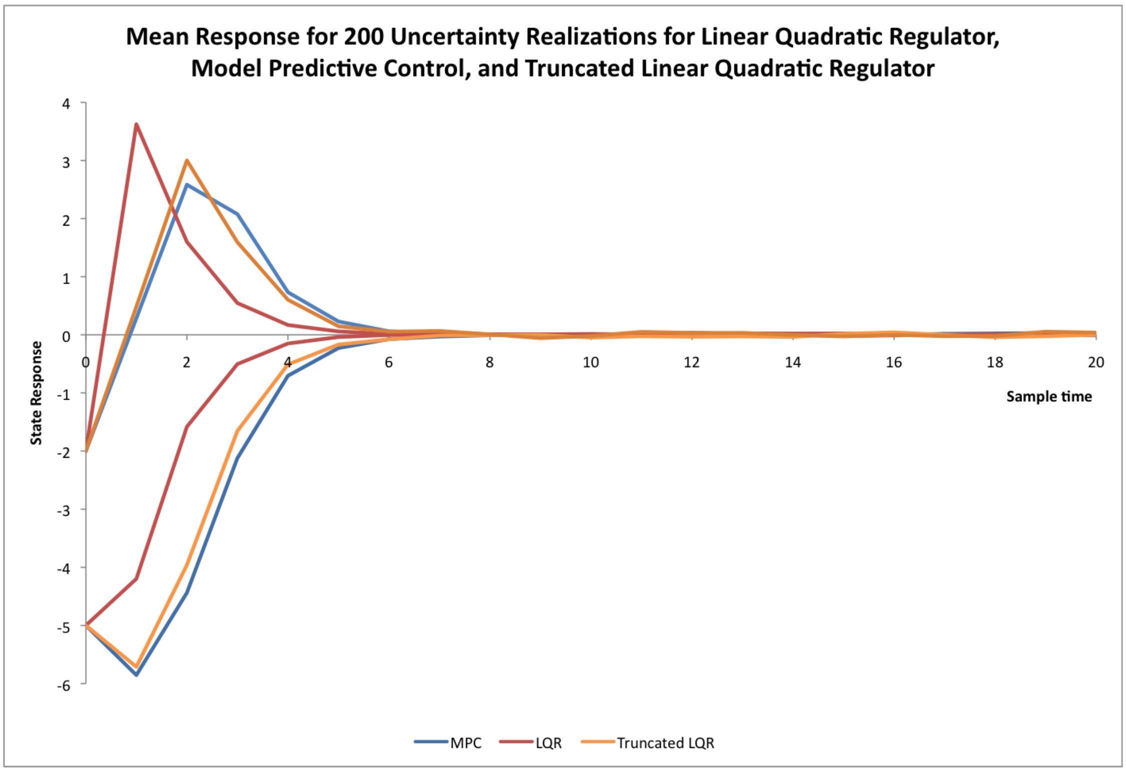

Figure A.1: Mean state response for 200 realizations of uncertainty for linear quadratic regulator, model predictive control, and clipped linear quadratic regulator control methods

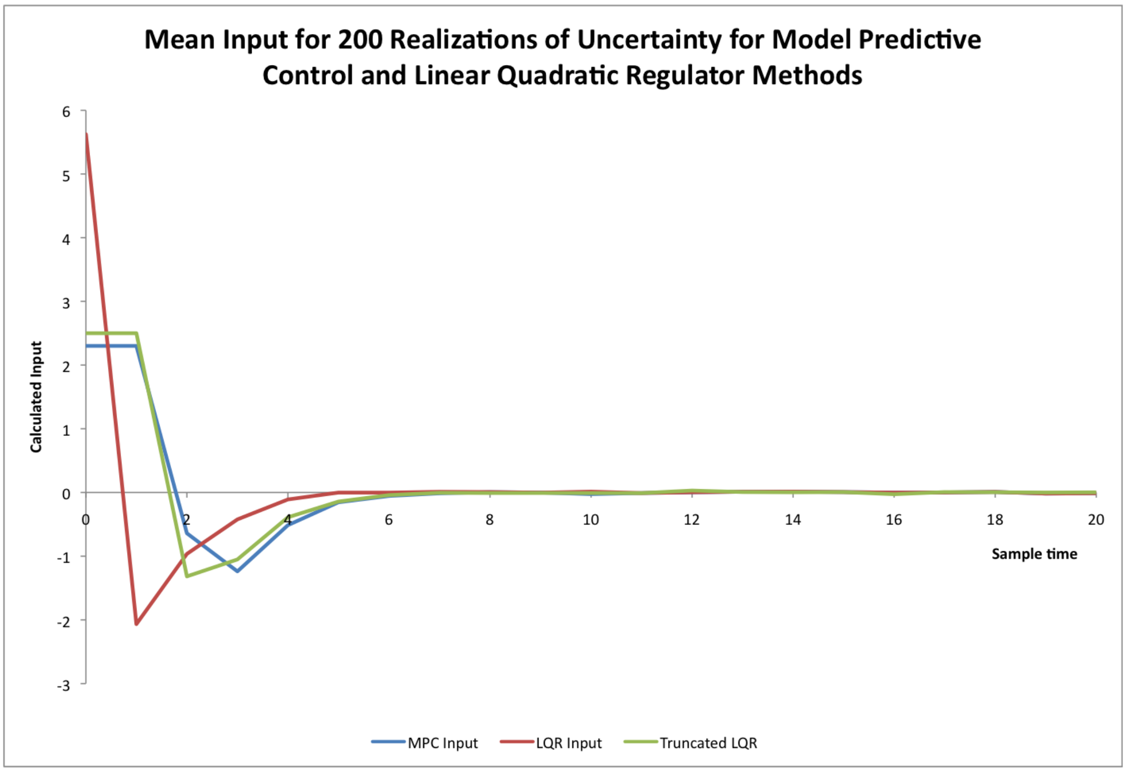

Figure A.2: Mean input for 200 realizations of uncertainty for linear quadratic regulator, model predictive control, and clipped linear quadratic regulator control methods

Appendix B

FalconSAT-5 Payload and Control Requirements

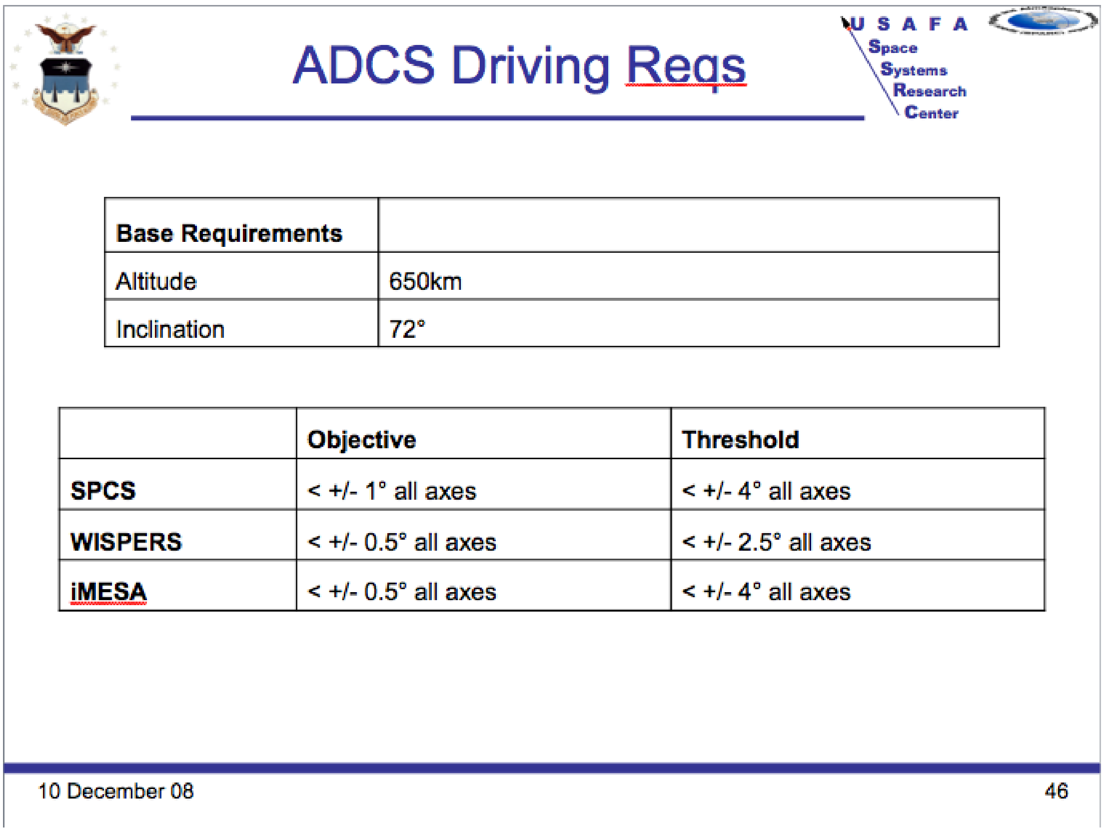

U S A F A
Space
Systems
Research
Center

ADCS Driving Reqs

Base Requirements	
Altitude	650km
Inclination	72°

	Objective	Threshold
SPCS	< +/- 1° all axes	< +/- 4° all axes
WISPERS	< +/- 0.5° all axes	< +/- 2.5° all axes
iMESA	< +/- 0.5° all axes	< +/- 4° all axes

10 December 08 46

Figure B.1: FalconSAT-5 ADCS driving requirements

ADCS CONOPS

USAFA Space Systems Research Center

Commissioning Phase	
De-tumble phase	Attitude/rate acquisition
	Detumble – torque rods (B-dot controller)
Stabilization, 3-axis control	Initial dampening of libration motion
	Torque rods and wheel(s)

Normal Operations	
3-Axis stabilization mode	Point in arbitrary direction
Downlink mode	Random/nadir pointing
Slew maneuver	Pointed at ground station during pass (90 deg / 10 min)
Safe hold	Torque rods only
Thermal control mode	Slew about yaw axis
Momentum dumping	Use torque rods to dump stored reaction wheel momentum

10 December 08 47

Figure B.2: FalconSAT-5 ADCS concept of operations (CONOPS)

Appendix C

FalconSAT-5 Calculations

C.1 Constants and Parameters

C.1.1 Orbital Parameters

$R_{earth} = 6378000$ m

$alt_{sat} = 650,000$ m

$r_{sat} = R_{earth} + alt_{sat} = 7228000$ m

Earth standard gravitational constant $= \mu = 3.985 \times 10^5 \frac{\text{km}^3}{\text{s}^2} = 3.985 \times 10^{14} \frac{\text{m}^3}{\text{s}^2}$

$\omega_{orbit} = \sqrt{\frac{\mu}{r_{sat}^3}} = .0011 \frac{\text{rad}}{\text{s}}$

C.1.2 Satellite Parameters

$$m_{RW} = 1.7 \text{ kg } r_{RW} = .0575 \text{ m } I_{RW} = \tfrac{1}{2}mr^2 = .0028 \text{ kgm}^2$$
$$\max(\omega_{RW}) = 5000 \text{ rpm} = 526.6 \tfrac{\text{rad}}{\text{s}}$$

$$I_{sat} = \begin{bmatrix} 12.77 & 0 & 0 \\ 0 & 11.15 & 0 \\ 0 & 0 & 7.59 \end{bmatrix} \text{kgm}^2$$

C.1.3 Coordinate Transforms

$$C_1 = \text{Rot}_3(\pi)\text{Rot}_2(\frac{\pi}{2})$$
$$C_2 = \text{Rot}_1(\frac{\pi}{2})$$

C.2 Disturbance Torques

C.2.1 Gravity Gradiant Torque

$$T_{gg} = \begin{bmatrix} \frac{3\mu|I_3 - I_2|}{r^3} \\ \frac{-3\mu|I_1 - I_3|}{r^3} \\ \frac{3\mu|I_2 - I_1|}{r^3} \end{bmatrix}$$

$$T_{gg} = \begin{bmatrix} -1.127 \times 10^{-5} \\ 1.6399 \times 10^{-5} \\ -5.1287 \times 10^{-5} \end{bmatrix} \text{Nm}$$

C.2.2 Solar Radiation

$$F_s = 1367\frac{\text{W}}{\text{m}^2} \; A_s = \text{surface area}$$
$$q = \text{reflectance factor} \approx .6 \; i = \text{ incidence angle} = 0$$
$$T_{sr} = \frac{F_s}{c} A_s(1+q)\cos i$$

$$T_{sr} \approx \begin{bmatrix} 3.26 \times 10^{-6} \\ 2.76 \times 10^{-6} \\ 2.52 \times 10^{-6} \end{bmatrix} \text{Nm}$$

C.2.3 Magnetic Field Torque

$$D = .1\text{Am}^2 \; M = 7.96 \times 10^{15}\text{Teslam}^3$$
$$T_m = DB = D\frac{2M}{r_{sat}^3}$$

$$T_m = \begin{bmatrix} 4.07 \times 10^{-6} \\ 4.07 \times 10^{-6} \\ 4.07 \times 10^{-6} \end{bmatrix} \text{Nm}$$

C.2.4 Aerodynamic Torque

$$\rho = \text{atmospheric density} \; C_d = \text{drag coefficient} \; A_s = \text{surface area}$$
$$v = \text{velocity} \; c_{pa} = \text{centre of atmospheric pressure} \; c_g = \text{centre of gravity}$$
$$T_a = .5(\rho C_d A_s v^2)(c_{pa} - c_g)$$

$$T_m = \begin{bmatrix} 2.1 \times 10^{-8} \\ 1.77 \times 10^{-8} \\ 1.62 \times 10^{-8} \end{bmatrix} \text{Nm}$$

Appendix D

Power Specifications

D.1 Power Modes

There are 6 different orbits for satellite operation and each has a different power draw. These orbits are described by their purpose and are given a numerical designation of PM (Power Mode) 1-PM6. Each orbit takes 97 minutes and the reaction wheels are operated for different amounts of time based on the specific orbit used. The following table shows the various power modes and the power draw from the reaction wheels for each power mode.

Table D.1: Power Modes

PM	Purpose	Power Draw
PM1	Survey	2425 Wmin
PM2	Sun Pointing	7275 Wmin
PM3	Acquisition	750 Wmin
PM4	Survey and Downlink	2425 Wmin
PM5	Sun Pointing and Downlink	7275 Wmin
PM6	Maintenance	7275 Wmin

D.2 Satellite Mission Life

The satellite lifespan is a minimum of 3 years and operation of the satellite occurs in cycles of 14 orbits. There are several different cycles of operation, each requiring a different power draw. The worst case orbital cycle uses a total power draw of 1209 Whr over the cycle, an average of 86.300 Whr per orbit. This, assuming the orbital cycle with worst case power draw was used at all times, would result in a power draw of 1.405 MWhr over the course of the satellite operation.

D.3 Savings from Probabilistic Contraints

By constraining the reaction wheels to 80 % of maximum power, a total of 281.087 kWhr can be saved over the course of satellite operation. This equates to an average of 10.69 W per orbit.

D.4 Discussion

These results are a worst case and assume the power draw of the reaction wheels to be maximum over the course of satellite operation. While the simulation results are particular to probabilistic constraint of 80 % of maximum power at a constraint satisfaction of 80 %, this value can be changed. It would be useful to investigate if, by changing the probabilistic constraint over time, better performance could be acheived. Furthermore, different probabilistic constraints could be used at beginning of life versus end of life, and the constraint value could be changed in orbits when the satellite is in eclipse versus in the sun.

Appendix E

Model Predictive Control for Pointing and Slew Maneuver

The goal of the model predictive algorithms described in Chapters 2, 3, and 4 was to drive the states to zero using a version of the linear quadratic regulator gain with additional free control moves as degrees of freedom. However, when the desired final state is non-zero, the algorithm changes. Rather than attempt to drive x_f to zero, the goal is to drive $x_f - x_g$, the error between the state (x_f) and the desired final state (x_g), to zero [Ming and Hasim, 2010].

Let x_g equal the desired state value and let u_g equal the input needed to maintain that desired set point. The goal now becomes a minimization of the following cost function:

$$J = \sum_{k=0}^{\infty} \mathbb{E}((x_k - x_g)^T Q (x_k - x_g) + (u_k - u_g)^T R (u_k - u_g) - L_{ss}) \tag{E.1}$$

Factoring in the measurement uncertainty and using the closed loop paradigm so that $u_k = K y_k + c$ and $u_g = K x_g$, the cost now becomes:

$$J = \sum_{k=0}^{\infty} \mathbb{E}((x_k + m_k - x_g)^T Q(x_k + m_k - x_g)$$
$$+ (Kx_k + Km_k + c_k - Kx_g)^T R(Kx_k + Km_k + c_k - Ku_g))$$
$$J = \sum_{k=0}^{\infty} \mathbb{E}((x_k - x_g)^T (Q + K^T RK)(x_k - x_g) + (x_k - x_g)^T K^T Rc_k + (x_k - x_g)^T (Q + K^T RK)m_k$$
$$+ c_k^T RK(x_k - x_g) + c_k^T Rc_k + c_k^T RKm_k + m_k^T (Q + K^T RK)(x_k - x_g) + m_k^T K^T c_k$$
$$+ m_k^T (Q + K^T RK)m_k)$$

The state is again augmented, but this time the augmented state vector becomes the following:

$$\chi = \begin{bmatrix} x_k - x_g \\ \bar{c}_k \\ 1 \end{bmatrix} \tag{E.2}$$

Using this state augmentation, the cost now becomes:

$$J = \sum_{k=0}^{\infty} \mathbb{E}(\chi_{k+i}^T \begin{bmatrix} Q + K^T RK & K^T RE & (Q + K^T RK)m_k \\ E^T RK & E^T RE & RKm_k \\ m_k^T (Q + K^T RK) & m_k^T K^T R & m_k^T (Q + K^T RK)m_k \end{bmatrix} \chi_{k+i}) = \sum_{k=0}^{\infty} \mathbb{E}(\chi_{k+i}^T \bar{Q} \chi_{k+i})$$

$$\tilde{Q} = \begin{bmatrix} Q + K^T RK & K^T RE \\ E^T RK & E^T RE \end{bmatrix}$$

Following the explanation found in Chapter 3, the cost of the tracking method can be written in quadratic form as follows:

$$\mathbb{E}(V_k) = \chi_k^T P \chi_k \tag{E.3}$$

$$P_{11} - \tilde{\Psi}^T P_{11} \tilde{\Psi} = \tilde{Q} \tag{E.4}$$
$$P_{22} = -\mathrm{trace}(\Theta P_{11}) \tag{E.5}$$

$$\begin{aligned}\Theta - \tilde{\Psi}\Theta\tilde{\Psi}^T =& ((\Phi^T\Phi - \Phi^T A - A^T\Phi + A^T A)\mathbb{E}(m_i m_i^T) \\ & + 2(\Phi^T D - A^T D)\mathbb{E}(w_i m_i^T) + D^T D\mathbb{E}(w_i w_i^T) \\ \Theta - \tilde{\Psi}\Theta\tilde{\Psi}^T =& (\Phi^T\Phi - \Phi^T A - A^T\Phi + A^T A)\Sigma + D^T D\Sigma\end{aligned} \tag{E.6}$$

Appendix F

Angular Velocity Response Plots for Pointing Control

F.1 Model Predictive Control

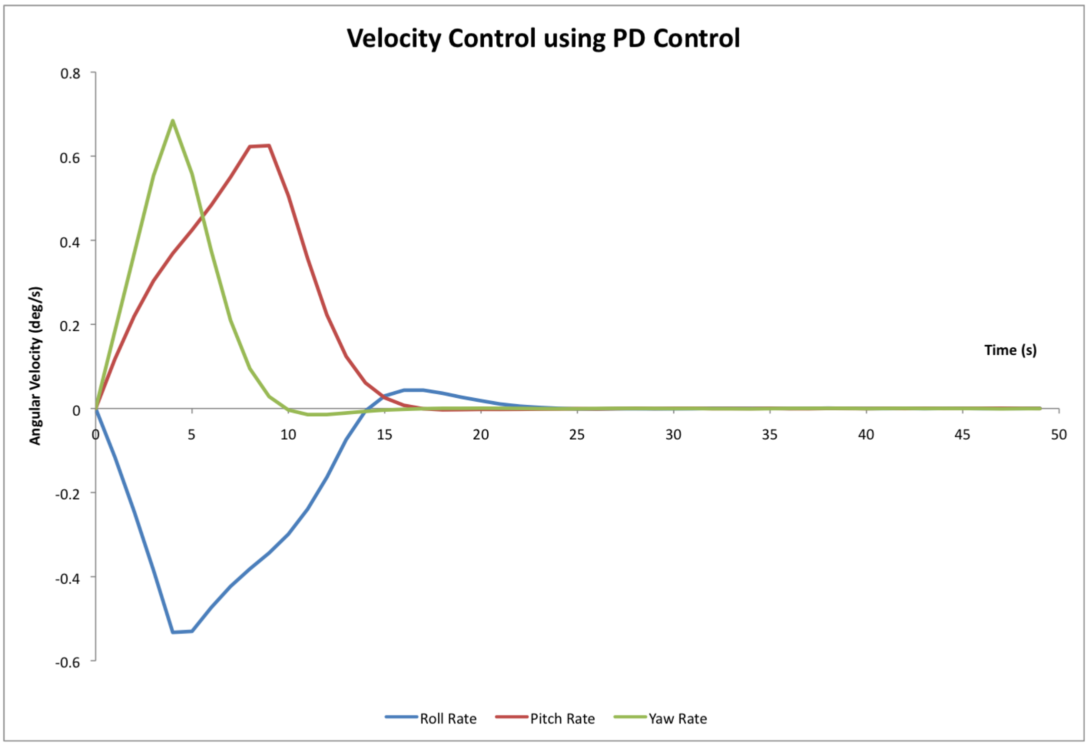

Figure F.1: Angular Velocity Response from Stationary

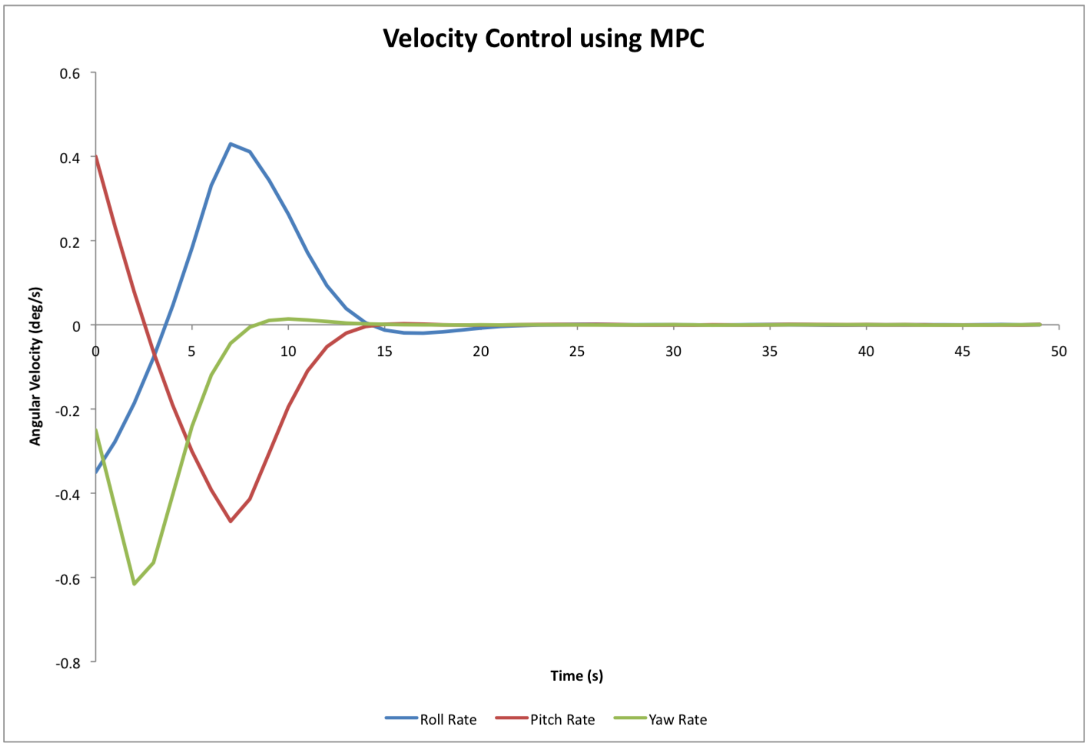

Figure F.2: Angular Velocity Response from Non-zero Initial Conditions

F.2 PD Control

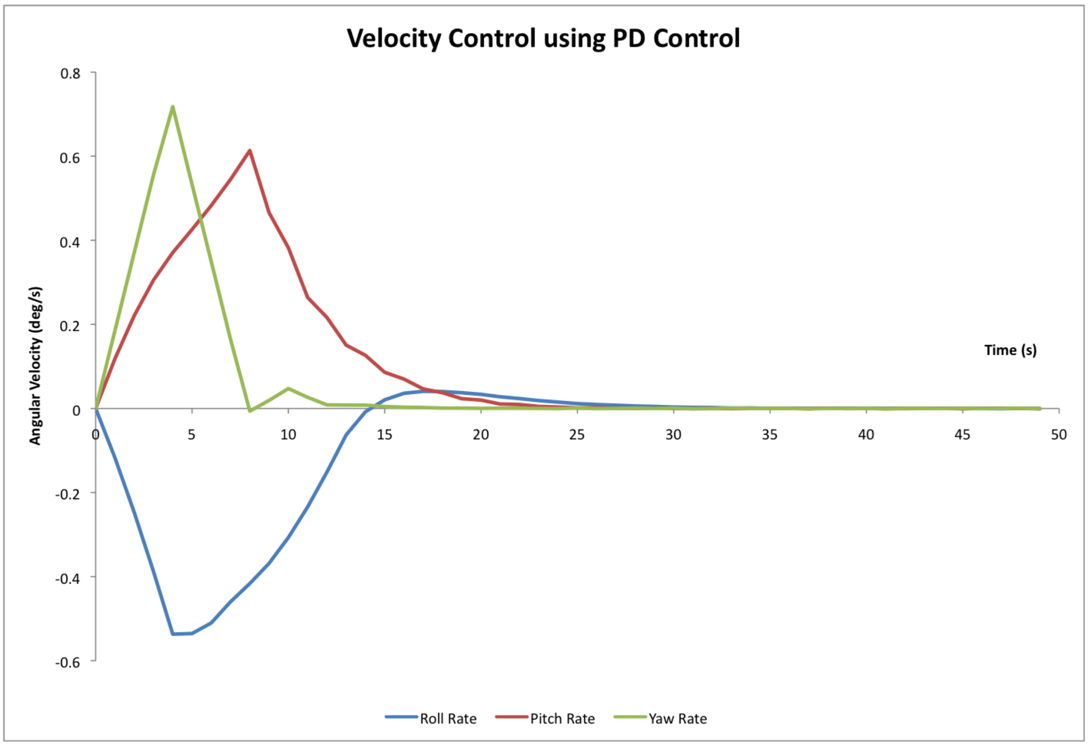

Figure F.3: Angular Velocity Response from Stationary

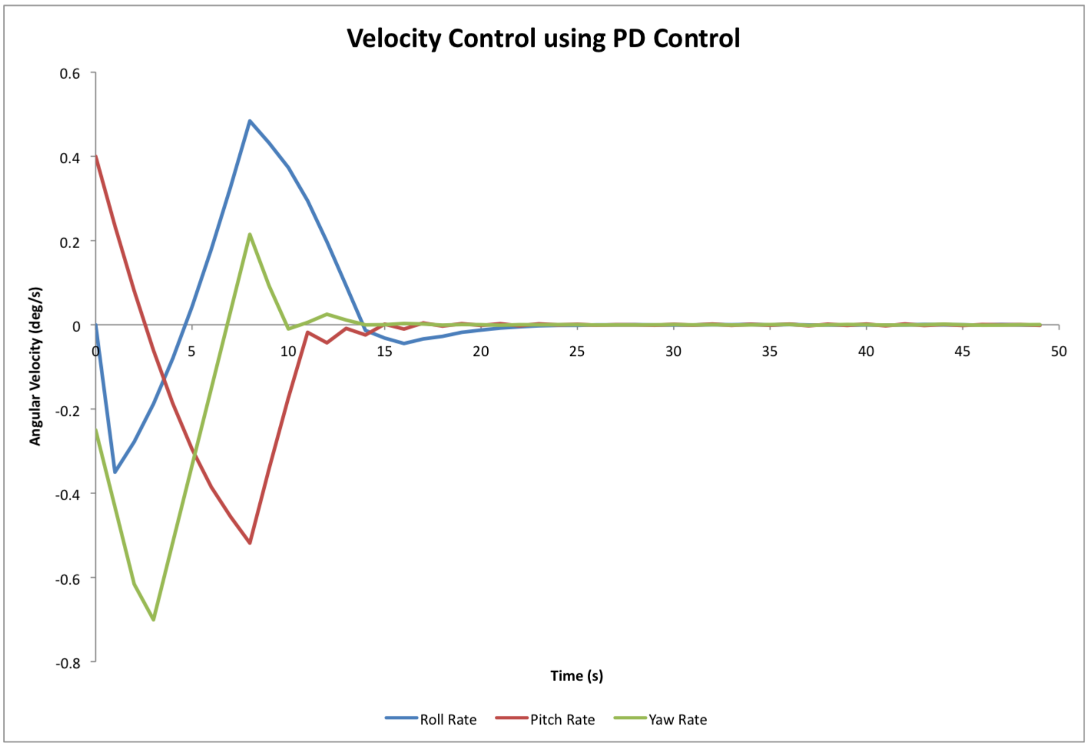

Figure F.4: Angular Velocity Response from Non-zero Initial Conditions

F.3 Comparison Between MPC and PD Control

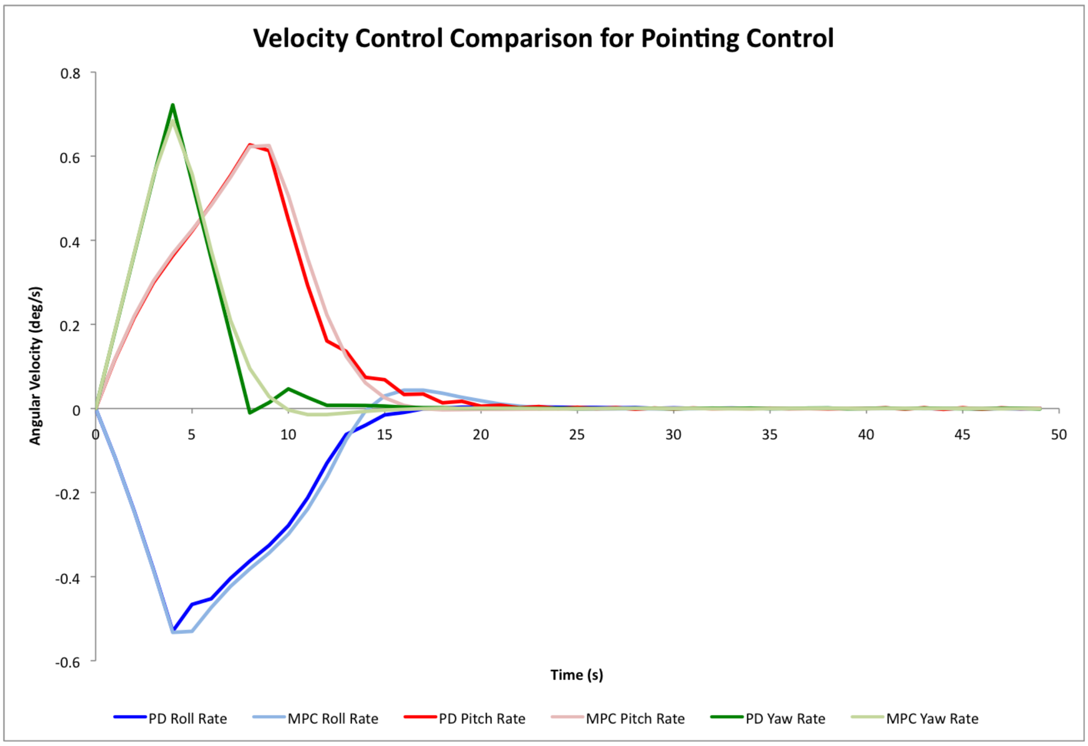

Figure F.5: Comparison of angular velocity response for pointing control from stationary

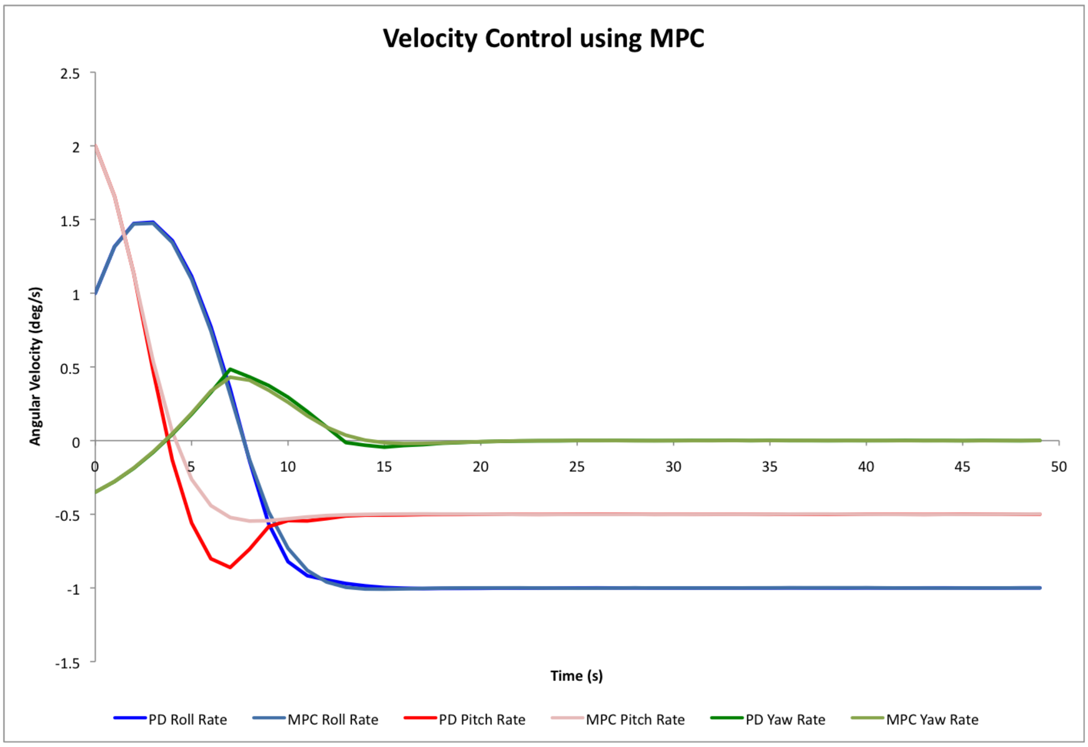

Figure F.6: Comparison of angular velocity response for pointing control from non-zero initial conditions

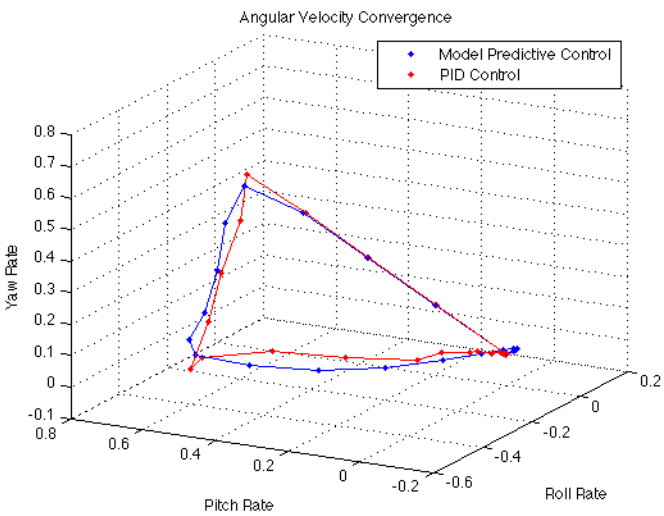

Figure F.7: Comparison of angular velocity convergence for pointing control from stationary

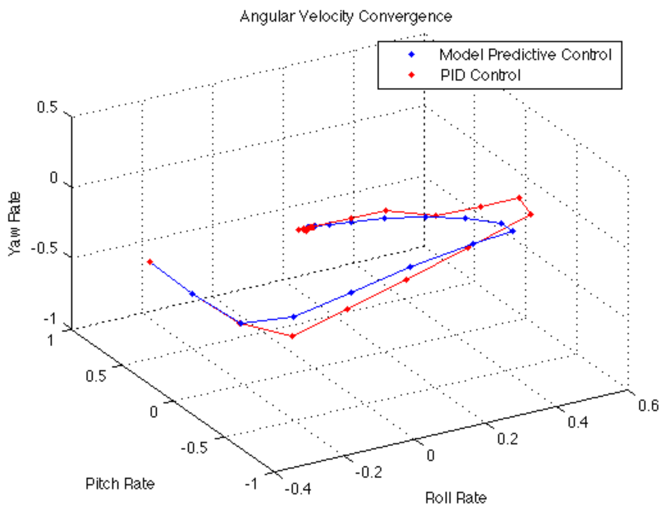

Figure F.8: Comparison of angular velocity convergence for pointing control from non-zero initial conditions

Bibliography

William Broad. Debris spews into space after satellites collide. *New York Times*, February 2009.

Eduardo Fernandez Camacho and Carlos Bordons. *Model Predictive Control*. Springer, London, 2 edition, 2004.

M Cannon, B Kouvaritakis, and X Wu. Probabilistic constrained mpc for multiplicative and additive stochastic uncertainty. *IEEE Transactions of Automatic Control*, 54(7): 1626–1632, July 2009.

M Cannon, Q Cheng, B Kouvaritakis, and S Rakovic. Stochastic tube mpc with state estimation. *Automatica*, 48(3):536–541, 3 2012.

CC Chen and L Shaw. On receding horizon feedback control. *Automatica*, 18(3):349–352, 1982.

David Clarke. *Advances in Model Predictive Control*, chapter Advances in Model Based Predictive Control, pages 3–15. Oxford University Press, Oxford, 1994.

USAFA DFAS. Falconsat program fact sheet. Technical report, United States Air Force Academy, 2009.

Rolf Findeisen and Frank Allgower. An introduction to nonlinear model predictive control. Technical report, Technical Institute for Systems Theory in Engineering, University of Stuttgart, 2002.

Bernard Friedland. *Control System Design: An Introduction to State-Space Methods*. Dover Publications Inc., New York, 1986.

E Gilbert and K Tan. Linear systems with state and control constraints: The theory and application of maximal output admissible sets. *IEEE Transactions of Automatic Control*, 36(9):1008–1020, September 1991.

VECTRONIC Aerospace GmbH. Vectronic reaction wheel vrw-1.

Marshall H. Kaplan. *Modern Spacecraft Dynamics and Control*. Wiley and Sons, Hoboken, NJ, 1976.

SS Keerthi and EG Gilbert. Optimal infinite horizon feedback laws for a general class of constrained discrete time systems: Stability and moving horizon approximations. *Journal of Optimization Theory and Applications*, 57(2):265–293, May 1988.

B Kouvaritakis, M Cannon, S Rakovic, and Q Cheng. Explicit use of probabilistic distributions in linear predictive control. *Automatica*, 46(10):1719–1724, October 2010a.

B Kouvaritakis, M Cannon, and R Yadlin. On the centres and scalings of robust and stochastic tubes. UKACC International Conference on Control, 2010b.

B Kouvaritakis, M Cannon, and D Munoz-Carpintero. On prediction strategies in stochastic mpc. pages 249–254. IEEE International Conference on Control and Automation, 2011.

Wiley J Larson and James R Wertz, editors. *Space Mission Analysis and Design*. Space Technology Library, 3 edition, 1999.

DQ Mayne, JB Rawlings, CV Rao, and POM Scokaert. Constrained model predictive control: Stability and optimality. *Automatica*, 36:789–814, 2000.

VT Ming and F Bin Mohd Hasim. Robust model predictive control schemes for tracking setpoints. *Journal of Control Sciences and Engineering*, pages 73–82, 2010.

Norman Nise. *Control Systems Engineering*. Wiley, 4 edition, 2003.

M Rast, G Schwehm, and E Attema. Payload-mass trends for earth-observation and space-exploration satellites. *ESA Bulletin*, March 1999.